LAWRENCE
LIVERMORE
NATIONAL
LABORATORY

LLNL-TR-405990

FY06 L2C2 HE program report Zaug et al.

J. M. Zaug, J. C. Crowhurst, W. M. Howard, L.E. Fried, K. R. Glaesemann, S. Bastea

August 4, 2008

Disclaimer

This work performed under the auspices of the U.S. Department of Energy by Lawrence Livermore National Laboratory under Contract DE-AC52-07NA27344.

Improvements to the fidelity of ASC-supported Cheetah/hydrocode simulations Campaign 2 Level 2 Milestone Report

Joseph M. Zaug, Jonathan C. Crowhurst,
W. Michael Howard, Laurence E. Fried, Kurt R. Glaesemann, Sorin Bastea

Lawrence Livermore National Laboratory
P. O. Box 808, Livermore, CA 94551, USA

Sept. 29, 2006

Abstract

The purpose of this project is to advance the improvement of LLNL thermochemical computational models that form the underlying basis or input for laboratory hydrodynamic simulations. Our general work approach utilizes, by design, tight experimental-theoretical research interactions that allow us to not empirically, but rather more scientifically improve LLNL computational results. The ultimate goal here is to confidently predict through computer models, the performance and safety parameters of currently maintained, modified, and newly designed stockpile systems. To attain our goal we make relevant experimental measurements on candidate detonation products constrained under static high-pressure and temperature conditions. The reduced information from these measurements is then used to construct analytical forms that describe the potential surface (repulsive energy as a function of interatomic separation distance) of single and mixed fluid or detonation product species. These potential surface shapes are also constructed using input from well-trusted shock wave physics and assorted thermodynamic data available in the open literature. Our potential surfaces permit one to determine the equations of state (P,V,T), the equilibrium chemistry, phase, and chemical interactions of detonation products under a very wide range of extreme pressure temperature conditions. Using our foundation of experimentally refined potential surfaces we are in a position to calculate, with confidence, the energetic output and chemical speciation occurring from a specific combustion and/or detonation reaction. The thermochemical model we developed and use for calculating the equilibrium chemistry, kinetics, and energy from ultrafast processes is named "Cheetah." Computational results from our Cheetah code are coupled to laboratory ALE3D hydrodynamic simulation codes where the complete response behaviour of an existing or proposed system is ultimately predicted. The Cheetah thermochemical code is also used by well over 500 U.S. government DoD and DOE community users who calculate the chemical properties of detonated high explosives, propellants, and pyrotechnics. To satisfy the growing needs of LLNL and the general user community we continue to improve the robustness of our Cheetah code. The P-T range of current

speed of sound experiments will soon be extended by a factor of four and our recently developed technological advancements permit us to, for the first time, study any chemical specie or fluid mixture. New experiments will focus on determining the miscibility or coexistence curves of detonation product mixtures. Our newly constructed ultrafast laser diagnostics will permit us to determine what chemical species exist under conditions approaching Chapman-Jouguet (CJ) detonation states. Furthermore we will measure the time evolution of candidate species and use our chemical kinetics data to develop new and validate existing rate laws employed in future versions of our Cheetah thermochemical code.

1. 0 INTRODUCTION

Laboratory experiments conducted on materials held at pressures in excess of several GPa provide insight into a realm of chemical and material properties that are significantly different from those encountered under ambient conditions. Such studies extend and test the theoretical framework which permits progress from properties at the atomic and molecular level to macroscopic behavior, constitute a potential source of novel materials and new tools for chemical transformation, and are important adjuncts to progress in other disciplines. There is no question that an improved general knowledge of electronic, physical, and chemical behavior of relevant constituent materials at high density is required, for example, for a less fragmented description of the processes that precede and govern dynamic exothermic chemical reactions. The same arguments are routinely made with regard to the structure and evolution of the major planets [1] and the deep interior of the Earth.

Increasing the predictive capability of LLNL hydrodynamic codes is an overarching goal of the Accelerated Strategic Computing program (ASC) and the Stockpile Stewardship Program in general. In the past, high explosive modeling was performed on an ad-hoc basis using the JWL (Jones-Wilkins-Lee) equation of state for the detonation products. The JWL is an empirical equation of state including separate cold compression and thermal terms. There is no fundamental basis for the functional form of the equation of state or for the parameters used in the equation of state. The JWL is highly successful for HMX-based conventional high explosives, but when applied to TATB-based insensitive explosives, the equation of state must be tuned on a per-part basis. This severely limits the predictive nature of the hydrodynamic simulations.

As part of the ASC program, we have undertaken to replace the empirical JWL with a scientific equation of state based on interacting individual detonation products. In order to carry out this project, we developed a high explosive equation of state package, Cheetah, which was numerically efficient and accurate. The Cheetah code, however, is semi-empirical in nature. Although it can calculate the equation of state of multiphase mixtures to better than 1% accuracy in many cases, it relies on potential interaction parameters for each individual molecular species. The only reliable way to derive these potential interaction parameters is through experiment.

Dynamical simulation based on approximate Born-Oppenheimer potentials plays a large and increasingly important role in chemistry and in the biological and materials sciences. More generally, knowledge of an effective interatomic potential function underlies any effort to predict or rationalize the properties of solids and liquids. While there exists an extensive body of experimental techniques and experience on computational methods appropriate to ambient conditions, the regime of strong repulsive interactions at very high densities has not been as extensively investigated [2-8]. We recognized that many of the materials used in the Cheetah code were not sufficiently well characterized by existing experiments. Gas gun experiments have been traditionally used to explore the equation of state of detonation product molecules. There are limitations to this approach, however. Gas gun experiments are very expensive. In addition, it is difficult to couple gas gun experiments with spectroscopic probes of speciation. This is an important issue, since chemical reactions can change the material being studied under conditions of high pressure and temperature. Also, simple gas gun experiments are confined to the so-called shock Hugoniot, which is a locus of points in P-V-T space. Moving off the shock Hugoniot in gas gun experiments is difficult, which further increases cost. Diamond anvil cell experiments have some potential advantages over gas gun experiments. Since the diamond anvil cell experiment is non-destructive, a large number of experiments can potentially be performed more rapidly and at lower cost than with a gas gun. We have coupled infrared and Raman spectroscopic diagnostics with our diamond anvil cell, allowing chemical speciation to be probed in situ. More importantly, we have developed a unique probe of the equation of state through the Impulsive Stimulated Light Scattering (ISLS) technique. ISLS allows us to determine the speed of sound in fluids or solids at high pressure and temperature conditions to an accuracy better than 1%. The speed of sound as a function of pressure and temperature can in principle be integrated to find the full P(V,T) equation of state. When combined with a heating apparatus, the diamond anvil cell can move through a full two dimensional set of P,T points.

We have designed sets of experiments to probe particular issues in the development and calibration of the Cheetah code. Those issues are:

1. Determine the equation of state at high P,T conditions for materials, which are not currently well characterized.
2. Validate models for molecular mixtures by performing measurements on mixtures.
3. Determine the important of electrostatic interactions at high P,T by studying molecules with large dipole moments.
4. Determine the importance of ionization at high P,T by studying strong acids and bases likely to dissociate into ions.

Although we have not fully resolved all of these issues, substantial progress has been made on all of them through the use of the ISLS technique. These advances have allowed us to substantially enhance the accuracy of the Cheetah code when applied to a wide range of materials. As the quantitative accuracy of the code has increased, its applicability to

hydrodynamic simulations has also increased. The following experiments were a necessary enabler in the development of a new approach to high explosive detonation modeling.

1.1 HIGH PRESSURE EXPERIMENTAL METHODS

We principally used spectroscopic probes to interrogate high pressure and temperature properties of detonation products. Raman and FTIR spectroscopy methodologies were employed to study chemical reactions at extreme pressure and temperature conditions. Impulsive stimulated light scattering was employed to provide direct measurements describing material thermodynamic states necessary to develop Cheetah's equation of state library. The speed of sound parameter plays a central role in the determination of fundamental equations of state for fluids. It is thermodynamically related to thermal property shapes (T-surface at (P,ρ)), and caloric parameters. ISLS is a nondestructive pulse-gated optical method exceptionally suited for measuring sound velocities [9-23]. It is also an extraordinarily versatile technique that has been used to measure or determine numerous material properties that include, fluid flow velocities [24], compressibilities [22], acoustic damping and structural relaxation rates [13, 23, 25-33], elastic constants [21, 22], energy transfer processes [34-43], chemical reaction kinetics [29, 44-49], population density kinetics [50, 51], electron-hole transport and decay rates [52-59], binary mass diffusion [60, 61], temporal and spatial coherence properties of laser beams [62, 63] and thermodynamic properties (*i.e.,* equations of state [15, 21-23] and thermal diffusion [9, 40, 55, 64-67]) on a very broad class of samples. Temperature and/or pressure induced phase transitions can be accurately characterized with ISLS techniques [20, 21, 68, 69]. A partial list of samples that have been investigated includes proteins [27, 28, 31, 80], thin film polymers [17, 18, 29], semiconductors [52-58], superconducting ceramics [16], metals [12], fluids [15, 19, 23, 26, 30, 32 64, 67], fluid mixtures [27, 60, 65], solutions [19, 25, 36-40, 43-49], glassy state amorphous structures [46, 66, 67], liquid crystals and crystalline solids [10-11, 13-14, 20-22, 33-35, 50, 68, 69]. In addition, ISLS experiments may be conducted on high-energy plasmas [42], and flames [70]. Unlike traditional frequency-domain measurement techniques (such as, pulse-echo and including the latest in resonant ultrasound spectroscopy, and Raman, including CARS), ISLS can effectively resolve heavily damped, or overdamped, modes that predominate in liquids and amorphous structures (glasses) at high-pressure. Traditional optical frequency-domain techniques (Raman spectroscopy and Brillouin scattering) tend to produce broad frequency linewidth spectra, when the sample medium is viscous, which yield indeterminate and/or ambiguous time-resolved measurements. Furthermore, the frequency range of ISLS experiments depend only on the large bandwidth intrinsic to ultrashort fs-ns laser pulses. The temporal resolution of the excited material modes is limited only by the pulse width. (In a more limited sense, the coherence time of the light dictates the time resolution of the experiment [84]). The competing qualities (resolution vs. intensity) found with even the largest spectrometers are rendered *non-issues* when using fast and gated electronic instruments within the context of time

resolved spectroscopy. Analyzing ~30 μm thick samples with diameters on the order of ~50 μm are considered routine using laser-induced ultrasonic methods, whereas transducer-induced ultrasonic methods are limited to samples that are >1000 μm thick and 200 μm in diameter. When such small samples are illuminated with an ~80 picosecond pulsed laser system acoustic phonons can be excited and probed within a frequency range of 10 MHz - 10 GHz. With today's of-the-shelf femtosecond laser systems, this range extends to THz (optical phonons), where nearly any motion of atoms or molecules (vibrations in condensed materials, molecular rotations and vibrations, or simply structural relaxations) can be time-resolved although at high frequencies frequency-domain techniques may well be preferable. ISLS can help resolve/characterize structural and liquid-glass transitions. It can also be used to detect ppm (parts per million) concentration changes in chemical binary solutions or mixtures, with temporal resolutions exceeding reaction or recombination times [77]. Perhaps one of the most convincing utilities of ISLS experiments is the determination of anisotropic properties of molecular environments. For all of the above, the essential requirements (aside from a good optical sample) are very short excitation pulse widths, and beam-material coupling mechanisms by which the optical pulses can initiate and monitor the time dependent results.

There is extensive literature describing experimental methods and computational models designed to provide insight into chemical behavior under ambient conditions. Yet, in terms of the universe that we live in one may argue that ambient conditions are a physical anomaly. Most chemical reactions occur under conditions of extreme temperature and pressure, the largest exception being reactions in biological systems. In general, knowledge of an effective interatomic potential function underlies any effort to predict or rationalize the properties of solids and liquids. The regime of strong repulsive interactions in condensed phases at very high densities, where many body interactions play a primary role has not been so extensively investigated.

Percy W. Bridgman [85] (1882-1961) opened the field of high-pressure studies with his piston-cylinder apparatus during the early part of the 20th century. His ideas were followed up, beginning in the mid 1940's, by groups at Norwell and General Electric who included high-temperature to the foray of evolving high-pressure devices. Diamonds were first proposed as having potential for high-pressure studies in 1887 [86]. However, it wasn't until Alvin van Valkenburg[*] (1913-) and C. E. Weir *et al.*, introduced [87] the modern diamond anvil cell (DAC), during the same time Schalwlow and Townes presented optical masers, that this potential became reality. Weir's device[§] opened a new era of high-pressure optical experimental characterizations of material properties. Smaller (palm size) diamond cells were designed to increase access in reciprocal lattice space illuminated by x-ray producing equipment [89]. In turn, these smaller DACs were found useful in phonon scattering of laser light (Brillouin

[*] It should be noted that Prof. John Jamieson, University of Chicago, made a diamond piston-cylinder device around the same time as Valkenburg.

[§] It should be noted that as early as 1956, [88] optical measurements were made using NaCl and synthetic sapphire windows.

scattering) [90]. The first ISLS experiment involving a DAC was conducted in 1988 on room temperature liquid methanol and ethanol up to 6.82 GPa [15].

The combination of DAC technology with ISLS experiments offers a powerful methodology for comprehensive studies of effective interatomic potential surfaces in the region of high repulsion. Results from such experiments are providing a means to further refine molecular dynamics calculations and more accurate determinations of intermolecular potential functions and correlations of high-frequency molecular equilibrium relaxation times. The experiments described in this body of work demonstrate the versatility found with ISLS when hydrostatic pressure is used to increase density. The results show that extrapolation and/or computational modeling from ambient properties for deduction of high-pressure chemical behavior (*i.e.,* sound velocities, the equation of state, lattice constants, compressibilities) can be inaccurate. The logical progression will be the incorporation of computational methods with new high-pressure ISLS data to accurately characterize the interatomic potentials at high density.

Photoacoustic spectroscopy is often the most appropriate form of optical spectroscopy when material absorption is weak. ISLS spectroscopy offers the advantages of photoacoustic detection in a geometry that is compatible with the requirements of a DAC. The ISLS approach enables the experimenter to *tune in* material modes for observation, by adjustment of the excitation pulse width and wavelength. Control of the probe wavelength permits observation of each contributing mechanism of the resulting diffraction grating. In this way material modulations can be optimized to increase the amount of diffracted probe light (signal). The excitation beams' intersection angle can also be configured to control the acoustic wavelength (grating spacing), or modulation of the induced longitudinal, quasilongitudinal and/or surface waves in the material. Picosecond pulse-widths are short enough to excite low-frequency material modes or acoustic phonons. Shorter femtosecond pulses may excite higher frequency material modes, or optical phonons, in materials. This enables observation of individual vibrational oscillations.

The optical generation of ultrasonic waves has been successfully employed to study a wide array of physical and chemical systems. ISLS represents one form of dynamic, or transient, grating experiments that have evolved from early optical endeavors. Since 1973, ISLS experiments have been successfully applied to a wide number of scientific problems including: determination of orientational relaxation times and singlet lifetimes for dye molecules in solution, thermal diffusion measurements of solutions (liquids and solids), phonon and excited-state phonon studies of crystals, characterization of acoustic behaviors in solids near structural phase transitions, characterization of various phases of liquid crystal thin films, energy transport in molecular solids, polariton scattering, observation of protein motions in hemoglobin and myoglobin, and nondestructive characterization of thermal and mechanical properties of thin films and thin film coatings. In addition, multiple-pulse ISLS experiments have been successfully applied to manipulate molecular motions along excited-state potential energy surfaces

In the remaining body of this report a description of the ISLS experiment and recent technological advancements are provided along with a description of our high-

pressure/temperature vibrational spectroscopy instrumentation. Subsequent to the experimental descriptions, theoretical formalisms are presented followed by experimental results from this project that have been used to improve LLNL thermochemical and ALE hydrodynamic LLNL codes. The current impact of this work on LLNL computational efforts will be discussed in section 3. Section 4 addresses our proposed future work and implications for ongoing LLNL computations with emphasis placed on our need to confidently predict the properties of newly designed or modified systems and/or chemical formulations. It is through our non empirical, strict science based approach and associated input to thermocehmical codes where arguably the most reliable design parameters will fall out from computationally derived predictions.

1.2 ISLS EXPERIMENTS

The beam configuration of a traditional impulsive stimulated light scattering experiment is displayed in Figure 1. Our bench top ISLS experimental layout is provided in Figure 2. The technique may be considered, with respect to nonlinear optics, as one version (partially degenerate) of the four-wave mixing experiment. At a pulse repetition frequency (PRF) of 3.8 kHz, two 100-picosecond near-infrared (1.064 μm) parallel-polarized laser pulses, converge spatially and temporally at an angle θ in a sample medium. The wave vectors of these pulses are given by $\mathbf{k}_1$ and $\mathbf{k}_2$ where $|\mathbf{k}_1| = |\mathbf{k}_2|$. (In this report, both vector and tensor quantities appear in bold typeface). The crossed light produces a spatially periodic electric field, which in turn produces a spatial modulation (grating) of material properties (population of excited electronic states, polarization, or vibration, of atoms, temperature, or molecular orientation). In an absorbing material, rapid radiationless relaxation may heat the sample at the interference maxima. Subsequently, in an anisotropic medium, thermal expansion impulsively launches one quasilongitudinal and two quasitransverse pairs of counterpropagating ultrasonic waves. Along symmetry directions pure longitudinal waves are generated. The material strain created by the acoustic waves causes a time-dependent and spatially periodic variation in the index of refraction of the sample (standing strain wave), which, in effect, modulates the optical properties of the sample (index of refraction and/or absorption).

Phonon excitations are dependent on the condition that the temporal width of the excitation pulses, τ_P, is short compared to the single acoustic oscillation periods ($1 / \tau_P > 1 / \tau_A$). Hence the interaction term "impulsive" is incorporated into the name ISLS. Material modes where $\tau_P > \tau_A$ will not be efficiently excited. The acoustic wavelength and wave vectors describing the two coherently excited elastic waves are (λ_A, $\pm \mathbf{k}_A$) where

$$d = \lambda_A = \lambda_E / 2\sin(\theta) \tag{1a}$$

and

$$\mathbf{k}_A = \mathbf{k}_1 - \mathbf{k}_2 \, . \tag{1b}$$

The diffraction grating only contains the fundamental wave vector $\mathbf{k}_A$, and so, with exception to a non-linear refraction response, higher order scattering vanishes. As mentioned above, density variations affect the index of refraction, n, (both real and imaginary parts) thus changing the optical properties of the material. Hence, density variations give rise to a transient, or dynamic, optical diffraction grating that remains long after the excitation pulses have departed from the sample. (A frequency offset between the two-excitation pulses would result in a traveling grating). In non-absorbing materials, density changes occur due to electrostriction. The broad frequency spectrum of the short excitation pulses provides a mix of optical Fourier components that couple with material modes to generate high-frequency phonons. In this way, the crossed electric field terms of the excitation pulses produce an electrostrictive force density. The elastic deformations resulting from this force are again impulsively launched counterpropagating acoustic waves, whose wavevector matches the optical pattern. If the polarization of the two-excitation pulses is not parallel then acoustic waves of particular polarizations along selected wave-vector directions can be produced. Within isotropic materials, pure transverse modes (shear waves) can be excited with perpendicular polarized pulses. (There is an inherent cost because transient diffraction gratings are significantly reduced in intensity for non-parallel beam polarizations). In other words, ISLS can generate acoustic modes (longitudinal, quasilongitudinal, quasishear, and shear) within the constraint of what the medium can support, in any orientation, in materials of any symmetry. However, the photosentivities vary widely, some to the point where the diffracted intensities are too weak to detect using the tradition ISLS technique. Since material properties govern the time-dependent behavior of the laser-induced grating, a third variably delayed *probe* beam, with wavelength and wave vector (λ_P, $\mathbf{k}_P$), is monitored as it coherently diffracts off the grating (λ_D, $\mathbf{k}_D$) at the phase matched Bragg angle. Measuring the scattered diffraction intensity, I, of the probe pulse as a function of delay time, given stable physical conditions of the experiment (*i.e.,* grating spacing, pressure and temperature), serves to determine the frequency, f_A, and attenuation, γ, of the induced acoustic standing waves and any observable structural modes. Dispersion properties are monitored by measuring sound velocity, u, as a function of f_A (under constant physical conditions) by varying λ_A (*i.e.,* changing the intersection angle θ). The sound velocity is determined by

$$u = \lambda_A \cdot f_A \qquad (2)$$

where again λ_A (in microns if λ_E = 1.064 μm) is the grating spacing or period. The grating spacing is determined by measuring f_A of a temperature-independent standard. The confirmed

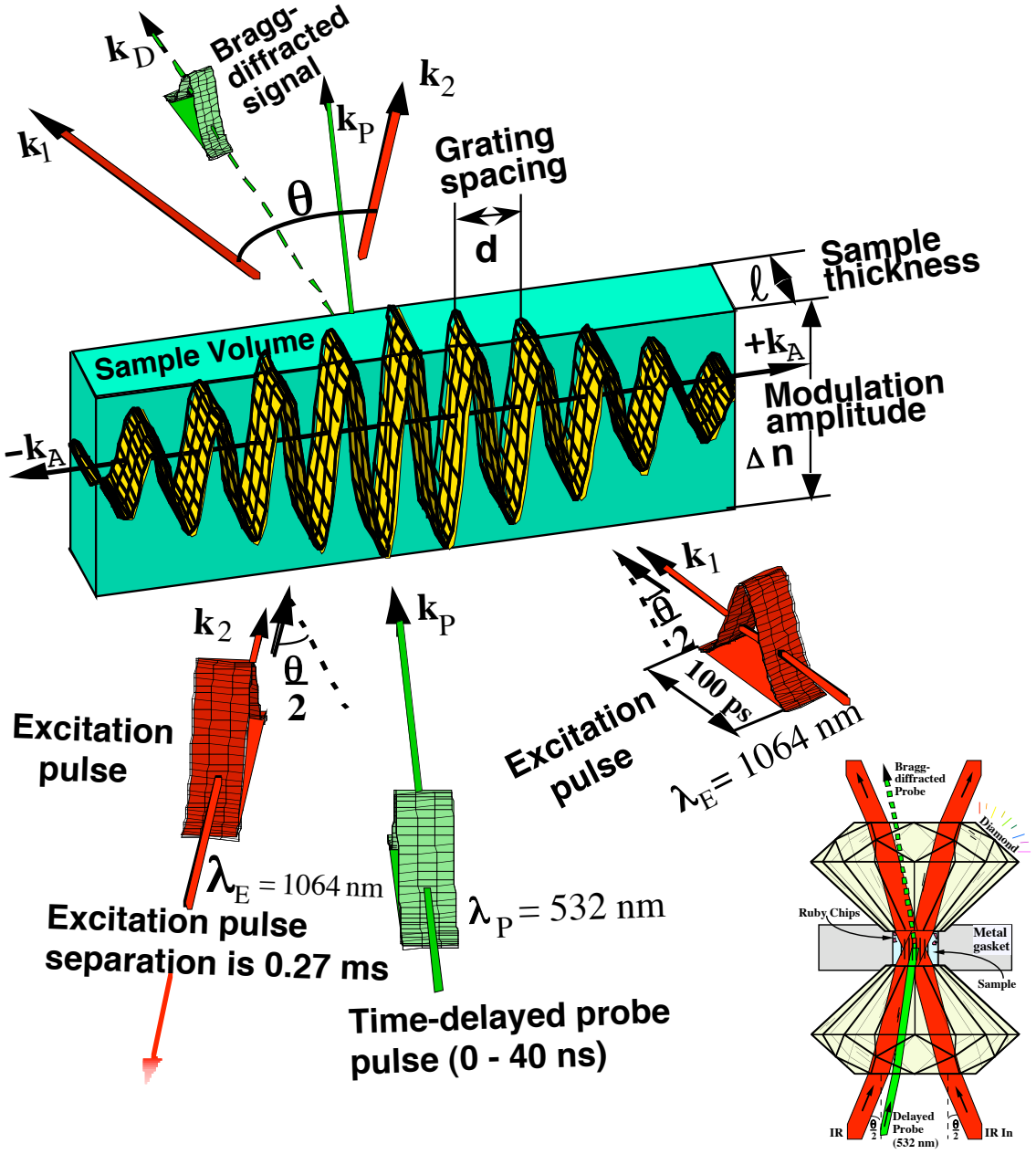

Figure 1. Laser-induced ultrasonic wave excitation and detection using ISLS. Two 100 picosecond infrared pulses converge spatially and temporally within a transparent sample medium. The time-dependant intensity or strength of the optical transient diffraction grating is monitored by a third frequency doubled pulse that, in the case for relatively low scattering strength, is systematically delayed in time. The time response of "stronger" gratings can be monitored using a continuous-wave laser probe.

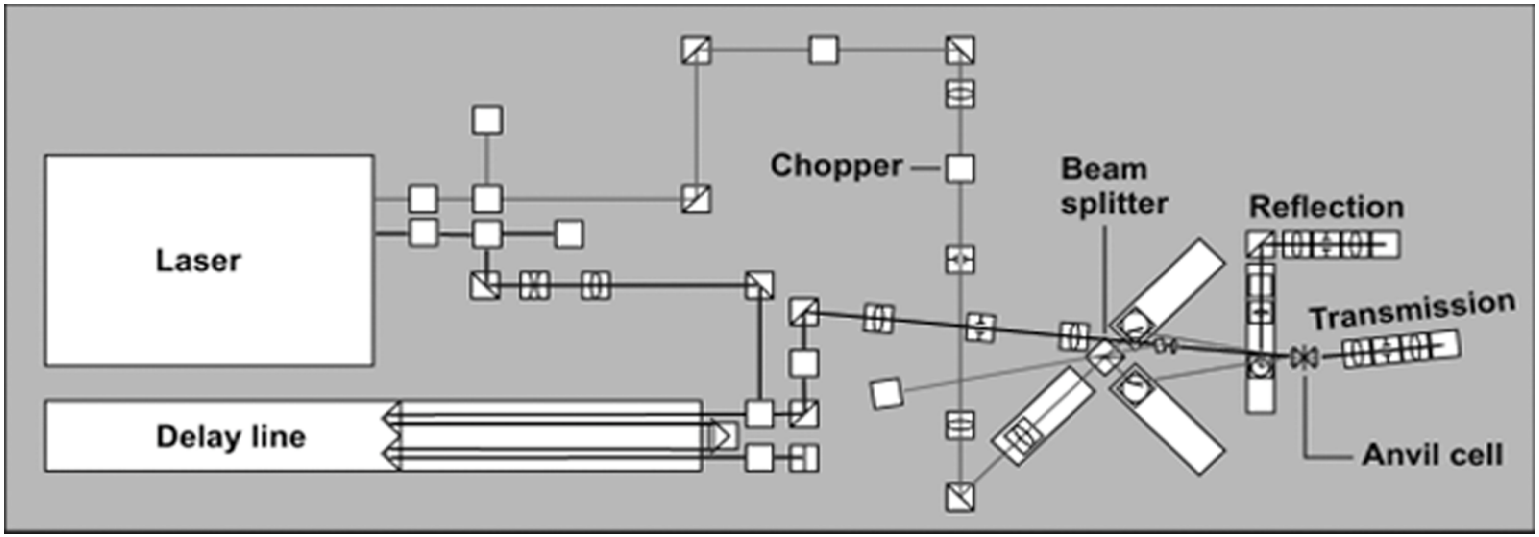

Figure 2. ISLS system. A Time-Bandwidth Jaguar Nd:YAG laser provides a continuous train of 100 ps 1064 nm excitation and 532 nm probe pulses at a fixed pulse repetition frequency. Every other near IR pulse is removed using a mechanical chopper wheel to provide a non-transient grating based parasitic scattering background that is then subtracted from grating diffracted signals. The 532 nm probe pulses are time-of-flight delayed by using a mechanical translator. Diffracted probe pulse signals are collected using a spatial filter and a digitally amplified photo multiplier tube. Use of a boxcar integrator increases the signal-to-noise ratio and a Labview® data acquisition board and software is employed to digitize and normalize time-domain ultrasonic data. The system can be used in either transmission or reflection geometries.

literature value for the velocity of the standard u_S, and the measured frequency provides an accurate determination of $\lambda_A \pm 0.2\%$ in the sample, provided the angle θ remains constant and the standard has a low thermal expansion coefficient with no dispersion. (For this study glass was the secondary standard and was calibrated against water and fused silica) [90-93]. If the diffracted signal intensity is high enough, then a record of the grating modulation intensity can be acquired using a continuous-wave (CW) laser probe source in conjunction with very fast transient recording devices. At a typical pulse repetition frequency (PRF) of 3.8 KHz, one second of averaging provides a substantial s/n advantage over averaging each shot from a systematically delayed pulsed probing source. In this way, the data acquisition time can be reduced by factors of 10^3 or more. The grating intensity, or diffractive strength, depends inherently on material modes coupling to the optical electric field and absorption of the excitation laser pulses. A more detailed account explaining how the electric fields of the crossed laser pulses couple to material modes and then induce a spatially periodic variation in index of refraction is published in one of our recent Elsevier Science book chapters ("The equation of state and chemistry at extreme conditions: applications to detonation products," J. M. Zaug, W. M. Howard, L. E. Fried, A. F. Goncharov, W. B. Montgomery, and J. C. Crowhurst, in *Chemistry Under Extreme Conditions*, ed. M. R. Manaa, Elsevier Science Ltd, 399-425, (2005).). References [71-76], and [78-83] also provide additional reading material.

Recently we discovered and somewhat refined an entirely new ISLS methodology that requires only one laser pulse to launch acoustic waves across the DAC sample chamber. This single pulse excitation (ISLS-SPE) process is essentially an opto-mechanical process that opens our ability to study, unlike traditional ISLS, any fluid material. Figure three provides an illustration of the ISLS-SPE technique. We have characterized this completely new experimental methodology to more precisely measure speeds of sound from fluid samples. Essentially we optimize and calibrate the ISLS-SPE system, including the DAC, using a material such as water or liquid argon where very precise ultrasonic data is available in the literature. We then scale our measured ultrasonic frequency to match our speed of sound (SoS) measurement to previously published ultrasonic results. In this way we determine the wavevector to be used for our samples. A conservative estimate of the error in our measurement precision is less than or equal to 0.5%. Examples that demonstrate the robust utility of the ISLS-SPE technique will be given in section 2. We (Zaug, Crowhurst, Glaesemann, Torralva, Howard, and Fried) are preparing a manuscript for publication in Applied Physics Letters that will discuss ISLS-SPE, Cheetah EoS results, and present data that extends the pressure range of previous ultrasonic measurements on supercritical argon and propane by nearly a factor of 10^2.

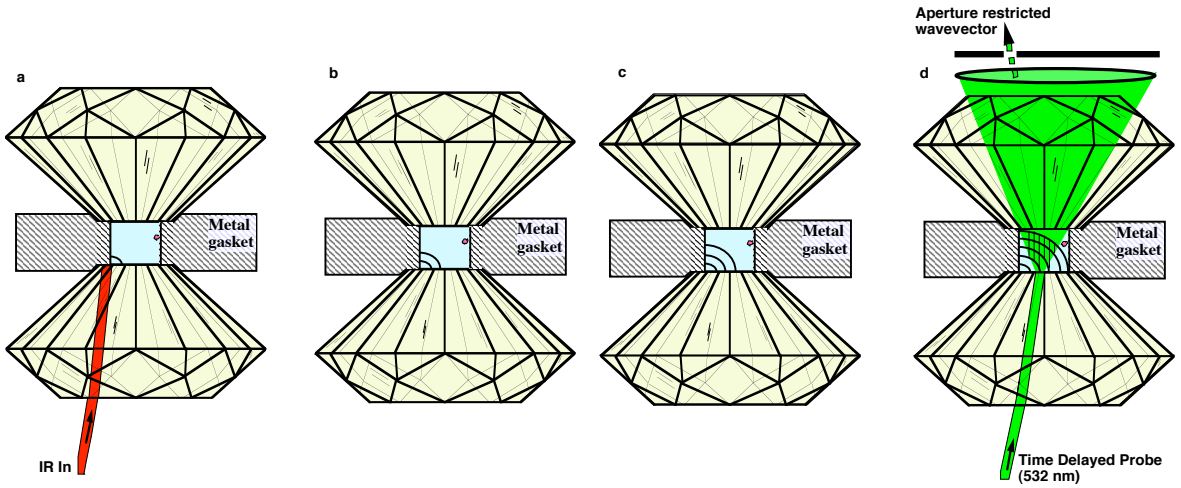

Figure 3. The ISLS-SPE process begins with a) the injection of a laser pulse (1 μJ, 100 ps, 1.065 μm, 100 μm diameter focused spot) at the metal-diamond interface. The laser energy is immediately absorbed by the metal gasket. The laser-shocked metal then expands and beats against the diamond culet. This in turn launches an ultrasonic wave into the sample chamber. The metal reverberates b) & c) at gHz frequencies. We then send in a time-delayed probe pulse (~0.5 μJ, ~80 ps, 0.532 μm, 25 μm diameter focused spot) to interrogate the transient acoustic grating. The probe pulse is made to scatter off of a scratch inscribed onto the entrance culet. This parasitically scattered light acts as a carrier wave that then mixes in a nonlinear fashion with light scattered from the acoustic grating. This heterodyne mixing process then provides a relatively stable amplification process thus enabling our ability to monitor what would otherwise be an imperceptible "signal." In order to enhance the precision of our measurements we restrict the frequency spread of our observed signal pulse by using a series of three collinear wavevector limiting apertures.

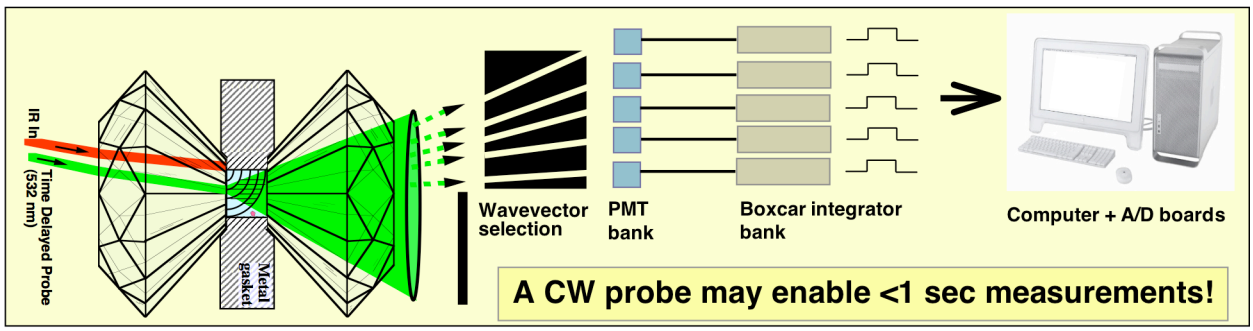

Figure 4. A conceptual diagram of how ISLS-SPE may be employed to simultaneously measure velocity dispersion of a viscoelastic or glass-like material. The frequency dependence of the velocity can be fit to acquire the acoustic absorption and determine structural relaxation dynamics. In some instances the high-frequency limit of the shear modulus can be calculated and correspondingly the viscosity.

In addition to SoS measurements the ISLS-SPE method may lend itself to high frequency velocity dispersion measurements. The traditional ISLS technique requires one to adjust the wavevector by either changing the excitation wavelength or the intersection angle of the two spatially and temporally overlapped pulses. Depending on the experimental geometry this can be a laborious and time-consuming venture. It may be possible to measure a range of ultrasonic frequencies using ISLS-SPE. Weather or not a significant frequency range is accessible remains to be determined. We also need to determine if ISLS-SPE signals can be detected using a CW laser probe. If this were possible then it is conceivable that a 3D picture (x,y,time) of ultrasonic waves traveling in the DAC sample chamber could be collected.

1.3 RAMAN AND FTIR EXPERIMENTS

We developed custom spectroscopic diagnostic tools to first determine the pressure of samples contained at extreme P-T conditions and second to monitor the chemical stability of our supercritical fluid samples. To determine pressure we originally we employed the ruby pressure-scale which requires only modestly sophisticated equipment [95]. However the precision of the ruby pressure marker drops precipitously with temperature and for the purposes of accurate EoS determinations it should not be used above 523K. Later we synthesized strontium tetraborate doped with samarium (SrB_4O_7:Sm^{2+}or SRB) which has three distinct advantages over the ruby pressure marker: 1) it yields a singlet spectral line and hence the peak fitting precision is more optimal 2) the spectral shift of SRB is nearly temperature independent, and 3) it can be used to temperatures approaching 1100K [96]. As our research moved toward the study of corrosive fluids the utility of our fluorescence pressure standards reached an end. Supercritical fluids such as H_2O or those that contain HCl, HF or NH3 chemically react with SRB. When SRB was attacked by corrosive supercritical fluids we obtained non sensible results. The carbon-13, ^{13}C, Raman pressure marker was first chosen to overcome chemical attack in highly corrosive environments. We never observed evidence of ^{13}C breaking down in any corrosive fluid. However our ^{13}C material is polycrystalline and the absolute highest precision attainable with such a sample is no better than ±0.3 GPa. A potential ten percent error in pressure at say 3 GPa is not acceptable for a high precision EoS study where measured sound velocities have sub 1% error. More recently we acquired single crystal cubic boron nitride (cBN) pressure markers. The cBN Raman pressure marker has at least two if not possibly three advantages over ^{13}C: 1) the transverse optical Raman mode (1055 cm^{-1} at ambient conditions) does not merge with the intense ^{12}C line from the diamond culet thus resulting in significantly more optimized peak fitting, 2) with an appropriately calibrated cBN pressure scale an extended single crystal effectively has no inhomogenities and hence can result in significantly more precise pressure determinations than ±0.3 GPa, and lastly 3) it has been reported that cBN may be less prone to chemical attack than diamond. We did discover two significant issues with concerning cBN as a pressure marker material. The Raman line positions became impossible to reproduce once

temperature was taken to 673K or higher. A search through the literature indicated that the cBN manufacturing process typically yields strained material. We solved this problem by twice annealing our cBN to 973K in a high-vacuum furnace. The second issue is that there is no suitably developed cBN pressure scale required for high precision EoS studies. Consequently the SoS and EoS values in this report where the cBN Raman marker is used are based on a provisional cBN pressure scale. We conducted a high pressure and temperature annealed cBN Raman study and compared, under exact same conditions, against SRB using supercritical argon as the pressure mediums. The complete analysis of this data and the development of our final cBN scale will occur, due to the significant amount of required analysis time, after the completion of this level-2 milestone report. We have conducted pressure calibration studies to further understand high temperature induced pressure calibration offsets between commonly used optical sensors (Goncharov A. F., E. Gregoryanz, J. M. Zaug, and J. C. Crowhurst, *J. Appl. Phys.* **97**, 094917 (2005).). We reported that the overall temperature dependence of ruby fluorescence becomes less significant at high pressure. The ruby scale in fact underestimates pressure by as much as 0.5 GPa, compared to all other conventional pressure sensors, at high P-T conditions. We provided a description of how to correct this issue.

A fluid or fluid mixture will chemically react or breakdown when subjected to sufficiently energetic pressure-temperature conditions. Fluid mixtures such as H_2O:HCl will become immiscible. In order to verify the integrity of our samples we employ traditional vibrational spectroscopy in the form of Raman and/or Fourier transform infrared (FTIR) absorption. For Raman spectroscopy we developed three separate systems: 1) a traditional CW Raman system, 2) a pulse-gated Raman system and 3) a near simultaneous FTIR/Raman system. We also added the ability to simultaneously conduct Raman spectroscopy and laser heat DAC encapsulated samples. For the completeness of this report each system will be briefly described.

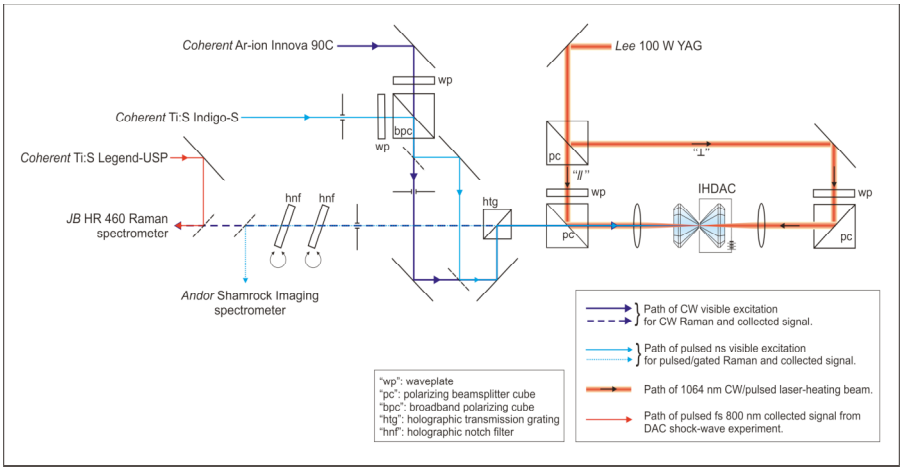

Figure 5. Schematic diagram of our pulse-gated, CW Raman, and double-sided laser-heating instrument. Additionally this system is used to image single shot femto second pulses providing a sensitive tool to interferometrically time-resolve ultrafast phenomena such as laser ablated surface displacement.

A schematic diagram of our CW Raman ands laser heating system is provided in figure 5. With the flip of two mirrors we can direct the 20 ns pulsed output from our 5 kHZ PRF Coherent® Indigo laser source to our sample and perform pulse-gated Raman spectroscopy. This capability enables us to discriminate weakly scattered Raman signals from huge thermal and/or fluorescence backgrounds thus dramatically extending our range of measurements by as much as a factor of three in temperature. Our double-sided laser-heating component enables us to heat samples to approximately 4000 Kelvin. Temperature is determined using one of three separate techniques: 1) collecting radiometric data and fitting it to a black body curve, 2) calibrating the spectral efficiency of our instrument and then using the ratio of Stokes to antiStokes Raman modes from the high temperature sample, and 3) exciting electrons in an already hot sample using our CW argon laser source and fitting the excited state Raman modes to a statistical Boltzmann distribution model. The system shown in figure 5 also incorporates our new FAST-DAC (ultrafast laser) instrumentation. We collect single shot femto second laser shot information from our Coherent® Legend laser source and image the spectral data on a CCD array coupled to our HR 460 spectrograph. We have used this system to perform several groundbreaking experiments that impact the fidelity of ASC supported Cheetah/hydrocode simulations. Our first experiment, developed in hand with Cheetah code predictions, the low pressure-temperature phase boundary for dynamically ionized water (Goncharov A. F., Goldman N., Fried L E., Crowhurst J. C., Kuo I-F., Mundy C. J., and Zaug J. M., *PRL*, **94**, 125508, (2005).). A second experiment determined the intramolecular potential surface of nitrogen and hydrogen under high pressure and temperature conditions (Goncharov A.F., and Crowhurst J. C. *PRL*, **96**(5), 055504, (2006).). The utility of our pulse-gated Raman instrument was first demonstrated on high temperature tungsten. In addition we used our instrument to determine the fluorescence decay lifetime of diamond (Goncharov A. F. and Crowhurst J. C., *RSI* **76**, 063905 (2005).). We also reported Raman measurements from cBN up to 40 GPa and 1700K (Goncharov A. F., Crowhurst J. C., Dewhurst J. K., Sharma S., *PRB* **77**, 100104, (2005).). However the temperature precision from this laser heating experiment is not suitable for our current EoS program studies.

In order to measure pressure and simultaneously monitor the chemical and physical state of our supercritical fluids during speed of sound studies we recently embedded a custom Raman and second fluorescence system. Figure 6a is a photo of the DAC sample region with associated ISLS pulses used for SoS measurements. Figure 6b is a photo of our embedded dual Raman and fluorescence spectrographic system (RFS). Our RFS system uses two spectrographs. In this way we do not need to move our diffraction gratings between pressure measurements and fluid Raman measurement settings. This dramatically increases data throughput and maintains a relatively low user effort required to maintain high precision spectroscopy/pressure measurements. All one is required to do is flip a motorized mirror after each measurement cycle. Our system also includes a high magnification CCD imaging system that enables one to take sample micrographs and easily aim our CW argon laser spot onto the fluid sample or a pressure sensor. This custom built instrument is arguably the most precise and efficient optical based speed of sound + vibrational spectroscopic analysis system on the planet. Within seconds of a

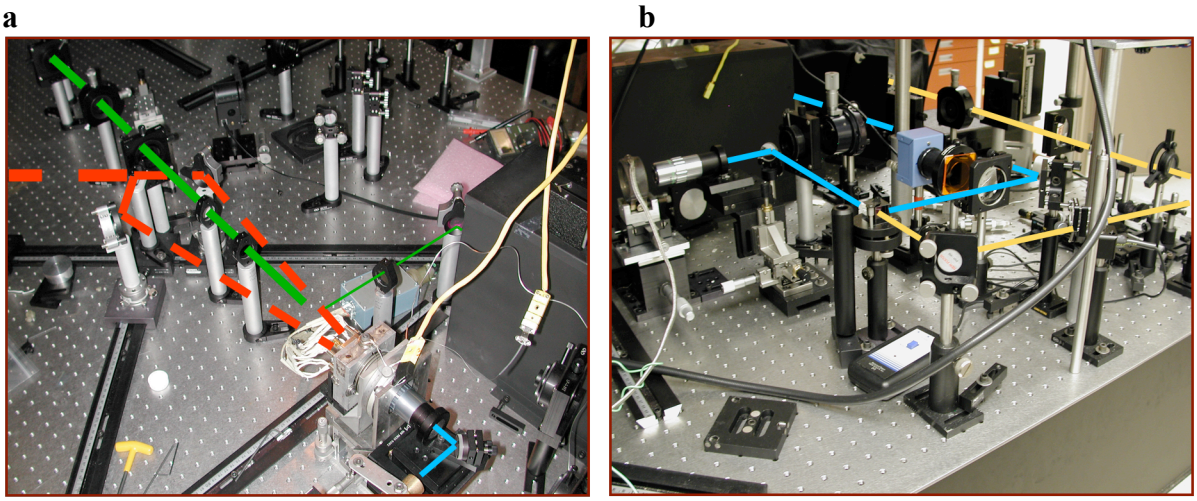

Figure 6. Photographs of our ISLS and Raman-fluorescence instruments. The sample remains stationary for (a) ISLS and (b) Raman and fluorescence measurements. ISLS is initiated by overlapping two 100 ps near IR pulses within the sample volume. The resulting transient holographic grating intensity is probed using a time delayed 532 nm pulses. The process is repeated at different probe delay times at a pulse frequency of 3.8 kHz. For visible spectroscopy we use an argon ion CW laser source (blue lines drawn in (b)). The scattered light (yellow lines shown in (b)) is collected and directed either to a dedicated Raman or a fluorescence spectrometer.

ISLS SoS measurement we can determine pressure with no more than 0.03 GPa error (SRB sensor) and collect a calibrated Raman spectrum (1 cm^{-1} resolution) on any fluid sample contained at simultaneous high-pressure temperature conditions.

In some instances it is not possible to collect meaningful CW or pulse-gated Raman spectra from a high temperature fluid. The background fluorescence intensity and lifetime can overcome our capabilities to detect a Raman signal. There are at least three possible techniques used to overcome this challenge: 1) collect Raman at two (ν_1, ν_2) slightly different pump frequencies ($\Delta\nu_{1,2}$ = a few cm^{-1}) and then difference the two recorded spectra, 2) conduct FT Raman measurements, and 3) conduct FTIR measurements. For a variety of reasons we chose to pursue option three. Our near-simultaneous Raman and Fourier transform infrared (FTIR) microscope was designed to accommodate long working distance and hot DACs (see Figure 7). A motorized rail permits rapid switching between probes. A Bruker® Optics Vector-33 interferometer is used as an IR glow bar source and data is collected via an external IR LN cooled CdTe detector. Raman fluorescence data is collected via a fiber optic channel and injected into a fast spectrograph and CCD detector. The nominal IR resolution is adjustable and typically we choose between 1 cm^{-1} or 4 cm^{-1} resolution. This instrument also has a sample visualization CCD camera that enables the user to confidently direct laser light onto the sample or a pressure sensor or to take still micrographs of a sample. Pressure is determined during melting and recrystallization studies by monitoring a calibrated optical pressure gauge such as the $SrB_4O_7:Sm2^+$ $\lambda_{0\text{-}0}$ line [96]

and/or the temperature-dependant ruby (Al_2O_3: $Cr3^+$) fluorescence line [95]. In the experiments discussed in this report we measure temperature using type-k thermocouples secured between the metal sample retaining gasket and a diamond anvil using gold foil. The thermocouple voltage is compared against calibrated and electronically set cold reference junctions. The differenced voltages are then converted to temperature. The precision of our temperature measurements is approximately 2 K.

We have used our FTIR/Raman instrument to successfully determine the chemical phase diagram of formic acid (Montgomery W., Zaug J. M., Howard W. M., Goncharov A. F., Crowhurst J. C., and Jeanloz R., *JPCB* **109**(41), 19443, (2005).), and nitromethane (unpublished work by Hart E., and Zaug J. M., 2004). Currently we are studying cyannuric acid, which is loosely considered to be an analogue material for TATB.

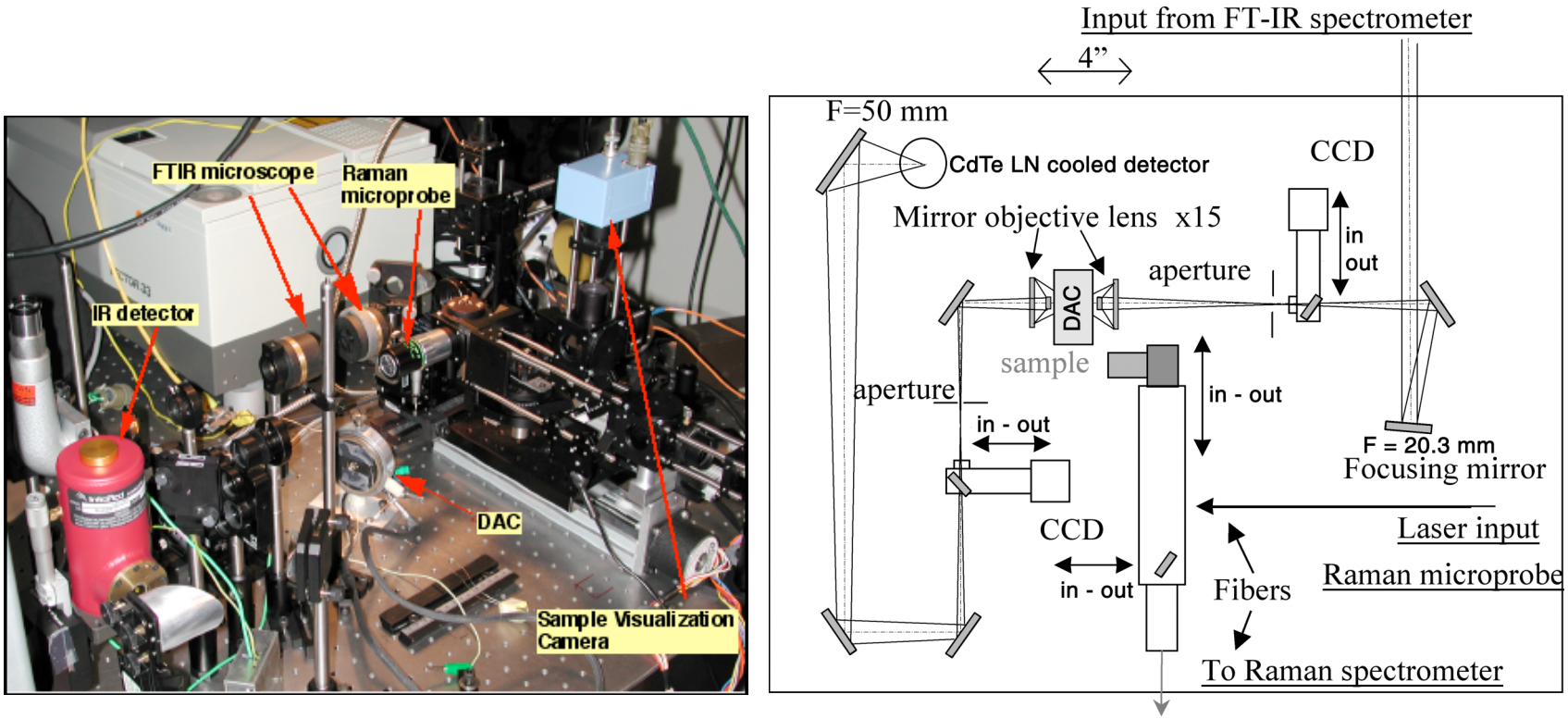

Figure 7. Raman/FTIR system. A custom designed vibrational spectroscopy instrument that accommodates a large variation of geometrically different diamond cells for both Raman and FTIR spectroscopy. For Raman, 488 nm or 514 nm CW light is injected into the instrument stage through a fiber optic cable. Spectra are collected in reflection geometry and coupled to a second fiber optic line that is fed into a spectrometer with a CCD array. The entire system can be rapidly switched over to FTIR data collection by use of a computer-interfaced motorized stage. A standard glow bar source housed in a Bruker® Vector 33 interferometer provides the near and mid IR source that is focused with a reflecting mirror into the DAC encapsulated sample. IR absorption data are collected in transmission with a second reflecting objective and focused into a CdTe detector. Care is taken to correctly aperture the IR light before and after the DAC. A minimum sample diameter of approximately 30 microns can be interrogated with this system. The microscope stage also includes a CCD camera to allow visual acuity of the DAC sample in either Raman or FTIR mode.

1.4 COMPUTATIONAL METHODS

We apply an accurate and numerically efficient equation of state for multiphase mixtures in the Cheetah thermochemical code to detonation, shocks, and static compression. The Cheetah thermochemical code is used to determine the properties of reacting energetic materials. We present a library of parameters for fluid and condensed high pressure molecules in Ref. [97]. We call this library "EXP6". Cheetah supports a wide range of elements and condensed detonation products. We have applied a Murnaghan [98] equation of state (EOS) form to a variety of metals, metal oxides and other solids. We have also matched experimental phase transition data for many of these solids. We have applied the EXP6 equation of state to numerous formulations containing the elements C, H, N, and O. We find that the EXP6 equation of state library improves significantly on previous equation of state libraries, without fitting to detonation properties. While there exists an extensive body of experimental techniques and experience on computational methods appropriate to ambient conditions, the regime of strong repulsive interactions at very high densities has not been as extensively investigated. The experiments discussed here are aimed both at enlarging the family of properties conveniently measured at high pressure and, principally, at providing data appropriate to develop Cheetah interatomic potentials. In this report we describe, in part, the experimental speeds of sound and computationally derived equations of state data of eighteen high-pressure fluids and mixtures including, methanol (CH_3OH), ethanol (C_2H_5OH), ethane (C_2H_6), propane (C_3H_8), heptane (C_7H_{16}), octane (C_8H_{18}), benzene (C_6H_6), water (H_2O), hydrogen chloride (HCl), formic acid (CH_2O_2), nitrogen (N_2), oxygen (O_2), argon (Ar), 50:50 w/w mixture of CH_3OH:C_2H_5OH, 50:50 molar mixture of N_2: O_2, 70:30 w/w mixture of H_2O:ammonia(NH_3), 63:37 w/w mixture of H_2O:HCl and a 49:51 w/w mixture of H_2O:hydrogen fluoride (HF). We find that these materials are present during the detonation of some common explosives. Ongoing experiments continue to improve the accuracy, versatility, and P-T range of our Cheetah thermochemical code.

The energy content of an energetic material often determines its practical utility. An accurate estimate of the energy content is essential in the design of new materials [99] and in the understanding of quantitative detonation tests [100]. The Cheetah thermochemical code is used to predict detonation performance for solid and liquid explosives. Cheetah solves thermodynamic equations between product species to find chemical equilibrium for a given pressure and temperature. The useful energy content is determined by the anticipated release mechanism. Since detonation events occur on a microsecond timeframe, any chemical reactions slower than this are not relevant when considering a detonation. Another way of looking at energy release mechanisms is through thermodynamic cycles. Detonation can be thought of as a cycle that transforms the unreacted explosive into stable product molecules (chemical equilibrium) at the Chapman-Jouguet state [101]. This is simply described as the slowest steady shock state that conserves mass, momentum, and energy. Similarly, the deflagration of a propellant converts the unreacted material into product molecules at constant enthalpy and pressure. Understanding

energy release in terms of thermodynamic cycles ignores the important question of the time scale of reaction. The kinetics of even simple molecules under high-pressure conditions is not well understood. Diamond anvil cell and shock experiments promise to provide insight into chemical reactivity under extreme conditions. Despite the importance of chemical kinetic rates, chemical equilibrium is often nearly achieved when energetic materials react. This is a consequence of the high temperatures produced by such reactions (up to 6000K). We will begin our discussion by examining thermodynamic cycle theory as applied to high explosive detonation. This is a current research topic because high explosives produce detonation products at extreme pressures and temperatures: up to 40 GPa and 6000K. Relatively little is known about material equations of state under these conditions. Nonetheless, shock experimentation on a wide range of materials has generated sufficient information to allow reasonably reliable thermodynamic modeling to proceed.

One of the attractive features of thermodynamic modeling is that it requires very little information regarding the unreacted energetic material under elevated conditions. The elemental composition, density, and heat of formation of the material are the only information needed. Since elemental composition is known once the material is specified, only density and heat of formation needs to be predicted. The Cheetah thermochemical code offers a general-purpose, easy to use, thermodynamic model for a wide range of materials.

Chapman-Jouguet (C-J) detonation theory [101] implies that the performance of an explosive is determined by thermodynamic states -the Chapman-Jouguet state and the connected adiabat. Thermochemical codes use thermodynamics to calculate these states, and hence obtain a prediction of explosive performance. The allowed thermodynamic states behind a shock are intersections of the Rayleigh line (expressing conservation of mass and momentum), and the shock Hugoniot (expressing conservation of energy). The C-J theory states that a stable detonation occurs when the Rayleigh line is tangent to the shock Hugoniot. This point of tangency can be determined, assuming that the equation of state P = P(V,E) of the products is known. The chemical composition of the products changes with the thermodynamic state, so thermochemical codes must simultaneously solve for state variables and chemical concentrations. This problem is relatively straightforward, given that the equation of state of the fluid and solid products is known.

One of the most difficult parts of this problem is accurately describing the equation of state of the fluid components. Efforts to achieve better equations of state have largely been based on the concept of model potentials. With model potentials, molecules interact via idealized spherical pair potentials. Statistical mechanics is then employed to calculate the equation of state of the interacting mixture of effective spherical particles. Most often, the exponential-6 potential is used for the pair interactions:

$$V(r) = \frac{\varepsilon}{\alpha - 6}\left[6\exp(\alpha - \alpha r / r_m) - \alpha (r_m / r)^6\right] \tag{3}$$

where, r is the distance between particles. r_m is the minimum of the potential well. ε is the well depth, and α is the softness of the potential well.

The JCZ3 EOS was the first successful model based on a pair potential that was applied to detonation [102]. This EOS was based on fitting Monte Carlo simulation data to an analytic functional form. Hobbs and Baer [103] have recently reported a JCZ3 parameter set called JCZS

The exponential-6 model is not well suited to molecules with a large dipole moment. Ree [104] has used a temperature-dependent well depth $\varepsilon(T)$ in the exponential-6 potential to model polar fluids and fluid phase separations. Fried and Howard have developed an effective cluster model for HF [98]. The effective cluster model is valid to lower temperatures than the variable well-depth model, but it employs two more adjustable parameters.

Many materials produce large quantities of solid products upon detonation. The most common solid detonation product is carbon, although some explosives produce aluminum and aluminum oxide [105]. Uncertainties in the equation of state and phase diagram of carbon remain a major issue in the thermochemical modeling of detonation. van Thiel and Ree have proposed an accurate Mie-Gruneisen equation of state for carbon [106]. Fried and Howard [107] have developed a simple modified Murnaghan equation of state for carbon that matches recent experimental data on the melting line of graphite. There is considerable uncertainty regarding the melting line of diamond. Fried and Howard argue based on reanalysis of shock data that the melting line of diamond should have a greater slope. Shaw and Johnson have derived a model for carbon clustering in detonation [108]. Viecelli and Ree have derived a carbon-clustering model for use in hydrodynamic calculations [109, 110].

In the present approach, we apply an accurate and numerically efficient equation of state for the exp-6 fluid based on Zerah and Hansen's hypernetted-mean spherical approximation (HMSA) [111] equations and Monte Carlo calculations to detonation, shocks, and static compression. Thermal effects in the EOS are included through the dependence of the coefficient of thermal expansion on temperature, which can be directly compared to experiment. We find that we can replicate shock Hugoniot and isothermal compression data for a wide variety of solids with this simple form.

The exp-6 potential has also proved successful in modeling chemical equilibrium at the high pressures and temperatures characteristic of detonation. However, in order to calibrate the parameters for such models, it is necessary to have experimental data for molecules and mixtures of molecular species at high temperature and pressure. Static compression data, as well as sound speed measurements, provide important data for these models. We validate Cheetah through several independent means. We consider the shock Hugoniots of liquids and solids in the "decomposition regime" where thermochemical equilibrium is established. We argue that this regime is reached for most organic materials above 50 GPa shock pressures. We also validate the code against high explosive overdriven shock Hugoniots, and more traditional metrics such as the detonation velocity and pressure. Overall, we find that Cheetah offers a highly accurate representation of high-pressure equation of state properties with no empirical fitting to detonation data.

The nature of the Chapman-Jouguet and other special thermodynamic states important to energetic materials is strongly influenced by the equation of state of stable detonation products. Cheetah can predict the properties of this state. From these properties and elementary detonation theory the detonation velocity and other performance indicators are computed. Thermodynamic equilibrium is found by balancing chemical potentials, where the chemical potentials of condensed species are just functions of pressure and temperature, while the potentials of gaseous species also depend on concentrations. In order to solve for the chemical potentials, it is necessary to know the pressure-volume relations for species that are important products in detonation

We now specify the equation of state used to model detonation products. For the ideal gas portion of the Helmholtz free energy, we use a polyatomic model including electronic, vibrational, and rotational states. Such a model can be conveniently expressed in terms of the heat of formation, standard entropy, and constant pressure heat capacity of each species. The heat capacities of many product species have been calculated by a direct sum over experimental electronic, vibrational, and rotational states. These calculations were performed to extend the heat capacity model beyond the 6000K upper limit used in the JANAF thermochemical tables (J. Phys. Chem. Ref. Data, Vol. 14, Suppl. 1, 1985). Chebyshev polynomials, which accurately reproduce heat capacities, were generated.

Experimental observables were placed into categories. We took the first category to be the volume along the shock Hugoniot and reshocked states. The second was the temperature along the shock Hugoniot and reshocked states. The third was the volume under static compression. The last category was the sound speed under static compression. For each category, we determined an average error.

The figure of merit is a weighted average of the category errors. We nominally assign a weight of 40% to shock volumes, 25% to shock temperatures, 25% to static volumes, and 10% to the speed of sound. Depending on the degree of chemical reactivity the optimization procedure is weighted more to shocks than static measurements, although we find below that we reproduce both well. A stochastic optimization algorithm was employed to minimize the figure of merit function. Our final parameters are listed in Ref. [97]. In the following subsections we analyze the performance of the resulting equation of state in reproducing a wide range of experimental measurements. Results for nitrogen are fully discussed in [111]. Although the parameters in that work are slightly different than those used here, the comparison to experiment is similar.

Other workers [112, 113] have shown that a chemical equilibrium model of hydrocarbons based on an exponential-6 fluid model using Ross's soft-sphere perturbation theory is successful in reproducing the behavior of shocked hydrocarbons. Our model of the supercritical phase includes the species H_2, CH_4, C_2H_6, and C_2H_4. We have chosen model parameters to match both static compression isotherms and shock measurements wherever possible. The ability to computationally match multiple types of experiments over expansive P-T conditions provides evidence in the general applicability of our experimental-theoretical approach and our high-pressure equations of state model.

2.0 FLUID EQUATIONS OF STATE AND PHASE DIAGRAMS

Speeds of sound measurements were made using ISLS and ISLS-SPE methods on a combination of eighteen different fluids and fluid mixtures contained at GPa pressures along isotherms ranging from of 295K to 700K. These results have been used to further develop the EXP6 library component of the Cheetah thermochemical code. We have also performed high pressure Raman experiments to learn more about the interatomic surfaces of nitrogen and hydrogen. In addition the chemical and physical phase stability of supercritical fluids has been determined using FTIR, Raman and ISLS techniques. These experiments have also served to improve the Cheeath code. Lastly we have begun to build a precise cubic boron nitride Raman pressure calibration scale that will be used to increase the precision of our previous and future SoS studies of highly corrosive or chemically reactive fluids and fluid mixtures.

2.1 FLUID SPEEDS OF SOUND AND EQUATIONS OF STATE

The experimental SoS and Cheetah derived EoS data for each fluid component will be presented below along with significantly relevant experimental information. For the sake of completeness some of additional experimental data used to develop each EXP6 fluid component will also be provided.

2.1.1 Argon

Argon does not absorb 1-micron light so we used our newly developed ISLS-SPE method to successfully measure the SoS of argon up to 5 GPa and 673K. The SRB pressure sensor was used and we also collected Raman data on annealed cBN in order to develop a precise scale. The Cheetah argon EXP6 library does not currently include this recently collected data. The ambient temperature ultrasonic, data plotted in figure 8, extends to the freezing pressure and it is taken from Kortbeek et al., *RSI* **56**(6), 1269, (1985).

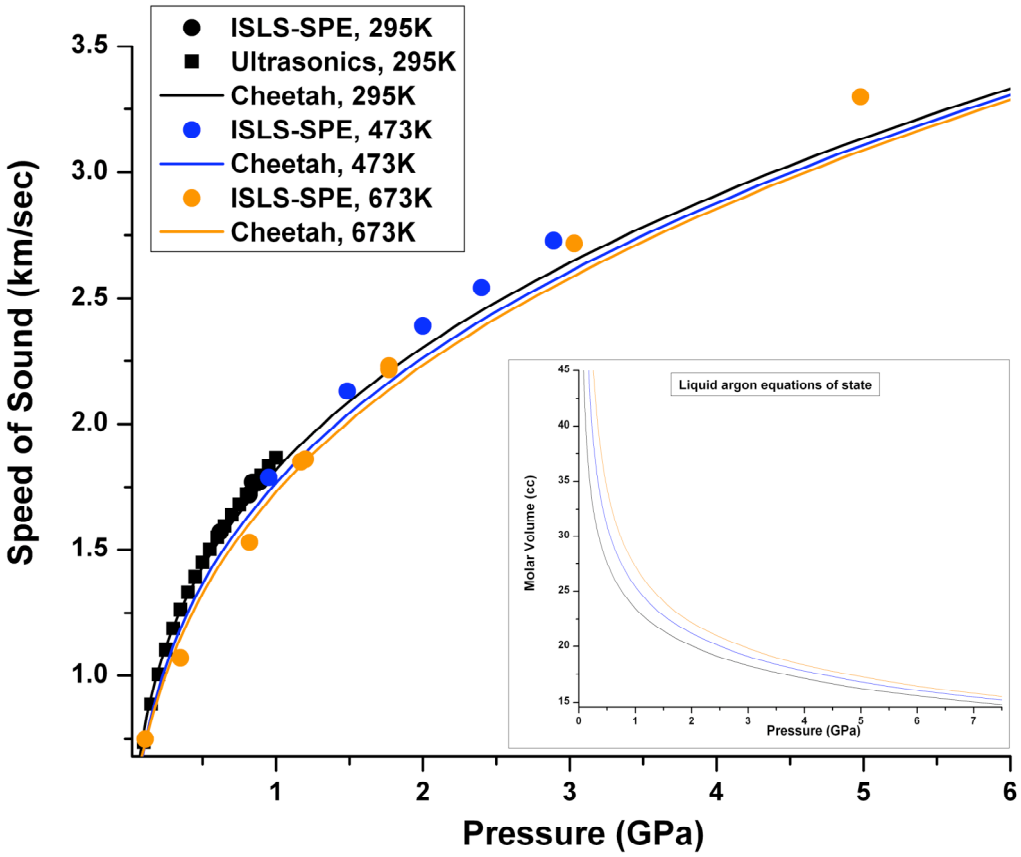

Figure 8. Argon SoS and EoS.

2.1.2 Nitrogen

Nitrogen also does not absorb 1-micron light so again we used our newly developed ISLS-SPE method to successfully measure the SoS of nitrogen up to 5.5 GPa at 473K. The SRB pressure sensor was used. The Cheetah nitrogen EXP6 library does not currently include this recently collected data set. It is striking to note that although the Cheetah N_2 EXP6 parameters are grounded principally on shock wave data it still quite reasonably fits our off-Hugoniot DAC SoS measurements. In part this is because nitrogen is a simple fluid that is thermodynamically stable over the entire range of measured shock wave and ISLS-SPE pressure temperature conditions.

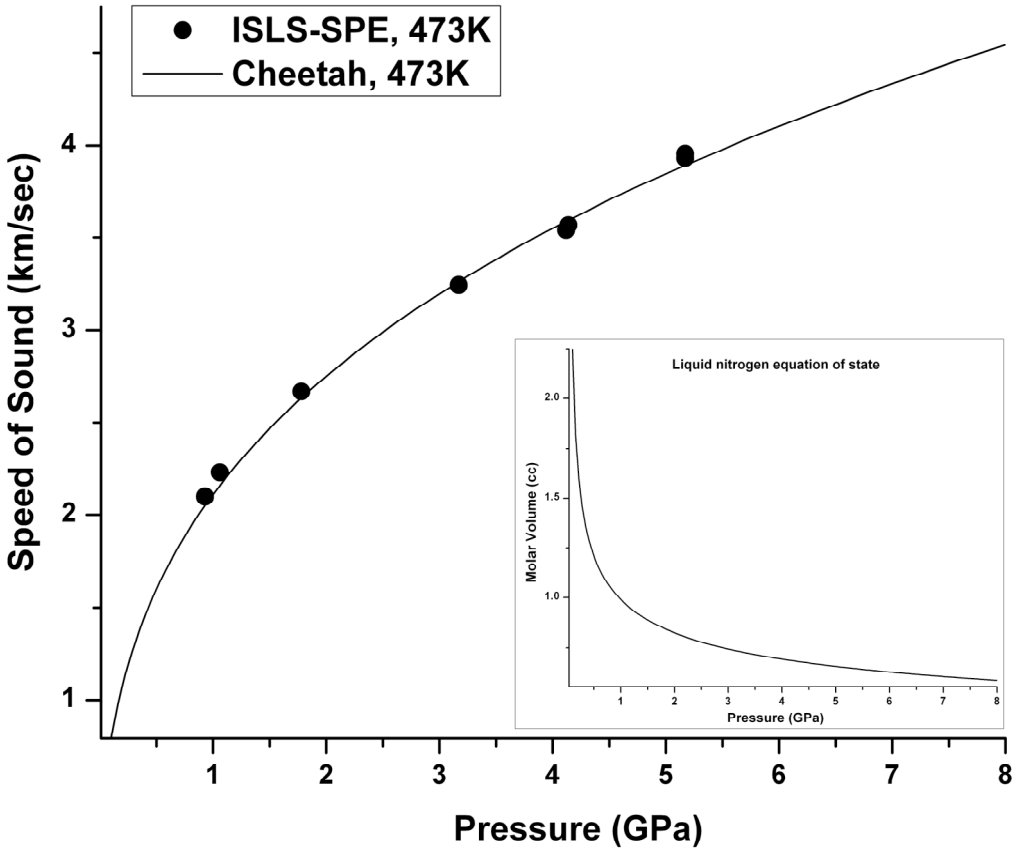

Figure 9. Nitrogen SoS and EoS.

2.1.3 Oxygen and a 50:50 molar mixture of nitrogen with oxygen

Oxygen is an exceptionally good optical absorber of 1-micron light. In this study, we collaborated with our university of Washington colleagues to use the ISLS method to measure the SoS of oxygen up to 11 GPa at 473K [118]. The ruby pressure sensor was used. The Cheetah oxygen EXP6 library was developed using our data. We also measured SoS velocities from a 50:50 molar mixture of N_2 + O_2 along a 250° C isotherm. (See Figure 11a.) In the case of oxygen

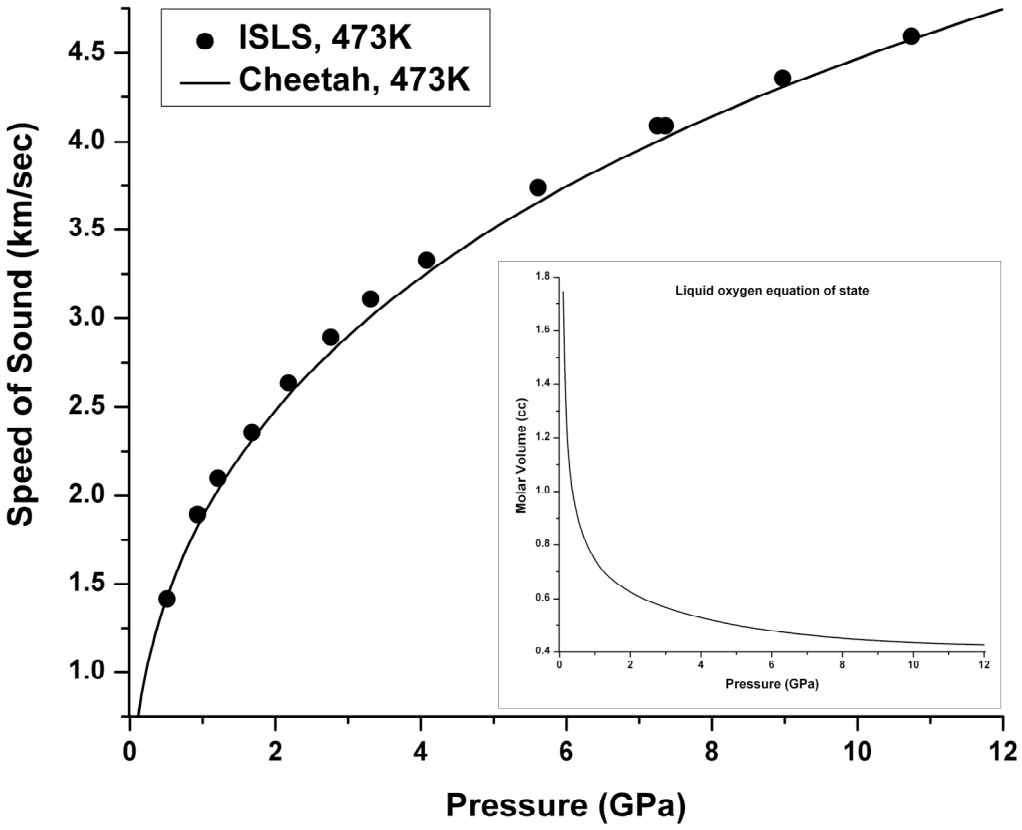

Figure 10. Oxygen SoS and EoS.

We independently determined the equation of state using known values of density, ρ, and specific heat, C_P. The thermodynamic equation of state is then calculated by recursive numerical integration of

$$\left(\frac{\partial \rho}{\partial P}\right)_T = (c_o)^{-2} + \left(\frac{\partial^2 T}{\partial C_P}\right) \text{ and } \left(\frac{\partial C_P}{\partial P}\right)_T = \left(\frac{\partial^2 V}{\partial T^2}\right)_P \quad (4)$$

where P, c_o, α, T, and V are respectively the pressure, zero frequency sound speed, thermal expansion coefficient, absolute temperature, and specific volume. In this work, initial values of ρ and C_P were taken from the EOS of Wagner *et al*. [132].

An overview of previous work on oxygen is given by Wagner and Schmidt (W&S) [132]. These authors have generated a thermodynamic potential based on experimental densities up to 0.08 GPa and at 130° C up to 0.03 GPa. In addition, they used combined density and heat capacities measured to 30° C and 0.03 GPa. Other data, not used by Wagner and Schmidt, are those of Tsiklis and Kulikova [133] who measured densities to 1 GPa and 400° C. The latter were used above 0.2 GPa by Belonoshko and Saxena (B&S) [134] to constrain a molecular dynamics simulation (based on an exponential-6 potential), which was in turn used to construct a P-V-T surface. A Shock Hugoniot for the 1:1 fluid mixture provides P-V-E data between 9.89 and 24.0 GPa [135].

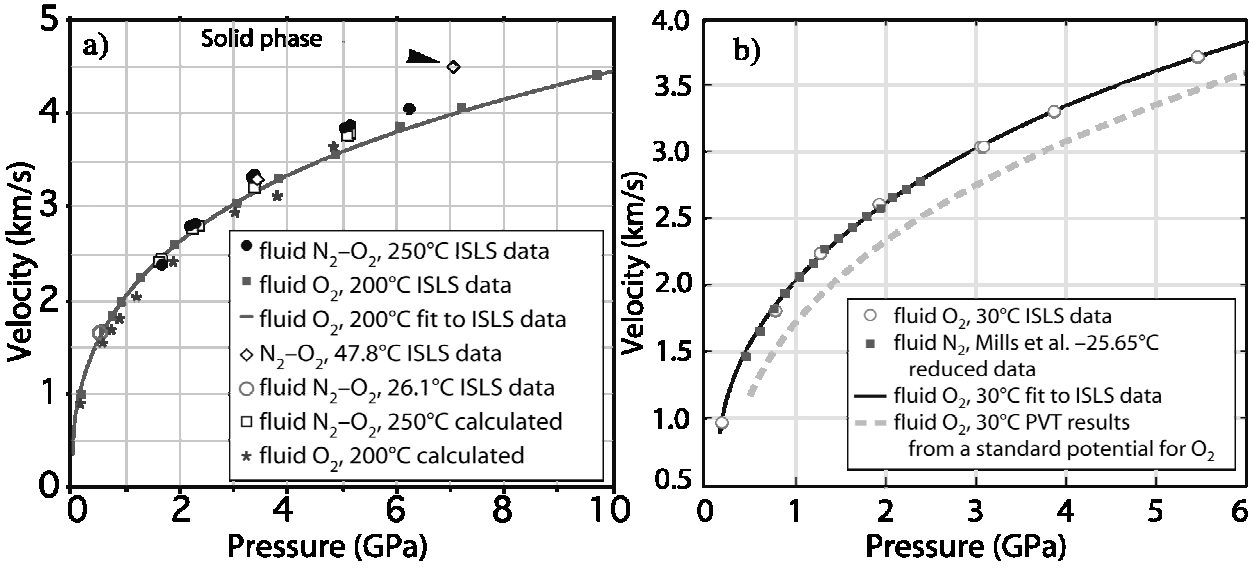

Figure 11. (a) ISLS sound speed data and corresponding calculations for oxygen and 1:1 molar ratio of fluid oxygen to nitrogen. (b) Example of the law of corresponding states for O_2 and N_2. The N_2 data [137] are reduced by the critical pressure, temperature and density and compared against ISLS O_2 data at 30˚ C [118]. The dashed line is a molecular dynamic result using a standard potential [134]. For O_2, a C_p at low pressure, where reasonably known, was used to start the integration necessary to generate the sound speeds.

The data presented here are currently insufficient to make a "positive" determination of the equation of state of O_2 from strictly thermodynamic principals. The high-pressure sound speed data, especially at higher temperatures, do not extend to the lower pressures at which values for C_p and ρ, are known. Further, the small variations in speed of sound within the experimentally useful range of temperatures used here are small enough to be confounded with the uncertainties

in the measurements of pressure. Consequently, several approximations have been made to yield a reasonably accurate EOS. The results are then compared with other data.

The assumptions made are that the sound speeds are linear in T over the stated range, that the W&S EOS correctly predicts the speeds up to 0.5 GPa, and that the form of the interpolating function is suitable to the task. At pressures higher than 0.7 GPa the speeds are assumed to vary linearly between 30° and 200° C, and an artificial data set is calculated at six temperatures from 30° to 100° C, based on the previous fits at the two stated end temperatures. Each isotherm is then fit individually, with the fits forced to conform to the W&S EOS for pressures between 0.02 and 0.05 GPa. The result is a velocity field in P and T in which the velocities are linear interpolations in T above 0.7 GPa, fairing into the W&S EOS below that. The usual equations are then iteratively solved to obtain the densities, heat capacities, entropies, etc. The results are reasonable, the densities increasing monotonically while remaining below those of the β phase. The heat capacities, C_P, are fairly constant in pressure, varying by at most 5% for each isotherm. They undergo several oscillations with increasing pressure, which probably derive from the cross over of dc/dT from a positive to a negative value at 0.5 g/cm^3.

At 30° C the O_2 densities determined here are 8% higher than the B&S results up to 0.5 GPa, then cross at about 1.5 GPa and are then uniformly lower than B&S, by 10% at 6 GPa. B&S densities are, however, always less than that of the solid, β phase. Given reasonable values of C_P (at 0.5 GPa), either from W&S results or those determined here, the speeds of sound inferred from the B&S EOS are uniformly low by about 10% (refer to Figure 11a). In comparison, this discrepancy is due to their higher compressibility below ~4 GPa and higher density above 2 GPa. In order to make their speeds of sound agree (approximately) with results here at 30° C it is necessary to assume an initial C_P at 0.5 GPa of 9.2 J/K/mole at 30° C which is about 5 times lower than expected.

Speeds of sound were measured at 30° C and 1.5 GPa at frequencies of 1.3, 0.77 and 0.27 GHz. Velocities matched to within the uncertainties, *i.e.* ±0.2% for the higher frequency and ±0.5% for the two lowest. The ISLS velocities fair nicely with those of the W&S model and are lower than the extrapolation of W&S. More dispersion may exist at lower frequencies. Between 22° C and 122° C the fluid β-phase boundary is well fit by the straight line P(GPa) = 0.0270 T(° C) + 5.153 with a two σ uncertainty on the slope of 10^{-4} GPa/° C. Each point of equilibrium was established by a visual observation of the simultaneous presence of both phases. Among observations, the volume of solid varied from approximately 5 to 95% of the sample; no correlation was apparent between the deviations of the data from the fit and the fraction of solid. Since one expects that any impurities will be concentrated in the fluid, this fact suggests strongly that impurities had no significant effect on the measurements

The measured oxygen velocities fit well to the form $\Sigma A_i \ln P^i$ with $i=\{0...4\}$. The 30° → 200° C fit parameters are A_0=2.0438→1.8665, A_1=0.7764→0.8462, A_2=0.1040→0.140, A_3=0.0078 → -0.0020, and A_4=0.0010 → -0.0016. In such fits the data were supplemented by data points at lower pressures generated from the W&S EOS. Additionally, the curve at 30° C was constrained to lie along the 200° C isotherm above 7 GPa. N_2-O_2 fit parameters from 1.3 to 6.5 GPa at 250° C are

A_0=2.0058, A_1=0.4490, A_2=0.8424, A_3= -0.2605, and A_4= -0.0015. A 1:1 molar ratio of N_2-O_2 at 25° C forms δ-N_2 at approximately 4.3 GPa [136], which accounts for the significant increase in velocity observed at 7.1 GPa. The calculated points in Figure 11a were derived from an accurate EOS for exp-6 type fluids [111] based on HSMA integral equation theory and Monte Carlo calculations. Figure 12 presents the Cheetah derived SoS and EoS for the N2:O2 mixture.

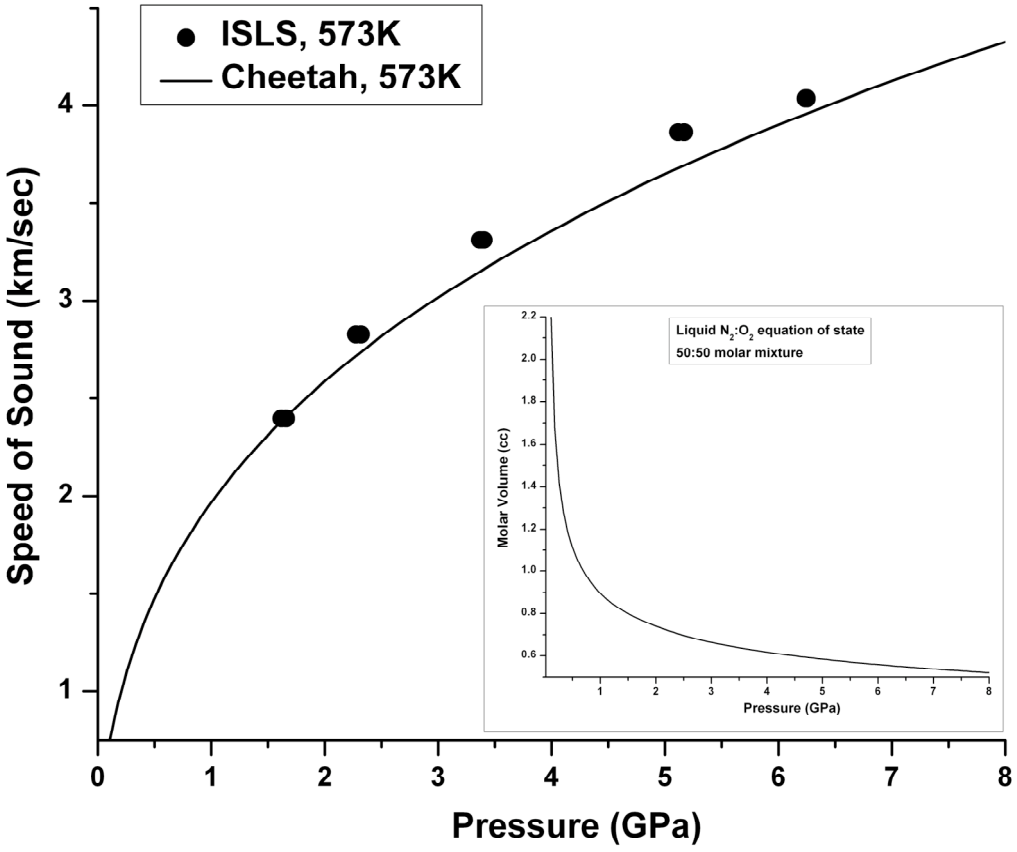

Figure 12. The SoS and EoS of a 50:50 molar ratio of N_2 + O_2.

According to simple theories, substances should behave the same when all variables are suitably scaled and the critical parameters are the most common scaling factors chosen. Figure 4b shows Mills et al. [137] –25.5° C data, which is equivalent to oxygen at 30° C when scaling by the critical temperatures. The N_2 sound speeds are reduced using critical pressures and densities.

$$c_{O_2}(equivlent) = c_{N_2} \frac{\sqrt{\frac{P_c(O_2)}{P_c(N_2)}}}{\sqrt{\frac{Mw(O_2)}{Mw(N_2)}} * \sqrt{\frac{\rho_c(O_2)}{\rho_c(N_2)}}} \tag{5}$$

Since O_2 and N_2 have the exact same compressibility factor (P_cV_c / RT_c=0.292), and no dipole moment, it may not be too much of a surprise that the sound speeds correlate well (figure 11b) with the empirical law of corresponding states. This result suggests that N_2 and O_2 molecules are approximately spherical up to 2.2GPa.

2.1.4 Methanol

Methanol is a reasonably good absorber of 1-micron light below approximately 25 GPa. Using the ISLS method and the ruby fluorescence pressure scale we measured the SoS of methanol along the 523K isotherm. Methanol was the first sample studied using the ISLS method at LLNL. The original laser technology used was much less efficient and prone to laser-heating samples during SoS measurement cycles. We did not have an embedded Raman system and so we measured the velocity of methanol after heating to compared against previous measurements of uncooked methanol. The process was excruciatingly slow as we were heating DAC samples in a vacuum furnace. Temperature equilibration took many hours to satisfactorily obtain. Still we observed no appreciable velocity differences between heated and unheated data sets. A methanol model was previously implemented in the Cheetah code. The model is now based on a combination of shock Hugoniot data and sound speeds determined via ISLS.

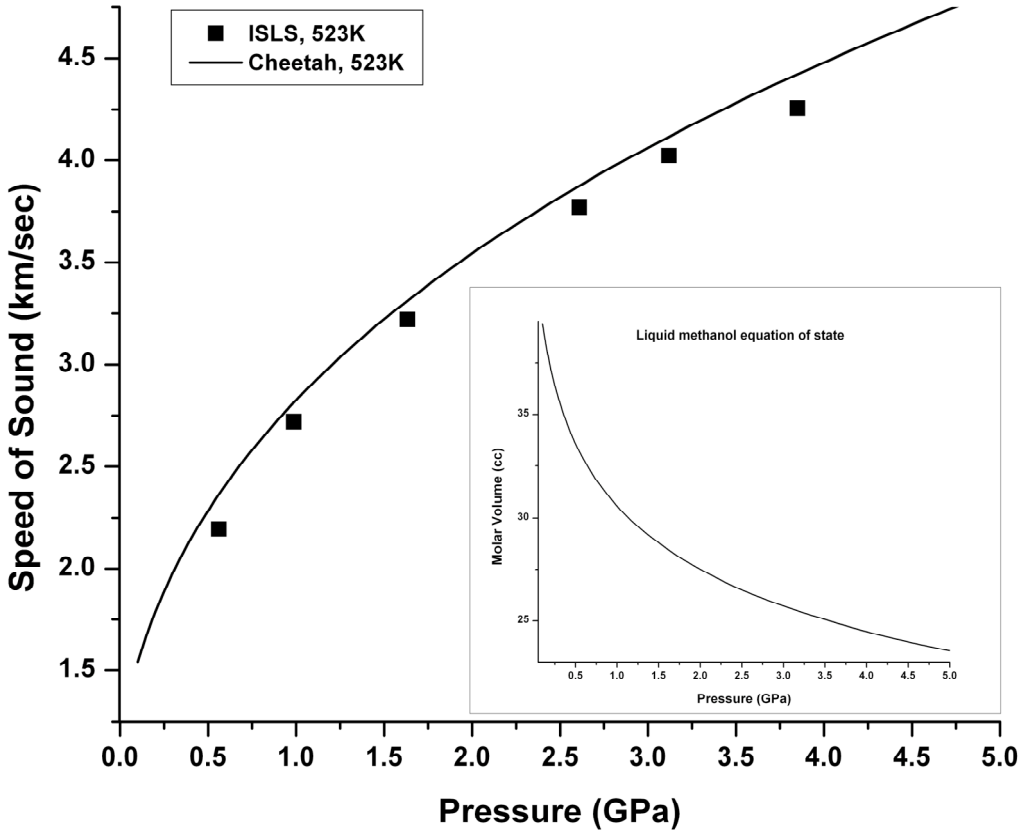

Figure 13. The SoS and EoS of methanol.

2.1.5 Ethanol

Like methanol, ethanol is a reasonably good absorber of 1-micron light and hence amenable to the ISLS technique. We synthesized our own SRB and now used its more precise and virtually temperature independent pressure scale. We used our own modified temperature correction curve for SRB (A maximum correction of -0.1 GPa is required at 573K!). Unlike in methanol we observed that ethanol would chemically attack SRB at or above 573K. A Cheetah exponential-6 potential model was parameterized to the ISLS measurements. The maximum 3% difference between data sets shows the utility of Cheetah and its ability to match well to both shock and static measurements.

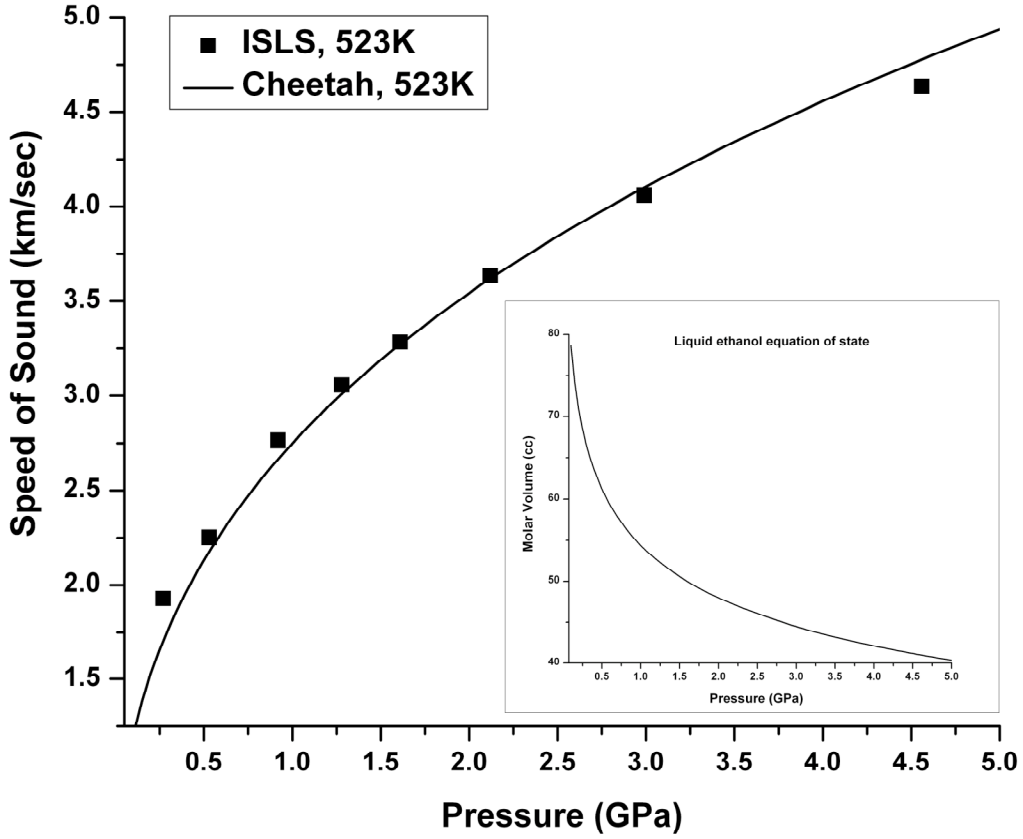

Figure 14. The SoS and EoS of ethanol.

2.1.6 50:50 volumetric mixture of methanol with ethanol

The Cheetah thermochemical code uses assumptions about the interactions of unlike molecules to determine the equation of state of a mixture. The accuracy of these assumptions is a crucial issue in the further development of the Cheetah code. We have tested the equation of state of a mixture of methanol and ethanol in order to determine the accuracy of Cheetah's mixture model. Cheetah uses an extended Lorenz-Berthelot mixture approximation [138] to determine the interaction potential between unlike species from that of like molecules:

$$\varepsilon_{ij} = \sqrt{\varepsilon_{ii}\,\varepsilon_{jj}}$$
$$r_{m,ij} = \kappa_{ij}(r_{m,ii} + r_{m,jj})/2 \qquad (6)$$
$$\alpha_{ij} = \sqrt{\alpha_{ii}\,\alpha_{jj}}$$

where, ε is the attractive well depth between two molecules and r_m is the distance of maximum attraction between two molecules. The parameter α controls the steepness of the repulsive interactions and κ is a non-additive parameter, typically equal to unity.

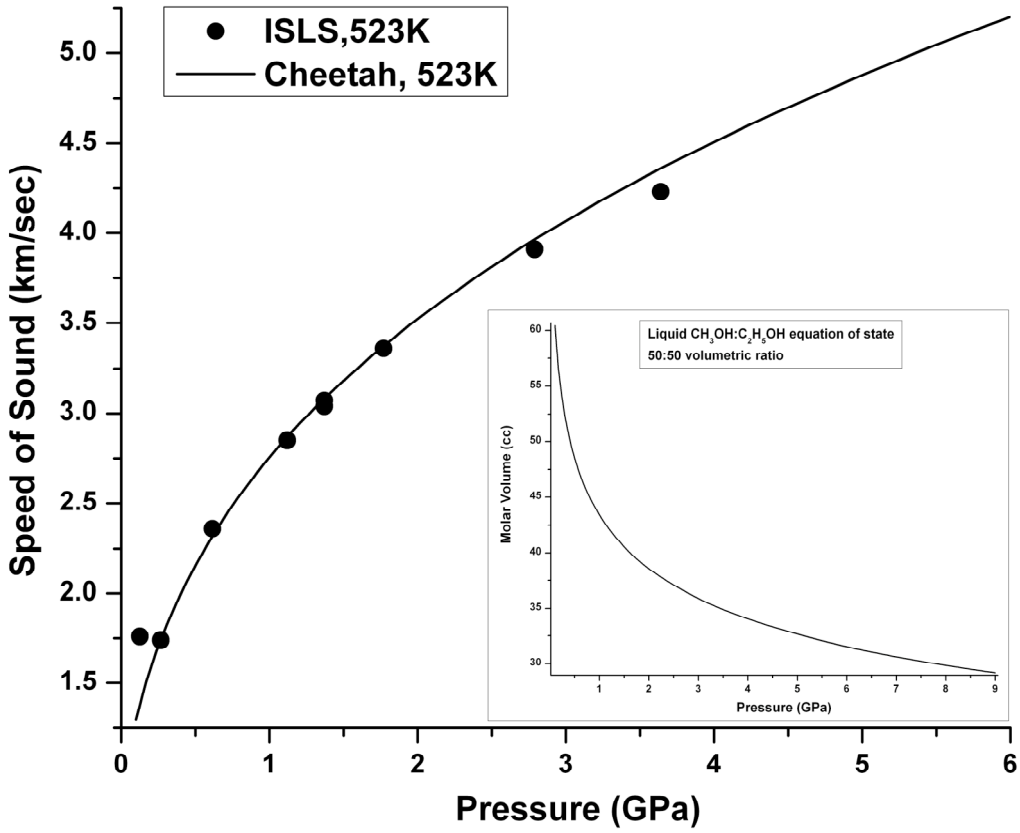

Figure 15. The SoS and EoS of a 50:50 volumetric ratio of methanol with ethanol.

The original comparison between "uncorrected" Cheetah results and ISLS data were essentially perfect [125]. The current beta version 5.0 of Cheetah greatly extends the predictive P-T range for alcohols. Even so, the agreement demonstrated in figure 15 at least partially validates the assumptions used in the Cheeath mixture rules.

2.1.7 Ethane

We found that the lighter hydrocarbons do not couple well to 1-micron light and so for these we used our new ISLS-SPE technique to generate and measure SoSs. The SRB pressure scale was used since it has a high (±0.03 GPa) precision. Ethane is the most recent sample we have studied and so a complete series of isotherms remains a work in progress. Figure 16 compares our measurements to highly accurate (<0.1% error) MHz transducer ultrasonic measurements taken from Younglove B.A., and Ely J. F., *JPCRD* **16**(4), 577-798 (1987). The Cheetah curve was constructed from ultrasonic and thermodynamic data sets prior to our measurements.

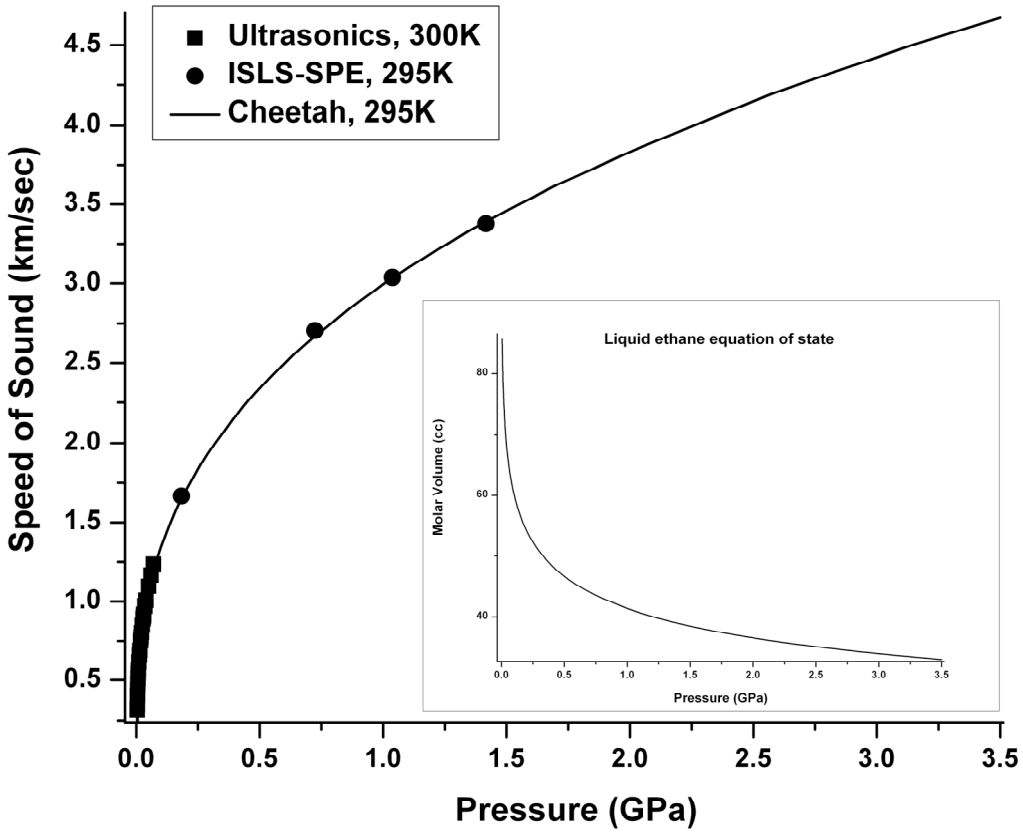

Figure 16. The SoS and EoS of ethane.

2.1.8 Propane

Propane was studied using the ISLS-SPE technique. The optical SRB pressure sensor and scale were used to determine pressure. We conducted measurements along three isotherms. The temperature effect to measured SoSs is apparent. Above approximately 3.5 GPa it appears that the SoS velocities depend very weakly on temperature. Here the Cheetah curve was based completely on one dubious ultrasonic study. Recently we discovered a more accurate ultrasonic study published in a foreign journal. The ultrasonic data shown in figure 17 were taken from Lacam A., *J. Rech Centre National Recherche Scientifique* **34**, 25-56 (1956). The EXP6 Cheetah model for propane is in the process of being updated using the French ultrasonic and ISLS-SPE data sets.

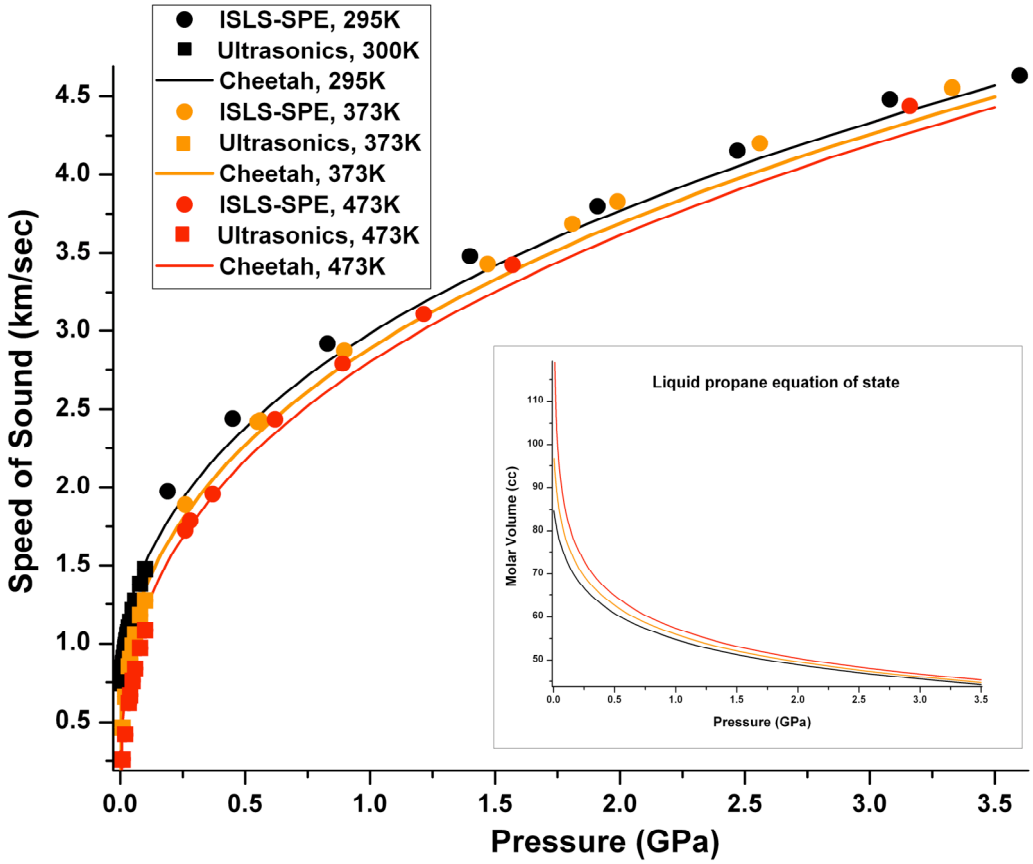

Figure 17. The SoS and EoS of propane.

2.1.9 Heptane

We found that heptane would couple to 1-micron light and so we were able to use the ISLS technique. In fact our heptane SoS study was conducted well before we discovered the ISLS-SPE process in May of 2006. The SRB sensor and scale were used to determine pressure. The EXP6 Cheetah parameters were fit exclusively to our ISLS results. Recently we found an accurate ultrasonics study published from the Netherlands group. The ultrasonic data plotted in figure 18 were taken from Muringer M. J. P., Trappeniers N. J. and Biswas S. N., *Phys. Chem. Liq.* **14**, 273-296 (1985). The 373K ultrasonic results came from extrapolation of Muringer et al. results, under the assumption that a linear velocity dependence on temperature is valid 63K above their 310K results. The Cheetah results at 298K indicate there is a need to further develop the propane EXP6 parameters. Muringer et al. results plus more ISLS data will resolve this issue.

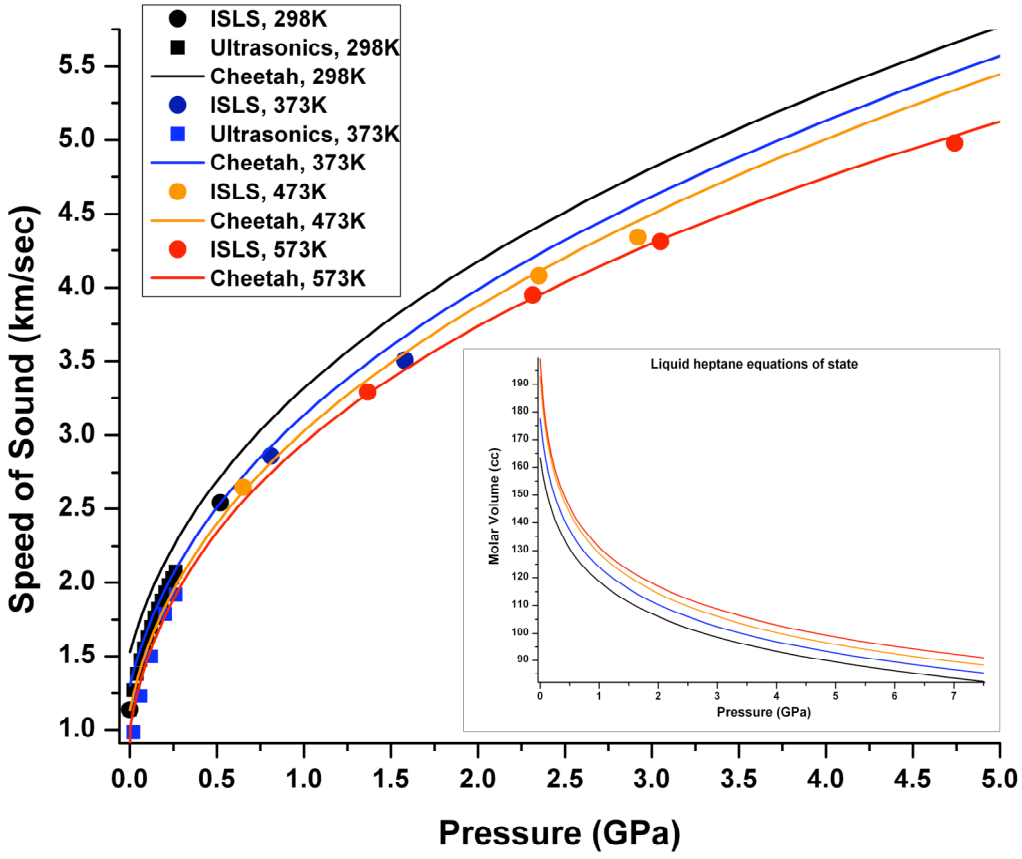

Figure 18. The SoS and EoS of heptane.

2.1.10 Octane

Octane was the first hydrocarbon studied using the ISLS technique. Under ambient conditions it is a liquid and hence easily loaded into a DAC. We used the SRB sensor and scale to determine pressure. Previously the EXP6 octane parameters were determined through matching to shock wave results. Our ISLS results were later used to ground the low P-T region of the potential surface. Recently we found two ultrasonic papers that may also help to develop the octane model. Figure 19 gives a comparison between ISLS, ultrasonics, and Cheetah results. The 298K ultrasonic data were taken from Ding Z. S., Alliez J., Boned C., and Xans P., Meas. Sci. Technol. 8, 154-161 (1997) and the 363K data were taken from an interpolation of J. W. M. Boelhouwer's paper found in *Physica* **34**, 484-492 (1967).

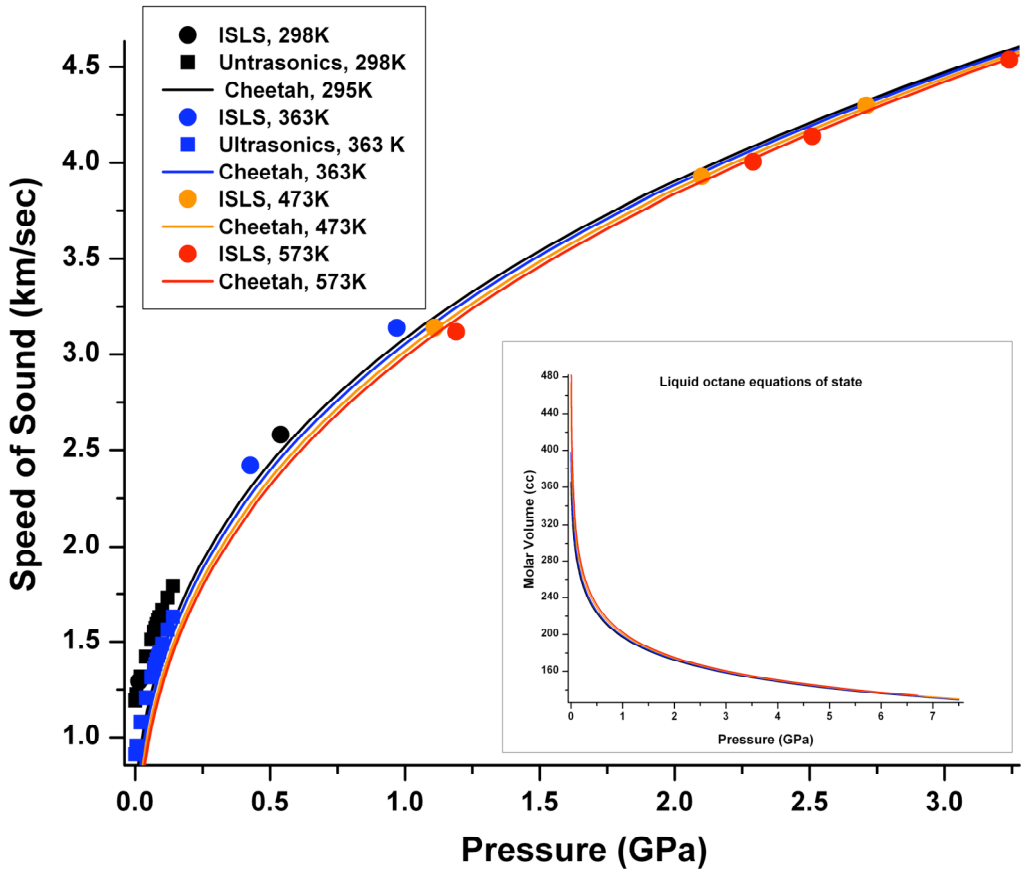

Figure 19. The SoS and EoS of octane.

2.1.11 Benzene

Benzene was the first high-pressure liquid-state ringed system to be studied using the ISLS technique. The melting curve of benzene is very steep and begins at 0.07 GPa at ambient temperature. It is then no surprise to see that the Cheetah model, developed for supercritical fluids, fails to match well to solid-state benzene. The ISLS data is a bit sparse but it is the only high-pressure static data available to help parameterize the EXP6 benzene model. Previously the model was fixed only to shock wave results. The recently found ultrasonic results plotted in figure 20 were taken from the Japanese group Takagi T. et al., *J. Chem. Thermodynamics* **36**, 659-664 (2004) and the Netherlands group Sun T. F., et al., *Phys. Chem. Liq.* **16**, 163-178 (1987). Takagi's results extend only to 0.03 GPa and Sun's results extend to the freezing pressure. During our ISLS measurements we observed that above 573K the benzene would fluoresce. Now that we have a sophisticated Raman system embedded into our ISLS instrument it would be worthwhile to conduct more definitive benzene measurements.

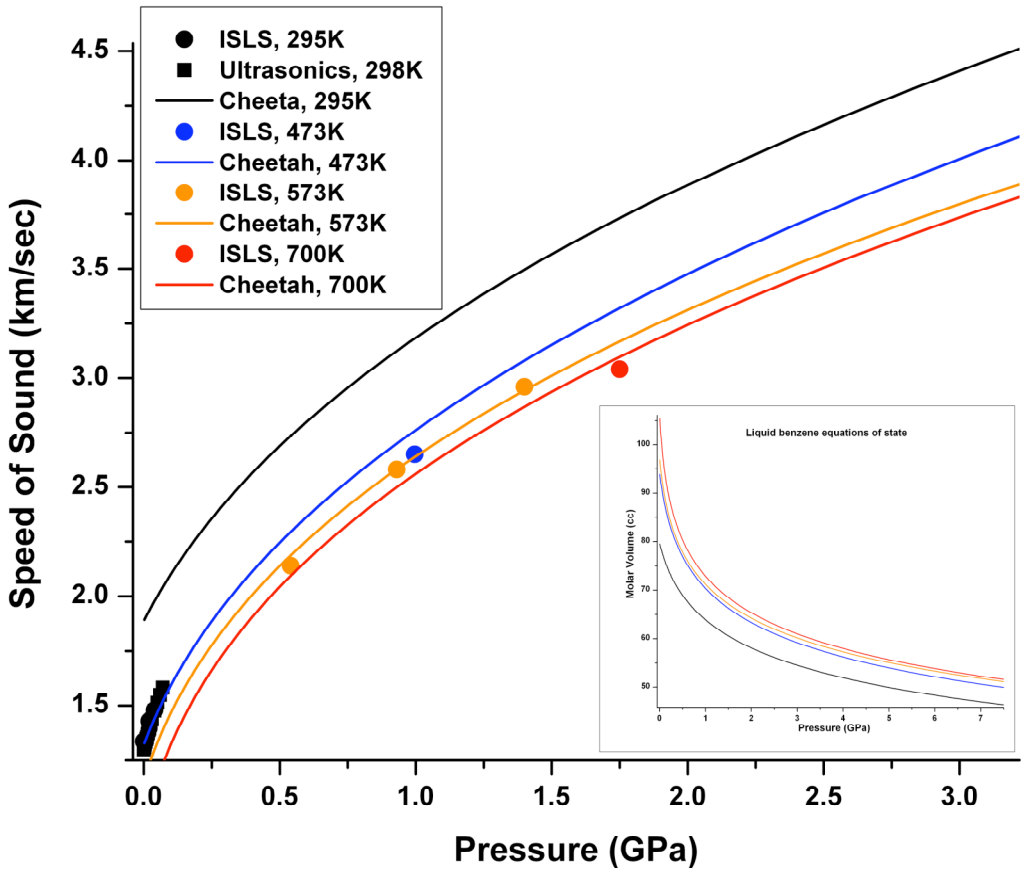

Figure 20. The SoS and EoS of benzene.

2.1.12 Pure formic acid

Inconsistent ISLS results on high P-T formic acid led to our initial suspicion that its 2D chemical phase stability region was relatively small. A definitive FTIR study later proved this to be true [129]. We thus conducted an ISLS measurement at as high of a temperature possible in a period of time where we knew reaction product formation would be negligible. Figure 21 shows the only known high-pressure static compression SoS data on formic acid. The EXP6 Cheetah model was parameterized to both shock wave and ISLS data. The near perfect fit is one more example of the versatility of our semi-empirical thermochemical model.

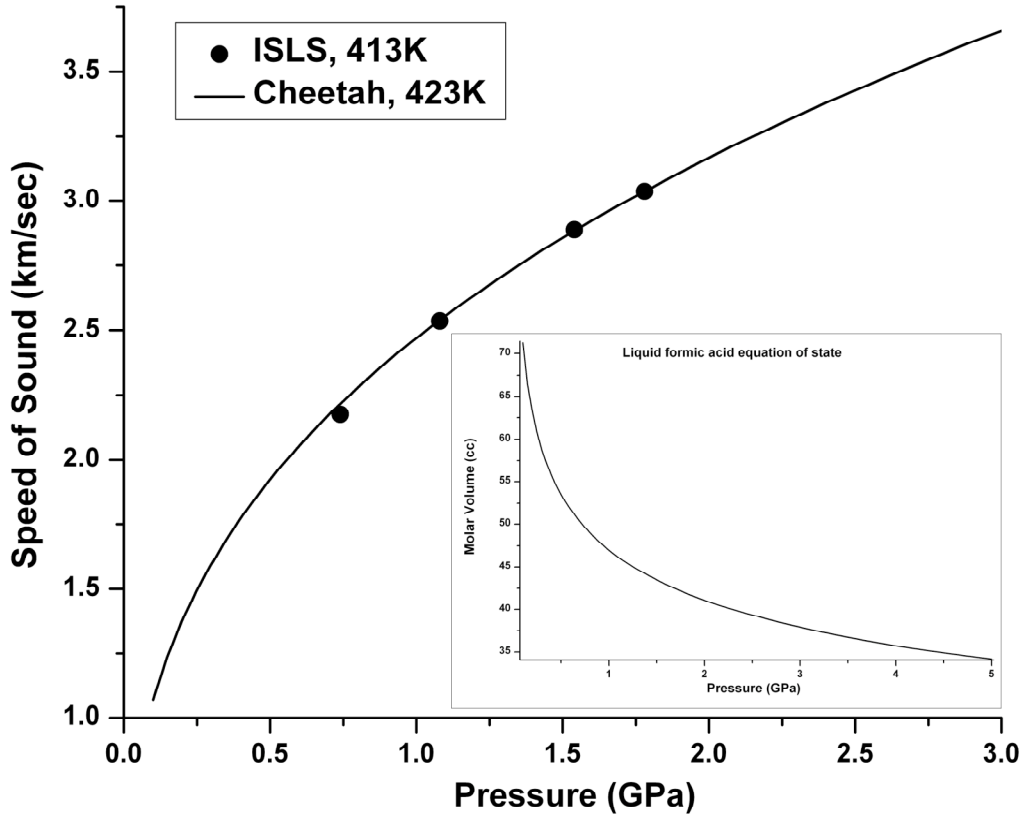

Figure 21. The SoS and EoS of pure formic acid.

2.1.13 Pure hydrogen chloride

We began a study of liquid HCl in early 2004. Unfortunately we could only conduct two measurements before our DAC (cBN pressure sensor) had to be used for an offsite synchrotron experiment. It then took 18 months to build a new sample preparation lab and re obtain ES&H approval to cryogenically load HCl in B235. We expect to conduct more ISLS measurements during the fall of 2006. In the complete absence of any shock wave or static data on HCl our ISLS data were used to begin development of an EXP6 model. Recently we discovered a Brillouin scattering study that was conducted, in part, on liquid HCl. The Brillouin data presented in figure 22 are taken from Shimizu H., Kamabuchi K., Kume T., and Sasaki S, *PRB* **59**(18) 11727 (1998). The Raman system used in 2004 was inferior to our currently embedded Raman system.

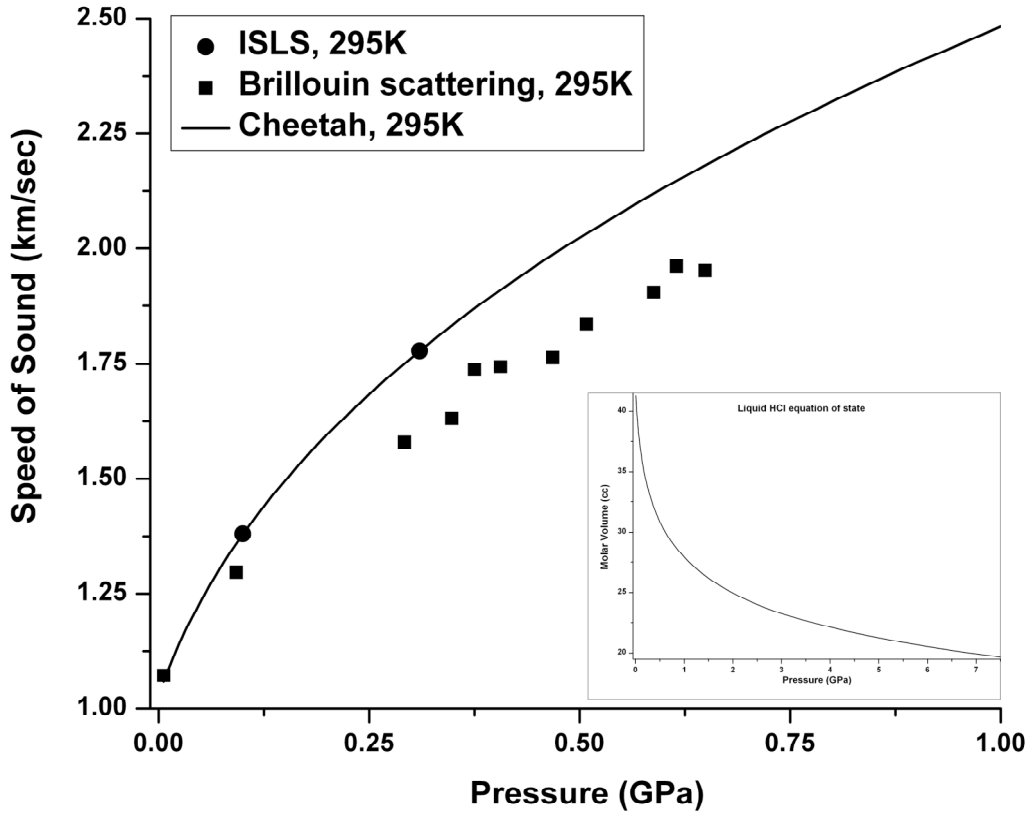

Figure 22. The SoS and provisional EoS of pure hydrogen chloride.

2.1.14 Pure water

We collaborated with our university of Washington colleagues on an ISLS study of pure water. The ruby fluorescence sensor and scale were used to determine pressure. Data were collected along five isotherms up to 673K and nearly 6 GPa. The EXP6 model was parameterized using both shock wave and static ISLS measurements. Above 6 GPa the measured velocity seems to be nearly temperature independent. The ultrasonic measurements shown in figure 23 were taken from Holton G. et al., *J. Acoustical Soc. America* **43**(1) 102 (1968). The 373K ultrasonic data is from a 20K extrapolation of Holton's data.

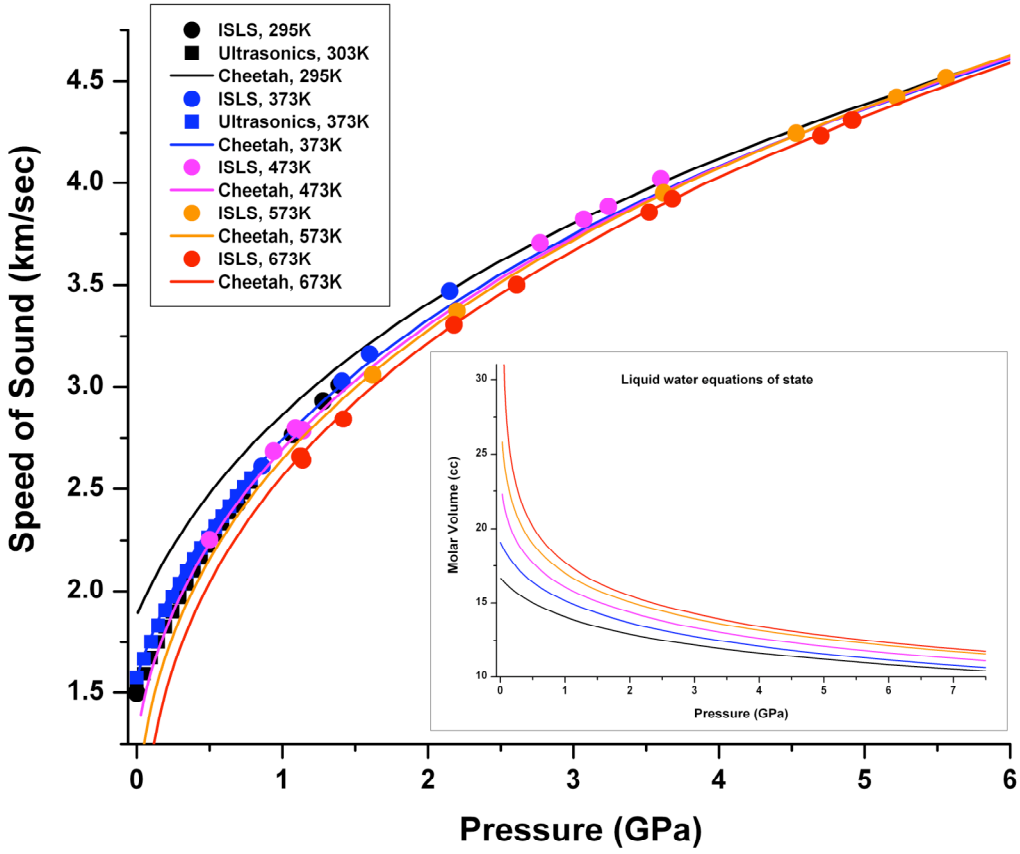

Figure 23. The SoS and EoS of pure water.

2.1.15 37:63 mass ratio mixture of HCl:Water

We conducted ISLS measurements on concentrated hydrochloric acid. We initially used an iridium gasket to contain the fluid. For these initial studies we used the SRB sensor and scale to determine pressure. During the time of this study we did not have a very robust Raman system embedded into the ISLS instrument. We were concerned that our measurements could be effected by reacted SRB so we then built a composite iridium cavity. One section contained just the fluid and the other contained a supersaturated solution of the fluid and SRB material. In this way our SoS measurements would be made on a pure fluid. Unfortunately it appears that our single cavity measurements are not valid. Note in figure 24 that composite cavity velocities are significantly slower than samples that may contain dissolved or reacted SRB material. Now that we have an optimal Raman system and are in the process of developing a precise cBN pressure scale it would be prudent f or us to make additional ISLS measurements on this fluid mixture.

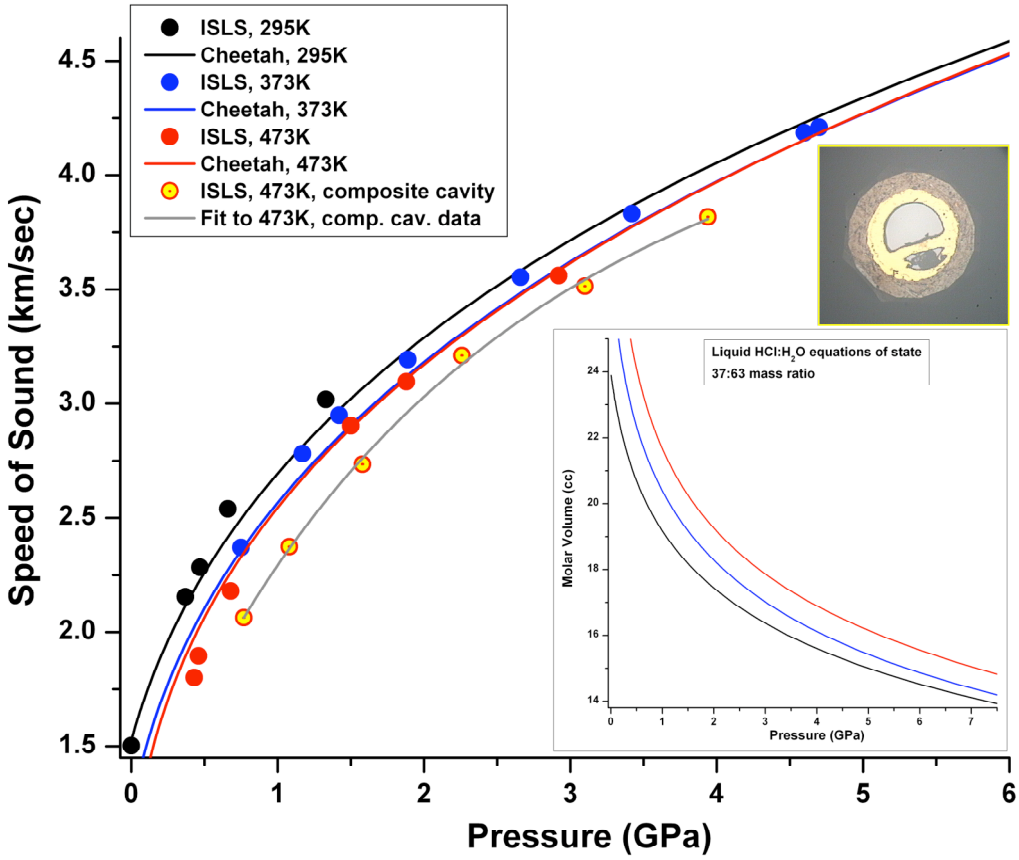

Figure 24. A provisional SoS and EoS of a 37:63 mass ratio mixture of HCl and water. The inset micrograph is an example of a composite cavity.

2.1.16 49:51 mass ratio mixture of HF:Water

We began our ISLS study of a concentrated hydrofluoric acid mixture with the knowledge that hydrochloric acid chemically attacks SRB. So we chose to skip the technological difficulties of making and preserving a composite metal cavity and instead use our cBN Raman sensor. We knew that at some point we would have to upgrade the cBN pressure scale using a suitably precise set of calibration data. Figure 25 is a plot of our HF:water data with no correction to the cBN pressure derived results. Clearly we need to collect more data and construct a new cBN scale. Still we were encouraged by the fact that we could relatively easily obtain an ISLS signal. The precision of our newly embedded Raman system now gives us reason to confidently conduct new SoS-pressure studies of the more corrosive fluid systems we ambitiously tackled earlier in this project's history.

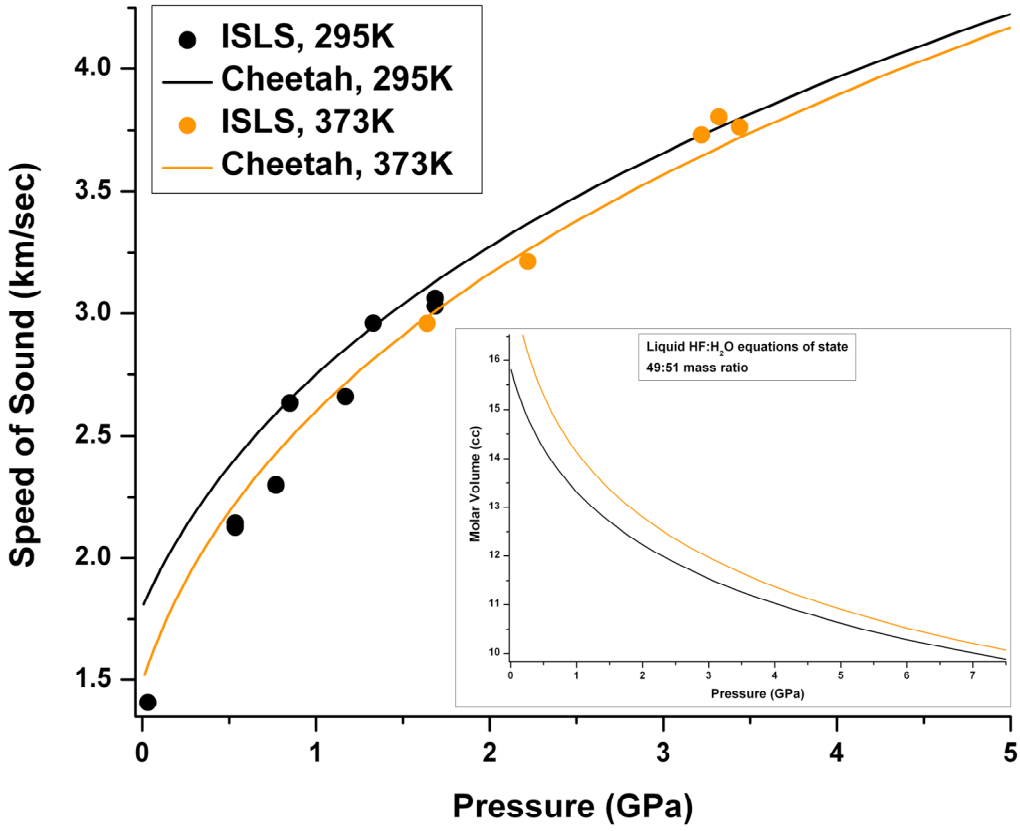

Figure 25. A provisional SoS and EoS of a 49:51 mass ratio mixture of HF and water.

2.1.17 30:70 mass ratio mixture of NH3:Water

Our ISLS study of ammonium hydroxide provided disconcerting results. This study was conducted at a time when we did not have a sufficiently robust Raman system embedded to within our ISLS instrument. So we used our SRB sensor and calibration scale to determine pressure. Our initial concern again was weather or not the NH_4OH would attack the SRB. To find out, we began by making 423K SoS measurements then followed by a set of 473K measurements. After an approximate 20-hour SRB exposure to high pressure and temperature ammonium hydroxide we made another 423K ISLS measurement. From the results shown in figure 26 one may conclude that either SRB yields significantly lower pressures after an extended exposure to high temperature NH_4OH or that the SRB is dissolving thus resulting in depressed velocity measurements or perhaps some combination of non optimal processes. This is another example where we can now use our new Raman instrumentation and the cBN sensor to mitigate the chemical attack issues that compromise the use of otherwise highly precise and reliable optical fluorescence sensors.

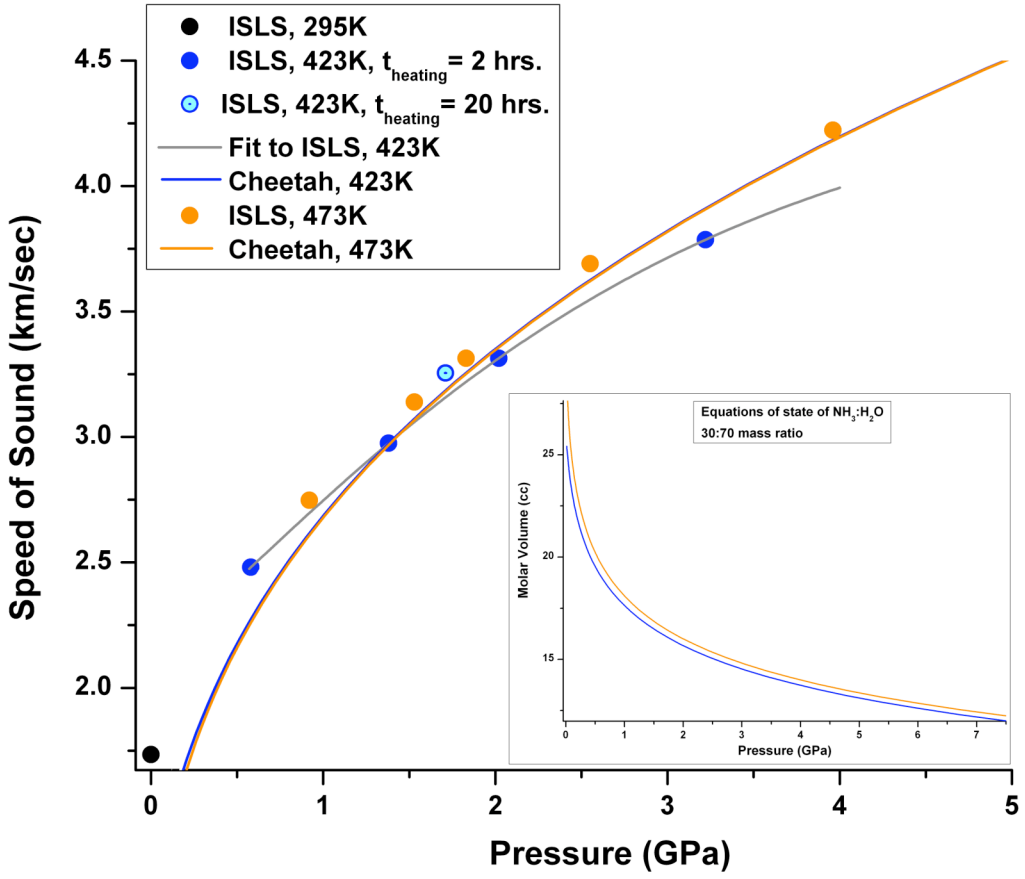

Figure 26. A provisional SoS and EoS of a 30:70 mass ratio mixture of NH_3 and water.

2.2 PRESSURE SENSOR DEVELOPMENTS

As we mentioned in section 1.3 there was a necessary evolution of optical pressure sensors necessary to improve the precision of our SoS measurements. Above 523K the temperature dependence and severe line broadening of ruby prohibits it use in our SoS measurements. We then set out looking for a more suitable sensor that would exhibit spectral characteristics that are not so severely affected by temperature. We opted for SRB and in the summer of 2000 we developed a recipe and synthesized SRB powder. A polycrystalline sample of SrB_4O_7:Sm^{2+} was prepared using a solid solution in air. H_3BO_3 and $SrCO_3$ were mixed in stoichiometric amounts (approximately 80 mol% H_3BO_3 and 20 mol% $SrCO_3$). A small amount (0.21 mol%) of Sm_2O_3 was added to obtain an Sm^{2+} dopant concentration of 0.4 mol%. Previously reported procedures suggested dopant concentrations of 1 mol% and 5 mol% Sm^{2+}.

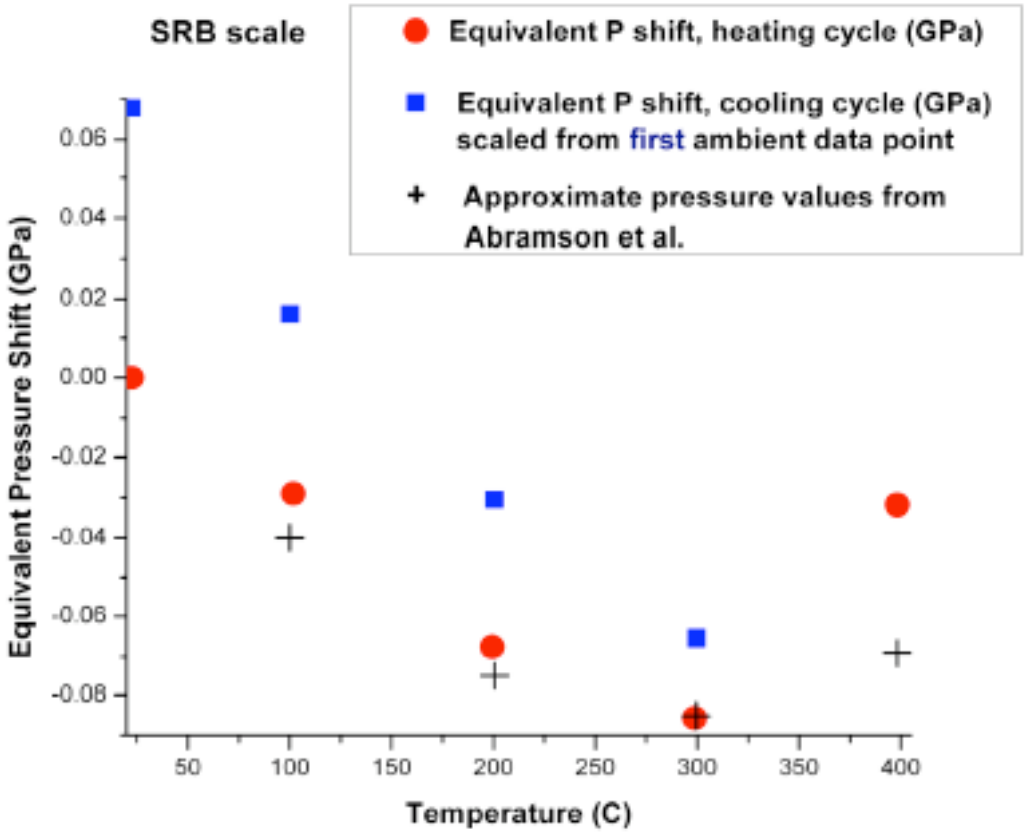

Figure 27. The effective temperature affect on the SRB pressure sensor is less than 0.1 GPa.

The mixture was baked at 973K for 66 hours in an alumina crucible. Once removed the sample was finely ground and placed back into the oven at 1073K for another 24 hrs. X-ray diffraction was used to verify the sample was SrB_4O_7:Sm^{2+}. The x-ray data also revealed a small impurity of SrB_2O_4. The sample was finely ground again and an additional 3 mol% H_3BO_3 was added to the

sample, in an effort to reduce the impurity concentration. The sample was baked a final time for 24 hours at 1123K. X-ray data was taken again on the final sample, with no appreciable decrease in SrB_2O_4 observed. The SrB_2O_4 does not produce an Sm^{2+} emission line and hence the impurity is regarded as insignificant. An ambient pressure, high-temperature spectral analysis of our SRB powder is given in figure 27. We compare our sample to larger single crystal samples made independently by E. Abramson at the university of Washington. Our SRB material has been an effective pressure sensor for our ISLS measurements. We also performed a spectral analysis of our cBN applied to a published cBN scale and compared it against our SRB scale. Figure 28 provides an indication of the pressure and temperature offset between SRB and cBN scales. Over a modest 1.4 GPa and 400°C range the "total" cBN effective pressure offset varies between -0.2 and nearly 0.3 GPa. This is a clear indication that the published cBN scale is not sufficiently precise for our SoS studies. We thus conducted a SRB plus cBN spectral study in liquid argon where both samples were under identical conditions (refer to figure 8). Analysis of this data is forthcoming.

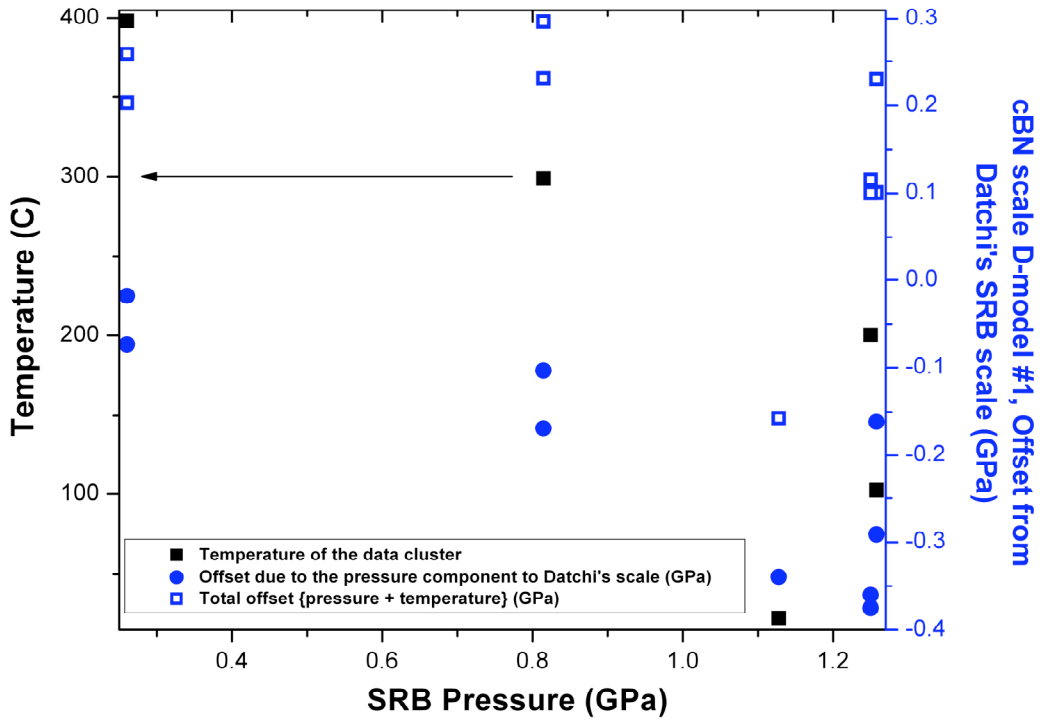

Figure 28. The effective total pressure offset between SRB and cBN scales warrants our independent development of a more precise cBN scale.

2.3 PHASE STABILITY DIAGRAMS

2.3.1 Formic acid

When measuring high-pressure and temperature sound velocities in supercritical organic fluids, one must verify the chemical nature of the system in question. Some of our preliminary measurements on formic acid gave indication through anomalous velocities and altered Raman spectra that reactions occurred above certain pressure-temperature conditions. Thus we began a program to development of a phase stability diagram for formic acid using FTIR and Raman spectroscopic techniques to differentiate between liquid, solid, and reacted states.

Formic acid is a simple monocarboxylic acid. A study of solid formic acid provides insight into the nature of hydrogen bonding with pressure. Unlike other carboxylic acids, formic acid does not form dimers in the solid state, but instead forms an infinite length network of hydrogen-bonded chains, linked by the hydroxyl group. Formic acid has *cis*- and *trans*- conformations that form chains. A phase transition was previously reported by Shimizu to occur at 4.5 GPa [139]. A subsequent study proposed a high-pressure crystal structure consisting of a more complex phase, which combines *cis*- and *trans*- isomers of HCOOH in symmetrically flat layers [140]. Our x-ray powder diffraction data indicates the low-pressure phase is stable to well over 30 GPa. Rather than a cis/trans conformational change it is most probable that Shimizu observed mode coupling between the O-D stretch and C=O stretch Raman bands resulting in the observed frequency inflection at 4.5 GPa.

Pure (99.99%) and neat formic acid was loaded into a membrane DAC chamber consisting of two counter opposed 500 μm diamonds (synthetic type II anvils) and a pure Ir disk indented to ~30 microns thick and cut with a 220 micron EDM spark erode cutter. A Eurotherm® control system is used to power an external heating ring surrounding the DAC. The metal membrane capillary pressure was repeatedly adjusted to maintain a constant sample pressure. Sample temperature was monitored using type-K thermocouples lodged between diamond and a metal containment gasket using gold leaf foil. The temperature precision was approximately ±0.5 K and the absolute accuracy decreases with increasing temperature and was approximated to be +0 K and –4 K up to 575 K.

Samples were heated at 1 K/min until melting was observed. Some samples were further heated at the same increasing rate until decomposition was observed. Changes in sample composition and structure were monitored by Raman and FTIR spectroscopy. Other samples were heated to achieve complete chemical decomposition. Temperature invariant FTIR spectral features indicated equilibrium was reached. A secondary indicator of a fully completed reaction was the evolution of a completely black and opaque sample. Some samples were cooled after melting had occurred, providing data on the solids of the system. There is not a smooth trend in pressure dependant crystallization temperatures due to inconsistent cooling rates. Constant

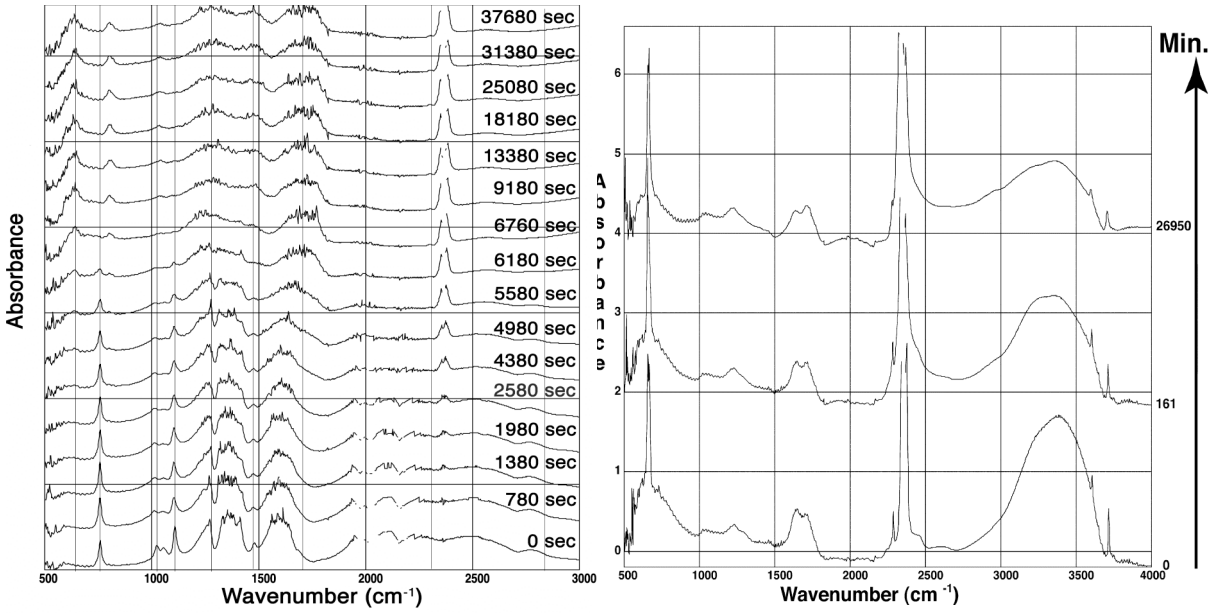

Figure 29. (a) Time-resolved FTIR spectra of pure formic acid at 5.9 GPa and 473K. Note the formation of CO_2 (662 cm^{-1}, 2364 cm^{-1}, and combination modes 3598 $cm^{-1}$and 3705cm^{-1} not shown in plot). (b) Time-resolved FTIR spectra of the products in (a) after rapid decompression to 0.2 GPa and temperature reduction to 298K.

pressure-temperature reactions were executed at 5.9 GPa and 4.2 GPa at 473K and 496 K respectively. In Figure 29a we display time-resolved FTIR spectra of formic acid held at 5.9 GPa and 473 K and in Figure 29b we show the evolution of the resultant products after temperature was reduced to 298 K followed by a rapid reduced to 0.2 GPa. The IR absorption background level decreased remarkably at this point. The reaction products are not apparently quenchable down to low pressure and room temperature conditions. The α-phase CO_2 band at 662 cm^{-1} provides evidence that the sample chamber remained sealed. There is a C-O bend mode at 1222 cm^{-1} and O-H and C=O and bending modes at 1638 cm^{-1} and 1710 cm^{-1} respectively. Over time, the I_{1638}/I_{1710} ratio decreases to less than unity. The broad background from 550-900 cm^{-1} provides evidence that H_2O is present. The number of O-H bonds (1638 cm^{-1}, 3345cm^{-1} and broad background centered around 720 cm^{-1}) decreased over the course of 18.7 days while the sp^2:sp^3 carbon bond ratio (3226 cm^{-1}: 2950 cm^{-1} C-H bonds) also seemed to be decreasing. When solid polymer-like reaction products, intensely orange in color, were exposed to air, they appeared to be photosensitive: attempts to measure Raman vibrational spectra using low-intensity (< 2 mW over a 5 μm diameter area) visible light from an argon laser resulted, after prolonged exposure to the laser light, in photochemical oxidation of the solid product where the nature of carbon bonds become completely graphitic in nature. In some instances, relatively short laser light exposures (< 30 sec) yielded diamond-like carbon bonding spectra only to become graphitized with continued laser light exposure.

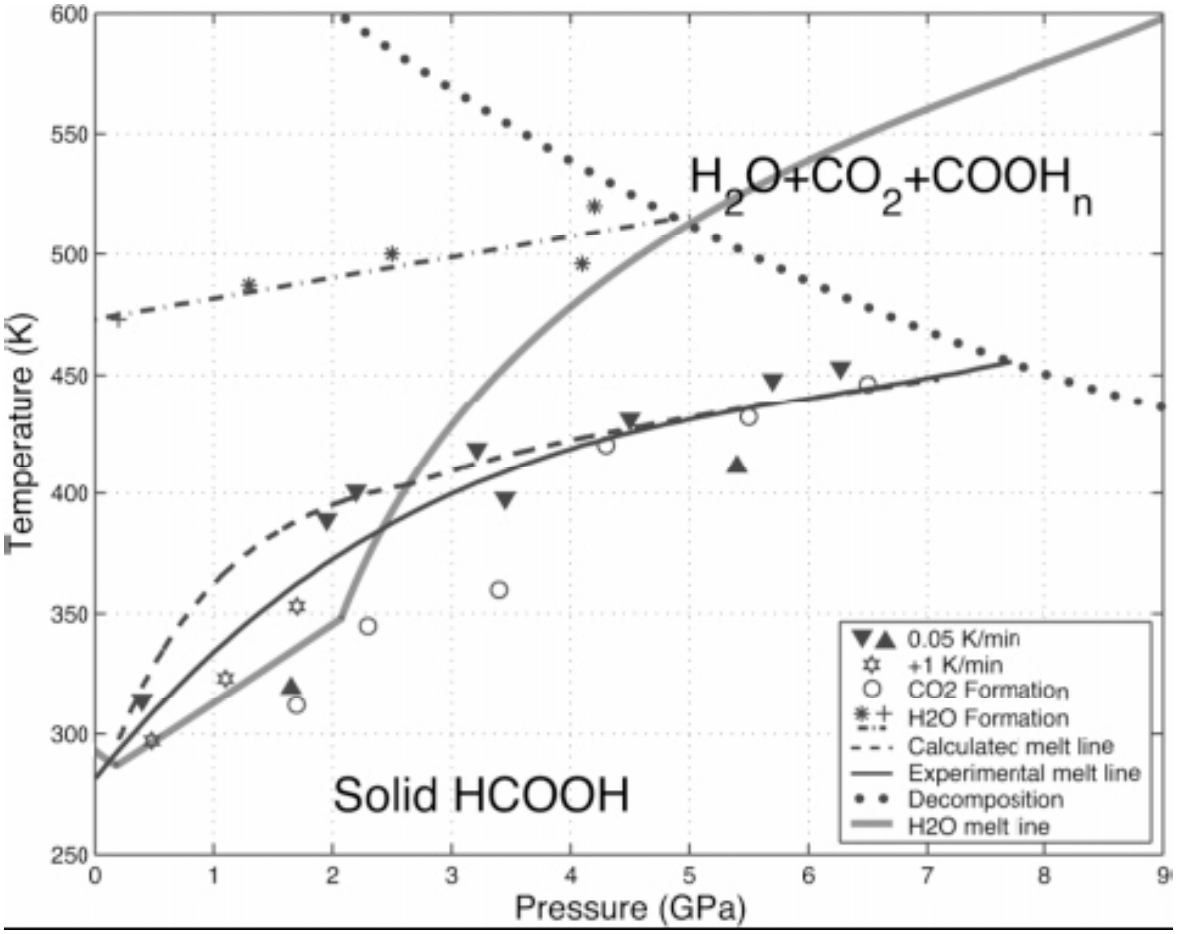

Figure 30. Experimentally determined phase and reaction diagram of formic acid, with solid and dashed lines indicating the experimental and theoretical melting curves, and the dotted lines indicating reaction boundaries. Solid triangles identify upper and lower bounds of the liquid-solid phase transition, as determined at slow heating/cooling rates of 0.05 K/min. A high-temperature chemical transformation to solid opaque products (•••) is distinguished from the decomposition of formic acid into CO_2 (and inferred H_2), which occurs near the melting line (-), and the higher-temperature decomposition of formic acid into H_2O and CO at pressures below 5 GPa (*); (+) data point taken from literature. For comparison, the melting line for H_2O is given by the solid gray line.

The phase and chemical stability of formic acid is summarized in Figure 30. Below 5.5 GPa, we have observed that solid formic acid will melt and simultaneously begin to chemically react forming liquid CO_2, CO and H_2O. Due to experimental difficulty, we cannot provide direct evidence for the creation of molecular hydrogen though it would seem necessary in order to form CO_2 and CO. The molar concentration of these species is dependent on pressure, temperature and cooking time. As mentioned above with increased heating, a second decomposition reaction occurs producing an orange colored solid reaction product. Threshold temperatures required to produce polymer-like solid products are inversely proportional to pressure. Above 6 GPa, CO_2

production is accompanied with solid products resulting in a chemical triple point. At pressures under 5.5 GPa and 498 K, CO_2 and CO production occurs from the following reactions.

$$HCOOH_{solid} \longrightarrow HCOOH_{liquid} \longrightarrow CO_2 + H_2 \quad (7)$$

$$CO_2 + H_2 \longrightarrow CO + H_2O \quad (8)$$

Below 4.5 GPa we observe, in some instances, H_2O and CO. At room temperature where gas phase formic acid is a dimer, reaction (14) has a standard energy of 152 kJ/mol and a standard entropy change of 42.4 J/mol·K. From $\Delta G = \Delta H - T\Delta S$ we know the activation barrier for this gas phase reaction increases with temperature. If we observe CO and H_2O at elevated temperatures then this implies a reduced activation barrier in the high-pressure liquid state and/or a significant change in ΔH. Reactions 7 and 8 are catalyzed from metal substrates and Ir, our metal support gasket, is considered a particularly good catalyst for these reactions [141]. Evidence of CO from FTIR is experimentally more difficult where $I\nu_3(CO_2)/I(CO)=213$ and this may partially explain why we see no spectral evidence above 5 GPa where IR background absorption levels from polymer-like products are relatively high.

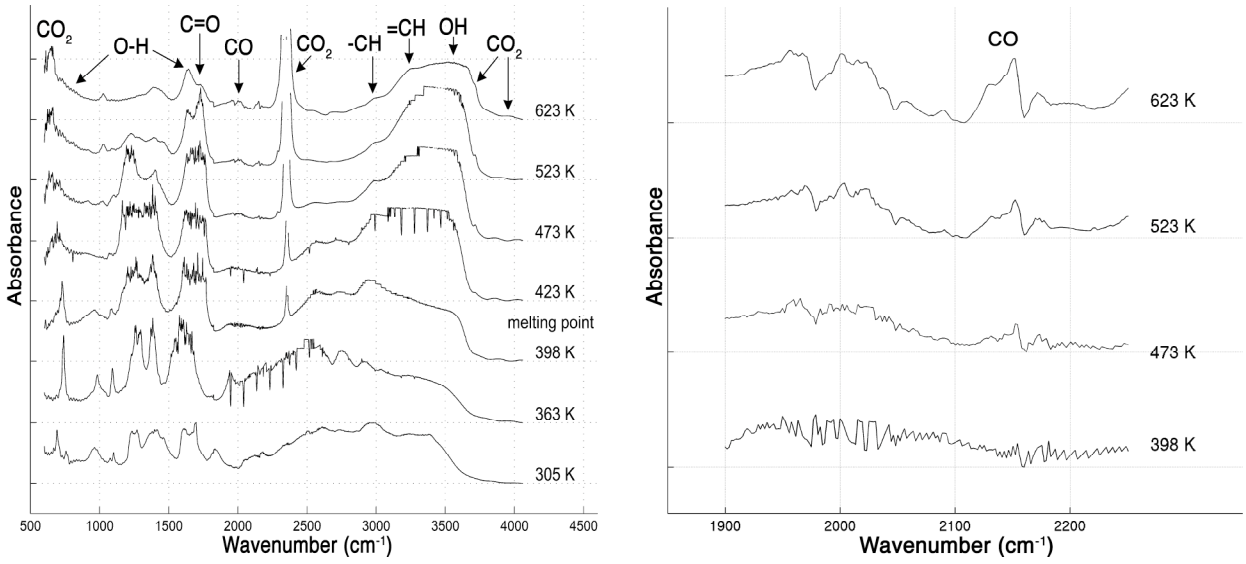

Figure 31. (a) Time-resolved FTIR spectra of pure formic acid at 3.0 GPa and a heating rate of 1K/min. At least three products from liquid formic acid, CO_2, H_2O and CO can be deduced from spectral assignments. (b) Expanded region in (a) centered around 2100 cm^{-1} showing the telltale IR absorption peaks of δ-CO.

The formation of hydrocarbons from thermal decomposition of formic acid at room pressure and high temperature (1696 K) has been reported by Muller *et al.* [142]. In our study we also

find evidence of hydrocarbons and note how their spectral features depend on reaction conditions. At 3 GPa and room temperature, the nature of O-H bonds from formic acid become more covalent-like with increasing temperature. Once a reaction occurs the long-range order of the O-H network in crystalline formic acid becomes disrupted with bond distances increasing to a more hydrogen-like bond length centered at frequency of approximately 3500 cm^{-1}.

We have yet to demonstrate the existence of the hydrocarbons produced in this pressure-temperature regime. In Figure 31a there is indication of H_2O products where a broad shoulder evolves at 600cm^{-1}- 800 cm^{-1}, and an O-H stretch mode forms at 1689 cm^{-1}. Figure 31b shows an expanded region of Figure 31a centered near 2100 cm^{-1} where a weak absorption doublet 2130cm^{-1} and 2148cm^{-1} intrinsic to δ-CO is observed. We also note CO spectral features appear at 4.2 GPa and T > 500 K. In this pressure regime, the infinite length hydrogen bond chains break following reaction (13) to form liquid HCOOH, where subsequently and CO_2 and presumably molecular hydrogen from. CO_2 combines with H_2 to produce CO, and some of the H_2 reduces the remaining HCOOH, producing amorphous hydrocarbons. A similar decomposition sequence occurs if the system is maintained at a fixed temperature and pressure.

At pressures above 5 GPa, for example at 8.3 GPa, there is no indication of CO formation. As the temperature is increased, CO_2 and hydrocarbon bands simultaneously appear, perhaps suggesting that formic acid is reduced by hydrogen created in reaction (13), and that reaction (14) does not occur at pressures over 5.5 GPa. Moreover hydrogen bond lengths remain invariant with temperature above 5.5 GPa and coincidently we see no evidence of water. As the reaction phase diagram shows, there seems to be two separate and identifiable reaction regimes delineated by the dotted curve in Figure 31. When thermally driven toward complete decomposition, each reaction region generates a different polymer-like product. Figures 32a and 32b show Raman and FTIR spectra of reacted samples recovered at STP respectively. The formation of C--C and C=C bonds at higher pressures, as indicated in Figure 32b where absorption occurs at 1027 cm^{-1} and 1585 cm^{-1} respectively, suggests that thermal decomposition of high-pressure formic acid may form what are perhaps complex organic compounds. Recovered samples appeared photochemically sensitive and their spectra may indicate how the nature of product carbon bonding depends on reaction conditions. The low-pressure (4 GPa) product (``Polymer 1'') shows graphite-like $sp^2$ bonding, while the high-pressure (8.5 GPa) product (``Polymer 2'') has a more diamond-like (sp^3) bonding nature. FTIR spectra indicates the presence of O-O, C-C, =C-H, and C=C bonds in Polymer 1 and Polymer 2 clearly contains –C-H bonds. Further analysis of recovered products from high-pressure DAC reactions will be conducted using conventional analytical chemistry techniques such as mass spectroscopy or perhaps nuclear magnetic resonance spectroscopy. It is an important challenge to systematically study chemical products prior to exposure of atmospheric oxygen and hydrogen. Chemical kinetic studies for the reactions discussed above are underway in our laboratory.

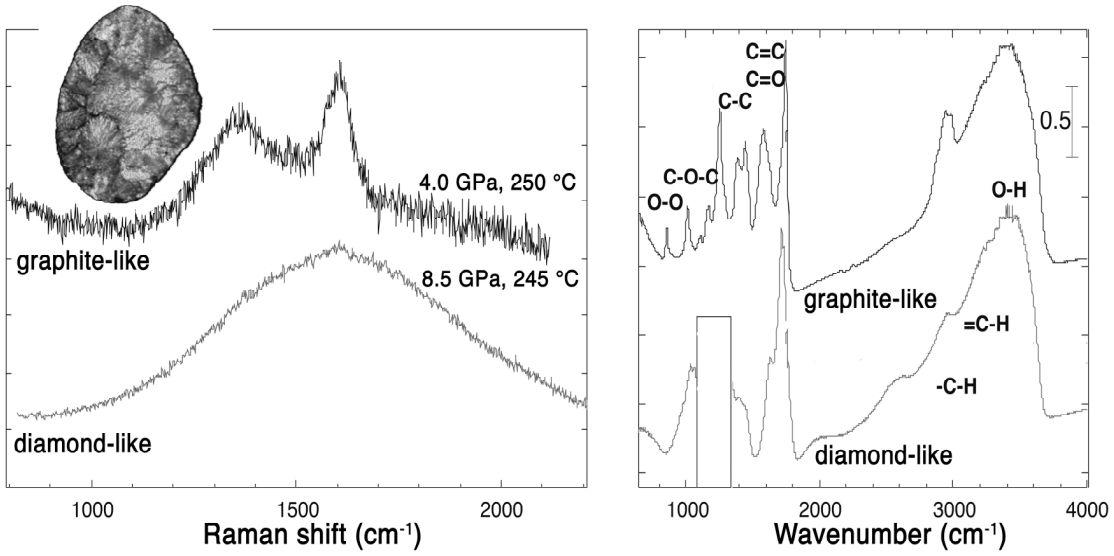

Figure 32. (a) Raman spectra (ambient conditions) of the C-H bend region of two different recovered products from formic acid. The inset is a photomicrograph of the 4.0 GPa products that are intensely orange. (b) FTIR spectra of the samples described in (a).

In Figure 30 we presented a calculated melt curve that compares favorably with our experimental results. This melt curve is the result of a minimized two-phase Gibbs free energy equation of state made to match accepted thermodynamic parameters and all available high-pressure experimental data including shock Hugoniot data [126], static cold compression volumes and compressibility from x-ray [128], and adiabatic ISLS sound velocity measurements [127].

The pressure dependant term for our Gibbs free energy was derived using a Murnagham form for volume. Given the relatively low temperature of melting for formic acid to 6 GPa, we chose to set thermal expansion in our model to zero thus resulting in a simplified temperature independent expression for the high-pressure Gibbs free energy component. Our equation of state is based on an explicit functional form for *G(P)*. The Gibbs free energy expression derived here appears to be appropriate from $0 \leq$ P (GPa) ≤ 6 where formic acid was observed to melt.

We begin by breaking the Gibbs free energy into a reference component [$G_0(T)$] accounting for properties at 1-atmosphere and a second pressure dependant component:

$$G(P,T) = G_0(T) + \Delta G(P) \tag{9}$$

First we consider $G_o(T)$ where from G = H – TS we have $G_0(T) = H_0(T) – TS_0(T)$. The enthalpy and entropy are conveniently expressed in terms of the constant pressure heat capacity at 1 atmosphere $C_{p,0}(T)$:

$$H_0(T) = \Delta H_0 + \int_{T_0}^{T} C_{p,0}(T)\, dT \tag{10}$$

$$S_0(T) = \Delta S_0 + \int_{T_0}^{T} \frac{C_{p,0}(T)}{T}\, dT. \tag{11}$$

In our present study T_0 = 298.15 K thus ΔH_0 and ΔS_0 are respectively, the standard heat of formation and entropy. In our computational model we consider the heat capacity for the liquid phase to be temperature independent and set it to 99.036 J/mole·K from literature data. For the solid phase, we employ a single Einstein oscillator to compute heat capacity:

$$C_{p,0}(T) = 7.5R^{*}\ E(\Theta/T) \tag{12}$$

where the Debye temperature Θ is set to 281K and the Einstein expression is

$$E(x) \equiv \frac{x^2 e^x}{(e^x - 1)^2} \tag{13}$$

At the limit $T \rightarrow \infty$, C_p = 62.358 J/mole·K or 7.5R. Integration of equation 16 yields

$$H_0(T) = \Delta H_0 + \theta \left[\frac{1}{e^x - 1} \right]_{x_0}^{x} \tag{14}$$

where $x \equiv \Theta/T$ and $x_0 \equiv \Theta/T_0$. We evaluate $S_0(T)$ analytically to yield:

$$S_0(T) = \Delta S_0 \left[\frac{x}{e^x - 1} - \ln(1 - e^x) \right]_{x_0}^{x} \tag{15}$$

This completes our definition of $G_0(T)$. The pressure dependant component of equation 15 follows from dG = VdP – SdT where we define ΔG(P) through postulation of a form for V(P). Our result is

$$\Delta G(P) = \int_{P_0}^{P} V(P)\, dP. \tag{16}$$

The Murnagham form uses the relation

$$V(P) = V_0 \left[n \kappa_0 P + 1 \right]^{-1/n} \tag{17}$$

This form is derived by assuming a linear pressure dependence for the bulk modulus:
$B = B_0 + nP$, where $B_0 = 1/\kappa_0$. The thermodynamic values that best minimize G(P,T) to all available experimental data are provided in table 1.

The heat capacity for the liquid is taken from JANAF tables, while that for the solid is taken from ref [131]. The enthalpy and entropy for the liquid at STP are also taken from experimental data [130, 131], as is V_o [128]. The enthalpy and entropy of the solid are determined by replicating the melt temperature and enthalpy of melting at 1 ATM pressure. The V_o for the solid is determined by an extrapolation of the static compression data [128] to 1 ATM. The B_o and n for the solid are fit simultaneously to the static compression data and the measured slope of the melt curve. Likewise, the B_o and n values for the liquid-phase are fit to sound speed data [127] and the slope of the experimental melt curve [129]. The relatively high error in fitting sound speed data was due to compromising these parameters relative to fitting the measured slope of the melt curve.

Table 1. Two-phase parameters of formic acid used to calculate a high-pressure melt curve.

Parameter	Liquid-Phase	Solid-Phase
C_p (J/mole·K)	99.036	62.358
ΔH_0 (kJ/mole)	-425.100	-436.750
ΔS_0 (J/mole·K)	131.840	88.241
V_o (cc/g)	1.22	1.57
B_0 (GPa)	1.63	10.67
n	6.65	5.60

We also reported the onset of symmetrical hydrogen bonding in formic acid above at approximately 20 GPa and ambient temperature [128]. At 45 GPa formic acid becomes amorphous in nature. These profound changes in interatomic bonding are important clues to further develop an understanding of the chemistry and physics of simple molecular systems under extreme conditions

2.3.2 Water

The possibility that transient ionic species form during a detonation process could have profound implications with regard to thermochemically predicted chemical reactions and hydrodynamic simulations. Previously published articles suggested from theory that a super ionic state exists for water and ammonia. We began a program that combined our experimental and theoretical expertise to investigate extreme condition water. We discovered that water may indeed have a dynamically ionized structure above 47 GPa beginning at approximately 1200K. At these conditions water appears to form a sublattice of oxygen where the protons become locally mobile. At higher temperatures the water may in fact become superionic where protons become highly mobile thus affecting charge transport properties. Our phase diagram is given in figure 33. The results of our study bring to attention the need to more thoroughly investigate the chemistry, structure, and transport properties at extreme P-T conditions.

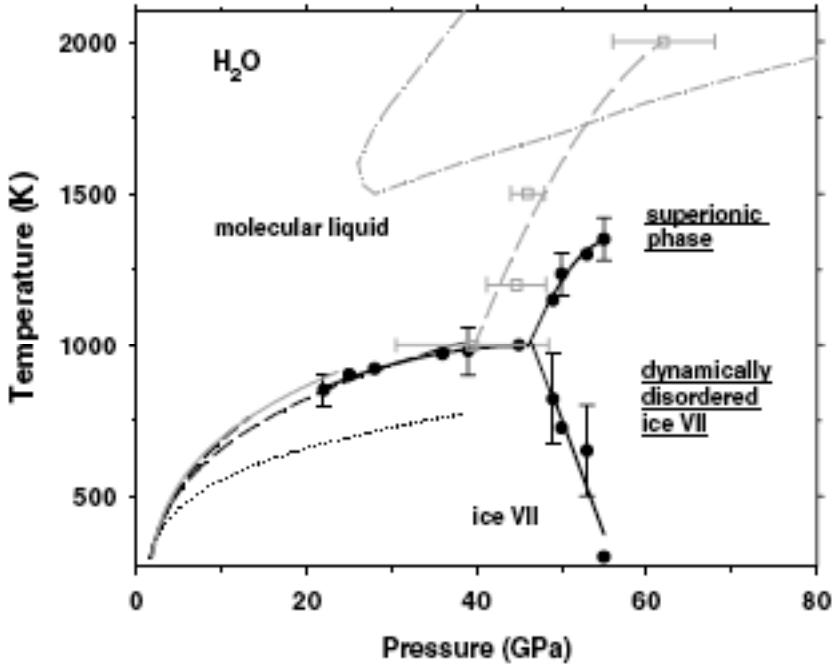

Figure 33. Phase diagram of H_2O. Solid circles correspond to the transformation points determined from the spectral data. Corresponding temperatures were chosen to be midpoints between experimentally determined temperatures in the various phases. Thick solid lines are guides to the eye for our experimental results; thin solid lines are extrapolations of the measured lines. Gray squares and the dashed line (guide to the eye) correspond to theoretically computed conditions for the freezing of oxygen. Thick, thin black dashed, gray dotted, and gray solid lines are interpolated data from literature references respect. Data from the previous references are much higher in temperature and are not shown. The gray dot-dashed line corresponds to the previously proposed [2] boundary of the superionic phase. The boundary between the dynamically disordered ice VII and superionic phase has not yet been determined.

2.3.3 General comments concerning the fluid and mixture phases discussed in section 2.1

In most cases we tend to measure the SoS of a fluid along an isotherm up to the pressure where the material freezes. We did make SoS measurements on liquid formaldehyde however it chemically reacted at very modest temperatures and pressures. Generally the material velocity will encounter a discontinuous increase when transitioning from the liquid to solid state. In fact SoS measurements are one reliable method to determine melt or freeze boundary lines. The acid:water mixtures encountered phase separations occurring at fixed pressures with increasing temperature. Fluid mixture coexistence lines are not so well known and are of significant value to the continued development of LLNL thermochemical models.

3.0 CURRENT IMPACT ON LLNL COMPUTATIONAL EFFORTS

The speed of sound measurements described here have allowed us to systematically improve the accuracy of the Cheetah code, especially for explosives comprised mostly of the elements C,H,N, and O. An explosive test suite with over 20 common explosives was run for Cheetah versions 2-5. The code dates spanned a range of 1996 to 2006. Results are shown in Figure 34.

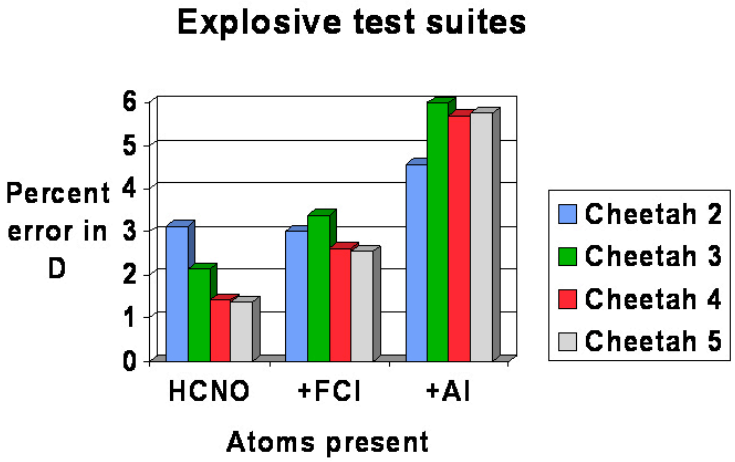

Figure 34: Error in the predicted detonation velocity D is shown for successive versions of the Cheetah code with HCNO explosive, HCNOFCl explosives, and HCNOAl explosives.

The code is almost 3 times more accurate when applied to explosives with the elements HCNO only. We plan to conduct more accurate measurements on compounds containing F and Cl to further reduce the errors in modeling these compounds. Explosives containing Al have slow reaction kinetics. The error in detonation velocity prediction for these compounds is dominated by the reaction kinetics rather than the high-pressure equation of state. This specific error highlights the need for kinetic measurements in addition to ongoing equation of state measurements.

SoS measurements on simple fluids are valuable so that we may baseline high-pressure burn experiments. Argon, nitrogen, and oxygen gases are typically compose the pressure medium used for large scale high explosive controlled burn experiments. Knowing the EoS of these gas materials helps us predict the chemistry and energy release of HE burn experiments. Materials such as water and weak acids intrinsically have with dipole moments. HE products contain species with dipole moments which govern the type of chemical interactions and time scales of interactions under extreme conditions. SoS studies on hydrocarbons are important since their EoS properties are used to predict the formation conditions for carbon. Carbon is a key component to insensitive high explosive detonation reactions. We still can not fully describe the chemical and kinetic roles that carbon plays in detonation chemistry reactions. SoS measurements on ionic species such as acid water mixtures is important as they ultimately help

us to understand if, when, and how electrical transport properties (conductivity) pin certain detonation reactions. Furthermore SoS mixtures help to further test and develop the underlying mixture rules that form the semi-empirical underpinnings to the Cheetah thermochemical code.

4.0 FUTURE WORK AND IMPLICATIONS TO LLNL COMPUTATIONAL EFFORTS

Our ISLS and ISLS-SPE SoS measurements have significantly contributed to the development of the Cheetah EXP6 interatomic potential surface library. Indeed without this effort it can arguably be said that no other SoS measurements on detonation products let alone mixtures would have been fed into our library. The recent ISLS-SPE development is huge. Now we can study any fluid or fluid mixture and with confidence that we will not laser heat our samples thereby inducing unwanted or unknown products. Our recent addition of a high precision Raman system in addition to our existing fluorescence instrument is exactly what we needed to extend our SoS range into 10s of GPa provided fluids do not freeze. Our ongoing effort to independently create a suitably precise Raman pressure sensor that can withstand chemical attack is the third leg of our project that now furnishes all of the parts required to transition what began as a semi-fundamental science effort into a full blown applied research project. The bottom line is that our experimental range and throughput will increase provided our future material studies involve samples that are reasonably simple to load into a DAC.

As was mentioned in section 3.0 there is a fundamental need to characterize extreme condition fluid mixture coexistence lines. The Cheetah code does not currently treat fluid-fluid phase separations. It is not clear whether this phenomenon is important for detonation. Experiments will help to direct the further development of the Cheetah code.

The CMLS FAST-DAC initiative is building toward measurements that will enable us to observe some of the chemical species that are predominate under equilibrium conditions. The closer our measurements can get to C-J pressures and temperatures the more rigorously we can test our thermochemical detonation predictions. We now have to potential to conduct Raman vibrational experiments using pulsed lasers and pulse-gated detection equipment (refer to figure 5). Over the next 12 months we intend to construct a single shot time resolved infrared (TRIR) absorption instrument. We may even be able to embed into the TRIR capability a radiometric determination of the temperature of a high-pressure deflagrating energetic material in one laser-shot. Recently we developed and tested a new instrument that can perform a single shot time resolved surface displacement from an ablated metal foil constrained at modestly high pressure in a DAC. This same system can be slightly modified to measure ultrasonic transit times in high-pressure bulk solids. It could be possible to determine the elastic properties of single crystal HE materials where the EoS has been previously determined. We can conceivably use our FAST-DAC system to create transient ionic fluids and then measure the chemical relaxation dynamics under extreme conditions.

Now that ultrafast fs laser systems and associated detection equipment can be purchased as off-the-shelf and reliable items, albeit at nontrivial fiscal expense, the extreme chemistry material science field is poise to finally focus on short-lived chemical processes. Our project team has already begun to develop the necessary tools required to begin exploring significant issues of concern to the detonation science community. We have used the start of this project to make significant measurements and also to push the technology to its cutting edge limit. This includes newly designed and constructed DACs that lend themselves to high-temperature studies and also to multi megabar sample pressures using remotely controlled pressure drive devices. Lastly we will once again emphasize that our tight scientific interactions between theorists and experimentalists is a key enabler for us to maintain a coherent and focused effort toward understanding the supremely complex nature of detonation chemistry.

ACKNOWLEDGEMENTS

The authors thank Dr. Alexander F. Goncharov for his preeminent involvement in this project during his tenure at LLNL. We thank Dr. P. Pagoria for preparation of pure CH_2O_2 and Donald W. Hansen for valuable technical assistance and SoS measurements of supercritical methanol and his presentation of our work on formic acid at the 226th annual ACS meeting. We thank Wren B. Montgomery for her contributions to our research on formic acid. We thank Elaine K. Hart for her work on the decomposition of nitromethane. We are grateful to Christopher Young for his synthesis of our SRB pressure sensor. We express our gratitude toward Dr. R. Simpson, Dr. L. Terminello, and Dr. P. Allen for their sustained support for our research. This work was performed under the auspices of the U.S. Department of Energy by the Lawrence Livermore National Laboratory under contract # W-7405-Eng-48.

APPENDIX A – Publications

Refereed Journal Publications

"Raman spectroscopy of hot compressed hydrogen and nitrogen: Implications for the intramolecular potential" Goncharov AF, and Crowhurst JC, *PRL* **96** (5), 055504 (2006).

"The melting curve and high pressure chemistry of formic acid to 8 GPa and 600 K," W. Montgomery, J. M. Zaug, M. H. Howard, A. F. Goncharov, J. C. Crowhurst, and R. Jeanloz, *J. Phys. Chem. B* **109**, 19443 (2005).

"Pulsed laser Raman spectroscopy in the laser-heated diamond anvil cell," Goncharov A. F. and Crowhurst J. C., *RSI* **76**, 063905 (2005).

"Dynamic ionization of water under extreme conditions," A. F. Goncharov, N. Goldman, L. E. Fried, J. C. Crowhurst, I-Feng W. Kuo, C. J. Mundy, J. M. Zaug, *PRL.* **94** 125508, (2005). *Featured research at Nature.com,* February 2005.

"Raman spectroscopy of cubic boron nitride under extreme conditions of high pressure and temperature," Goncharov AF, Crowhurst JC, Dewhurst JK, Sharma, *PRB* **72** (10), (2005).

"Optical calibration of pressure sensors for high pressures and temperatures," A. F. Goncharov, E. Gregoryanz, J. M. Zaug, and J. C. Crowhurst, *J. Appl. Phys.* **97**, 094917 (2005).

"Polymerization of formic acid under pressure," A. F. Goncharov, M. R. Manaa, J. M. Zaug, R. H. Gee, L. E. Fried, and W. B. Montgomery, *Phys. Rev. Lett*. **94** 065505, (2005).
Highlighted in the journal Nature, March 2005.

"Measured sound velocities of H_2O and CH_3OH," J. M. Zaug, L. E. Fried, E. H. Abramson, D. W. Hansen, J. C. Crowhurst, and W. M. Howard, *Int. J. of High Pressure Research* **23**(3), 229-233, (2003).

"Molecular dynamics simulations of HMX crystal polymorphs using a flexible molecule force field,"D. Bedrov, C. Ayyagari, G. D. Smith, T. D. Sewell, R. Menikoff, and J. M. Zaug, *Journal on Computer Aided Materials Design* **8**, 77-85, (2002).

Book Manuscripts

"The equation of state and chemistry at extreme conditions: applications to detonation products," J. M. Zaug, W. M. Howard, L. E. Fried, A. F. Goncharov, W. B. Montgomery, and J. C. Crowhurst, in *Chemistry Under Extreme Conditions*, ed. M. R. Manaa, Elsevier Science Ltd, 399-425, (2005).

"The equation of state and chemistry of detonation products," L. E. Fried, W. M. Howard, and J. M. Zaug, in *Energetic Materials: Decomposition: Crystal and Molecular Properties*, ed. P. A. Politzer and J. S. Murray, Elsevier Science Ltd, 193-221, (2003).

Refereed Conference Proceeding Publications

Contributed

"Detonation product EOS studies: using ISLS to refine CHEETAH," J. M. Zaug, W. M. Howard, L. E. Fried, and D. W. Hansen, (AIP Press, New York, 2002), edited by Furnish/Dandekar, *Proceedings of the 2001 AIP conference,* APS Shock Compression of Condensed Matter, Atlanta, GA, June 23-29, 177-180, (2002).

Invited

"Sound speed and thermal measurements of inert materials: laser spectroscopy and the diamond-anvil cell," J. M. Zaug, (AIP Press, New York, 1998), edited by Schmidt/Dandekar/Forbes, *Proceedings of the 1997 AIP conference*, APS Shock Compression of Condensed Matter, 73-78, (1998).

First-Place Presentation Award

"Elastic constants of β-HMX and tantalum, equations of state of supercritical fluids and fluid mixtures and thermal transport determinations," J. M. Zaug, *Proceedings of the Eleventh International Detonation Symposium*, Aspen, CO, August, 498-509, (1998).

DoD/DOE TCG-III published reports

"Kinetic modeling of non-ideal explosives with Cheetah," L. E. Fried, W. M. Howard, Joint DoD/DOE Munitions Technology Development Program, 1998.

"Detailed equations of state models for Cheetah: compounds containing F, Cl, and C," L. E. Fried, W. M. Howard , Joint DoD/DOE Munitions Technology Development Program, 1999.

"Development of a high temperature capability in the Cheetah thermochemical code," L. E. Fried, W. M. Howard, Joint DoD/DOE Munitions Technology Development Program, 2000.

"Detonation energies from the cylinder test and Cheetah v3.0," P. C. Sourers, L. E. Fried, W. M. Howard, S. Anderson, S. Dawson, P. Vitello, and R. Garza, Joint DoD/DOE Munitions Technology Development Program, 2001.

"Improved equations of state for the Cheetah thermochemical code," L. E. Fried, A. F. Goncharov, W. M. Howard, P. Vitello, D. W. Hansen, and J. M. Zaug, Joint DoD/DOE Munitions Technology Development Program, 2002.

"Detonation modeling using Cheetah," L. E. Fried, W. M. Howard, K. R. Glaesemann, J. M. Zaug, J. C. Crowhurst, Joint DoD/DOE Munitions Technology Development Program, 2003.

"Improvements in the Cheetah thermochemical code," L. E. Fried, J. Crowhurst, K. R. Glaesemann, A. F. Goncharov, W. M. Howard, and J. M. Zaug, Joint DoD/DOE Munitions Technology Development Program, 2004.

"Improvements in the Cheetah thermochemical code in FY05," K. R. Glaesemann, L. E. Fried, J. Crowhurst, A. F. Goncharov, W. M. Howard, J. M. Zaug, S. Bastea, and N. Goldman, Joint DoD/DOE Munitions Technology Development Program, 2005.

Secular Publications and Notations

"Giant planets may host superionic water," BioED and Nature Online, March 22, 2005.
http://www.bioedonline.org/news/news.cfm?art=1673
http://www.nature.com/news/2005/050321/full/050321-4.html

"Hydrogen bond," published online references to our formic acid study
http://en.wikipedia.org/wiki/Hydrogen_bonds
http://www.answers.com/topic/hydrogen-bond

"Revealing the mysteries of water," G. Rennie, edited by Lawrence Livermore National Laboratory, *Science and Technology Review*, October 2005.

"Going to extremes," M. S. Sherman, edited by Lawrence Livermore National Laboratory, *Science and Technology Review*, 14-19, August 2004.

APPENDIX B – Relevant Public Presentations

Invited lectures

"The equation of state of supercritical fluids and fluid mixtures: Refinements to thermochemical based predictions" J. M. Zaug, Naval Surface Warfare Center, Indian Head Division, Indian Head MD, July 31, 2006.

"The application of visible light scattering techniques to opaque materials in the diamond anvil cell," J. C. Crowhurst, Research at High Pressure Gordon Research Conference, Meriden, NH, June 27-July 1, 2004.

"Chemistry Under Extreme Conditions," J. C. Crowhurst, Energetic Material Gordon Research Conference Chaired by L. E. Fried, Tilton School, NH, June 20-25, 2004

"High pressure light scattering," J. C. Crowhurst, Workshop on Phonons in Crystalline Materials, European Synchrotron Research Facility, Grenoble, France, 2004.

"Critical phenomena in high pressure fluids," J. M. Zaug, American Physical Society March meeting, Austin, TX, March 2-7, 2003.

"Improved high-pressure scales at high temperatures," A. F. Goncharov, and J. M. Zaug, Open Commission workshop on High-Pressure-Temperature Calibration Standards, EHPRG-41/AIRAPT-19, International meeting, Bordeaux France, July 6-10, 2003.

"High pressure ultrasonic and thermal property studies of materials using the diamond cell," J. M. Zaug, University of California Santa Cruz, Santa Cruz, CA, October 16, 2002.

"High pressure thermal property studies of materials using the DAC," J. M. Zaug, CLRC Daresbury Synchrotron Laboratory, Warrington, UK, September 3, 2003.

"High pressure thermal properties of energetic materials and detonation products," J. M. Zaug, Atomic Weapons Establishment, Aldermasten, UK, September 2, 2003.

"High pressure studies of HE and Rxn products," J. M. Zaug, Gordon Research Conference, Energetic Materials, Tilton School, NH, June 16-21, 2002.

"Laser-Matter interactions and high pressure material science studies," J. M. Zaug, Rocketdyne-Boeing, West Hills, CA, March 8, 2001.

"Sound speed and thermal measurements of inert materials: laser spectroscopy and the diamond anvil cell," J. M. Zaug, LLNL, American Physical Society Topical Meeting: Shock Compression of Condensed Matter, Amherst, MA, June-July 1997.

Conference Proceedings Session Chairmanships

Extreme Chemistry Session, J. M. Zaug, 13th International Detonation Symposium
Norfolk VA, July 23-28, 2006

Extreme Chemistry Session, J. M. Zaug, Energetic Material Gordon Research Conference Chaired by L. E. Fried, Tilton School, NH, June 20-25, 2004

Contributed lectures

"Improved Wood-Kirkwood detonation chemical kinetics," K. Glaesemann, 13th International Detonation Symposium, Norfolk VA, July 23-28, 2006.

"Recent advances in Modeling Hugoniots with Cheetah," K. Glaesemann, 14th APS Topical Conference on Shock Compression of Condensed Matter, Baltimore, MD, July 31- August 5, 2005.

"Experimental studies of high-pressure formic acid: extreme chemistry decomposition reactions," J. M. Zaug, 42nd European High Pressure Research Group Meeting, Lausanne, Switzerland, September 1-4, 2004.

"FTIR studies of high-pressure formic acid reactions: extreme chemistry decomposition kinetics," J. M. Zaug, 227th American Chemical Society Meeting and Exhibition, March 28-April 1, 2004.

"Water under extreme conditions," N. Goldman, 227th American Chemical Society Meeting and Exhibition, March 28-April 1, 2004.

"Kinetics of formic acid at high pressure and temperature," W. M. Howard, American Physical Society March Meeting, Montreal, Quebec, Canada, March 22-26, 2004.

"Polymerization of formic acid under high static pressure," A. F. Goncharov, American Physical Society March Meeting, Montreal, Quebec, Canada, March 22-26, 2004.

"Liquids in the diamond anvil cell: high pressure-temperature chemistry of formic acid, " W. B. Montgomery, presented at the annual American Geophysical Union Meeting, San Francisco, CA, December 2003.

"High pressure-temperature EoS of dense organic fluids," J. M. Zaug, Joint AIRAPT-19th-EHPRG-XXXXI meeting, Bordeaux, France, July 7-11, 2003.

"High pressure-temperature chemistry of formic acid," J. M. Zaug, Joint AIRAPT-19th-EHPRG-XXXXI meeting, Bordeaux, France, July 7-11, 2003.

"Infrared synchrotron study of high pressure-temperature reaction products from supercritical methanol," J. M. Zaug, COMPRES-II annual meeting, Santa Cruz, CA, June 18-20, 2003.

"High-pressure supercritical fluid reactions, 1. Formic Acid," D. W. Hansen, presented at the 226th American Chemical Society Meeting, New Orleans, LA, March 2003.

"Detonation product EOS studies: using ISLS to refine CHEETAH," J. M. Zaug, *2001 AIP conference,* APS Shock Compression of Condensed Matter, Atlanta, GA, June 23-29, (2002).

"Elastic constants of β-HMX and tantalum, equations of state of supercritical fluids and fluid mixtures and thermal transport determinations," J. M. Zaug, *Eleventh International Detonation Symposium*, Aspen, CO, August, (1998).

LLNL/LANL/SNL invited lectures and LLNL Work In Progress Lectures

"Transient chemical and mechanical processes under extreme conditions," J. M. Zaug, LLNL, CMS, Directorate Review Committee, May 23, 2006.

"Decomposition of nitromethane in a diamond anvil cell," E. K. Hart, Lawrence Livermore National Laboratory, presented at the CMS Undergraduate Summer Institute Symposium, August, 2004.

"Overview of laboratory components" activities in X-chem," J. M. Zaug, Extreme Chemistry Group Meeting, Lawrence Livermore National Laboratory, March 3, 2004.

"Progress in diamond anvil cell research," J. C. Crowhurst, Extreme Chemistry Group Meeting, Lawrence Livermore National Laboratory, November 25, 2003.

"The chemistry and material science experimental high pressure group," J. M. Zaug, Lawrence Livermore National Laboratory, presented to the University of Illinois ASC consortium, July, 7, 2003.

"Chemistry at extreme conditions –or- scaling effects in multi phase component transitions," J. M. Zaug, Lawrence Livermore National Laboratory, presented to the B-program division WIP, September 6, 2002.

"High pressure thermal transport properties of detonation products," J. M. Zaug, Lawrence Livermore National Laboratory, presented to the Physics and Applied Technology division WIP, August, 8, 2002.

"Experimental high-pressure DAC research in CMS: chemistry and materials science at extreme conditions," J. M. Zaug, prepared presentation for by C. Mailhiot at Los Alamos National Laboratory, CEA review, September 2001.

"Chemistry at Xtreme Conditions, J. M. Zaug, Lawrence Livermore National Laboratory, invited presentation at the Undergraduate Summer Institute in Applied Science, August 6-17, 2001.

"Impulsive stimulated light scattering (ISLS): a dedicated experimental component to Cheetah," J. M. Zaug, Joint DoD/DOD Munitions Technology Review, TCG-III, Albuquerque, NM, July 11-12, 2000.

"Energetic materials equation of state," J. M. Zaug, Lawrence Livermore National Laboratory, invited presentation to the CMS Strategic Advisory Review Committee, March 1-3, 2000.

"Sound speed, thermal transport, and solid phase stability measurements in the diamond anvil cell," J. M. Zaug, Materials Research Institute Lecture Series, Livermore, CA, Oct. 17, 1999.

"Impulsive stimulated light scattering (ISLS): accurate mechanical, transport, and thermodynamic properties," J. M. Zaug, Lawrence Livermore National Laboratory, invited presentation to the CMS Strategic Advisory Review Committee, May 12-14, 1998.

"The pressure and temperature dependence of all 13 elastic constants of β-HMX," J. M. Zaug, Lawrence Livermore National Laboratory, presented at the Safety Working Group WIP Meeting, May, 25, 1997.

APPENDIX C – Our Collaborators

University professors

L. J. Slutsky, University of Washington, Seattle, WA
J. M. Brown, University of Washington, Seattle, WA
E. H. Abramson, University of Washington, Seattle, WA

R. Jeanloz, University of California, Berkeley, CA

Private Institution researchers

A. F. Goncharov, The Carnegie Institute, Washington D.C.

Graduate students

W. B. Montgomery, 2002-2006, University of California, Berkeley, CA

Undergraduate students

Elaine K. Hart, 2004-2005, Harvey Mudd College, Claremont, CA, recipient of a 2006 Barry M. Goldwater Scholarship. (see: http://www2.hmc.edu/www_common/chemistry/news.html)

Christopher Young, 2000-2004, University of California, Davis, CA. Awarded a 2005 COMPRES internship position at BNL, Currently employed by H-E-L Group, United Kingdom, http://www.helgroup.co.uk/ .

5.0 REFERENCES

[1] D. J. Stevenson, Ann. Rev. Earth Planet. Sci., 10 (1982) 257.
[2] A. J. Cohen, and R. G. Gordon, Phys. Rev. B, 14 (1976) 4593.
[3] M. Waldman, and R. G. Gordon, J. Chem. Phys., 71 (1979) 1325.
[4] R. LeSar, and R. G. Gordon, J. Chem. Phys., 78 (1983) 4991.
[5] E. H. Abramson, J. M. Brown, and L. J. Slutsky, Ann. Rev. of Phys. Chem., 50 (1999) 279.
[6] M. Parinello and R. Carr, Phys. Rev. Lett., 55 (1985) 2471.
[7] J. A. Barker, in: Simple Molecular Systems at Very High Density, A. Polian, P. Loubeyre, and N. Boccara, Eds., NATO ASI Series B: Physics 186 (Plenum Press, NY, 1989) p. 331, ibid, p. 341.
[8] A. M. Stoneham, and J. H. Harding, Annu. Rev. Phys. Chem., 37 (1986) 53.
[9] H. Eichler, and H. Stahl, J. Appl. Phys., 44 (1973) 3429, ibid, 44 (1973) 5383.
[10] K. A. Nelson, and M. D. Fayer, J. Chem. Phys., 72 (1980) 5202.
[11] S. De. Silvestri, J. G. Fujimoto, E. P. Ippen, E. B. Gamble Jr., L. R. Williams, and K. A. Nelson, Chem. Phys. Lett., 116 (1985) 146.
[12] A. F. Goncharov, J. C. Crowhurst, and J. M. Zaug, Phys. Rev. Lett., 92 (2004) 155502.
[13] T. P. Dougherty, G. P. Wiederrecht, and K. A. Nelson, J. Opt. Soc. Am. B., 9 (1992) 2179.
[14] G. Eyring, M. D. Fayer, J. Chem. Phys., 81 (1984) 4314.
[15] J. M. Brown, L. J. Slutsky, K. A. Nelson, and L.-T. Cheng, Science, 241 (1988) 65.
[16] C. D. Marshall, I. M. Fishman, and M. D. Fayer, Phys. Rev. B, 43 (1991) 2696.
[17] A. R. Duggal, J. A. Roggers, and K. A. Nelson, J. Appl. Phys., 72 (992) 2823.
[18] J. A. Roggers, and K. A. Nelson, SPIE-INT. Soc. Opt. Eng., 1861 (1993) 314.
[19] K. A. Nelson, R. D. Miller, D. R. Lutz, and M. D. Fayer, J. Appl. Phys., 53 (1981) 1144.
[20] M. R. Farrar, L.-T. Cheng, Y.-X. Yan, and K. A. Nelson, IEEE J. QE., 22 (1986) 1453.
[21] E. H. Abramson, L. J. Slutsky, and J. M. Brown, J. Chem. Phys., 100 (1994) 4518.
[22] J. M. Zaug, E. H. Abramson, J. M. Brown, and L. J. Slutsky, Science, 260 (1993) 1487.
[23] J. M. Zaug, L. J. Slutsky, and J. M. Brown, J. Phys. Chem., 98 (1994) 6008.
[24] M. Fermigier, P. Jenffer, J. C. Charmet, and E. Guyon, J. Phys. Lett., 41 (1980) 519.
[25] D. W. Phillion, D. J. Kuizenga, A. E. Siegman, Appl. Phys. Lett., 27 (1975) 85.
[26] K. A. Nelson, R. Casalegno, R. D. Miller, and M. D. Fayer, J. Chem. Phys., 77 (1982) 1144.
[27] L. Genberg, Q. Bao, S. Gracewski, and R. D. Miller, Chem. Phys., 131 (1988) 81.
[28] L. Genberg, L. Richard, G. McLendon, and R. D. Miller, Science, 251 (1991) 1051.
[29] D. E. Hare, and D. D. Dlott., Appl. Phys. Lett., 64 (1994) 715.
[30] S. Palese, L. Schilling, P. R. Staver, W. T. Lotshaw, and R. J. Miller, J. Phys. Chem., 98 (1994) 6308.
[31] L. Genberg, Q. Bao, S. Gracewski, and R. J. Miller, Chem. Phys., 131 (1981) 81.
[32] R. J. Miller, R. Casalegno, and K. A. Nelson, Chem. Phys., 72 (1982) 371.
[33] X. Wen, S. Chen, and D. D. Dlott, J. Opt. Soc. Am. B, 8 (1990) 813.
[34] J. R. Salcedo, A. E. Siegman, D. D. Dlott, and M. D. Fayer, Phys. Rev. Lett., 41 (1978) 131.
[35] J. R. Salcedo, and A. E. Siegman, IEEE J. Quant. Electron., 15 (1979) 250.
[36] K. A. Nelson, D. R. Lutz, M. D. Fayer, and L. Madison, Phys. Rev.B, 24 (1981) 3261.
[37] R. D. Miller, M. Pierre, and M. D. Fayer, J. Chem. Phys., 78 (1983) 5138.
[38] R. S. Moog, M. D. Ediger, S. G. boxer, and M. D. Fayer, J. Phys. Chem., 86 (1982) 4694.
[39] D. D. Dlott, M. D. Fayer, J. Salcedo, and A. E. Siegman, Topics in Chemical Physics, vol. 4; Picosecond Phenomena (Springer-Verlag, New York, 1978) 230.
[40] J. R. Andrews, and R. M. Hochstrasser, Chem. Phys. Lett., 76 (1980) 207.
[41] P. Günter, Phys. Rept., 93 (1982) 199.

[42] C. Joshi, Y. Kitagawa, and A. Lal, Int. J. Nonlinear Opt. Phys., 1 (1992) 1.
[43] D. R. Lutz, K. A. Nelson, C. R. Gochanour, M. D. Fayer, Chem. Phys., 58 (1981) 325.
[44] F. Rondelez, H. Hervet, and W. Urbach, Chem. Phys. Lett., 53 (1980) 138.
[45] D. M. Burland, Acc. Chem. Res., 16 (1983) 218.
[46] F. Rondelez, H. Hervet, and W. Urbach, Chem. Phys. Lett., 53 (1978) 138.
[47] C. Bräuchle, and D. M. Burland, Agnew. Chem. Ed. Engl., 22 (1983) 582.
[48] D. M. Burland, IEEE J. Quant. Electron., 22 (1986) 1469.
[49] F.-W. Deeg, J. Pinsl, and C. Bräuchle, IEEE J. Quant. Electron., 22 (1986) 1476.
[50] R. J. Miller, M. Pierre, T. S. Rose, and M. D. Fayer, J. Phys. Chem., 88 (1984) 3021.
[51] A. Von Jena, and H. E. Lessing, Opt. Quant. Electron., 11 (1979) 419.
[52] C. A. Hoffman, K. Jarasiunas, and H. J. Gerritsen, Appl. Phys. Lett., 36 (1978) 536.
[53] R. K. Jain, and M. B. Klein, Appl. Phys. Lett., 35 (1979) 454.
[54] R. K. Jain, Opt. Eng., 21 (1982) 199.
[55] S. C. Moss, J. Ryan Lindle, H. J. Mackey, and A. L. Smirl, Appl. Phys. Lett., 39 (1981) 227.
[56] H. J. Eichler, and F. Massmann, J. Appl. Phys., 53 (1982) 3237.
[57] D. H. Auston, C. V. Shank, and P. LeFur, Phys. Rev. Lett., 35 (1975) 1022.
[58] C. A. Hoffman, H. J. Gerritsen, and A. V. Nurmikko, J. Appl. Phys., 51 (1979) 1603.
[59] M. G. Moharam, T. K. Gaylord, and R. Magnusson, J. Appl. Phys., 50 (1979) 5642.
[60] H. Hervet, W. Urbach, and F. Rondelez, J. Chem. Phys., 68 (1978) 2725.
[61] D. Pohl, Phys. Lett. A, 77 (1980) 53.
[62] H. J. Eichler, U. Klein, D. Langhans, Appl. Phys., 21 (1980) 215.
[63] H. J. Eichler, G. Enterlein, and D. Langhans, Appl. Phys., 23 (1980) 299.
[64] E. V. Ivakin, A. M. Lazaruk, I.P. Petrovich, and A. S. Rubanov, Sov. J. Quant. Electron., 7 (1977) 1382.
[65] K. Thyagarajan, and P. Lallemand, Opt. Commun., 26 (1978) 54.
[66] D. Pohl, Phys. Rev. Lett., 43 (1979) 143.
[67] H. Eichler, G. Enterlein. P. Glozbach, J. Munschau, and H. Stahl, Appl. Optics., 11 (1972) 372.
[68] M. M. Robinson, Y-X Yan E. B. Gamble Jr., L. R. Williams, J. S. Meth, and K. A. Nelson, Chem. Phys. Lett., 112 (1984) 491.
[69] M. R. Farrar, L.-T Cheng, Y-X. Yan, and K. A. Nelson, IEEE J. Quant. Electron., 22 (1986) 1453.
[70] J. T. Fourkas, T. R. Brewer, H. Kim, and M. D. Fayer, J. Chem. Phys., 95 (1991) 5775.
[71] F. V. Bunkin, M. I. Tribelskil, Sov. Phys. Usp., 23 (1980) 105.
[72] K. A. Nelson, J. Appl. Phys., 53 (1982) 6060.
[73] L. Cheng, Y. Yan, and K. A. Nelson, J. Chem. Phys., 91 (1989) 6052.
[74] A. M. Weiner, D. E. Learid, G. P. Weidderecht, and K. A. Nelson, Science, 247 (1990) 1317.
[75] G. P. Wiederrecht, T. P. Dougherty, L. Dhar, K. A. Nelson, Mat. Res. Symp. Proc., 293 (1993) 431.
[76] M. D. Fayer, Ann. Rev. Phys. Chem., 33 (1982) 63.
[77] H. J. Eichler, P. Günter, and D. W. Pohl, Optical Sciences; vol. 50, Laser-Induced Dynamic Gratings, (Springer-Verlag, Berlin, 1986).
[78] Y. R. Shen, IEEE J. Quant. Electron., 22 (1986) 1196.
[79] M. D. Fayer, IEEE J. Quant. Electron., 22 (1986) 1437.
[80] R. D. Miller, Annu. Rev. Phys. Chem., 42 (1991) 581.
[81] L. Dhar, J. A. Roggers, and K. A. Nelson, Chem. Rev., 94 (1994) 157.
[82] R. Y. Chiao, C. H. Townes, and B. P. Stoicheff, Phys. Rev. Lett., 12 (1964) 592.
[83] E. Garmire, and C. H. Townes, Appl. Phys. Lett., 5 (1964) 84.
[84] T-S Yang, R. Zhang, and A. B. Myers, J. Chem. Phys., 100 (1994) 8573.
[85] P. W. Bridgman, Amer. Acad. Proc., 49 (1914) 627; ibid. page 4.
[86] H. Carvill Lewis, Geol. Mag., 4, (1887).

[87] C. E. Weir, E. R. Lippincott, A. Van Valkenburg, and E. N. Bunting, J. Res. Natl. Bur. Stand. Sec A, 63 (1959) 55.
[88] E. Fishman, and H. G. Drickamer, Anal. Chem., 28 (1956) 804.
[89] L. Merrill, and W. A. Bassett, Rev. Sci. Instrum., 45 (1974) 290.
[90] C. H. Whitfield, E. M. Brody, and W. A. Bassett, Rev. Sci. Instrum., 47 (1976) 942.
[91] American Institute of Physics Handbook (McGraw-Hill, New York, 1957).
[92] W. D. Wilson, J. Acoust. Soc. Am., 31 (1959) 1069.
[93] M. Greenspan, and C. E. Tshiegg, J. Acoust. Soc. Am., 31 (1959) 75.
[94] M. Born, and E. Wolf, in: Principles of Optics, (Pergamon Press 6th ed., Oxford, 1980).
[95] H. K. Mao, J. Xu, and P. M. Bell, J. Geophys. Res., 91 (1986) 4673.
[96] F. Datchi, R. LeToullec, and P. Loubeyre, J. Appl. Phys., 81 (1987) 3333.
[97] L. E. Fried, W. M. Howard, P. C. Souers in 12th Symposium (International) on Detonation, J.L.M.a.J.M. Short, Eds., NSWC, Indian Head, San Diego, CA, (2002).
[98] L. E. Fried, and W.M. Howard: J. Chem. Phys., 110 (1999) 12023.
[99] L. E. Fried, M. R. Manaa, P. F. Pagoria, and R. L. Simpson, Ann. Rev. Mat. Sci., 31 (2001) 291.
[100] P. C. Souers, J. W. Forbes, L.E. Fried, S. Anderson, S. Dawson, P. Vitello, and R. Garza, Prop. Explos. Pyrotech., 26 (2001) 180.
[101] W. Fickett, W. C. Davis, Detonation, (University of California Press, Berkeley, 1979).
[102] M. Cowperthwaite and W. H. Zwisler, Sixth Detonation Symposium, (1976) p.162.
[103] M. L. Hobbs, M. R. Baer, and B. C. McGee, Prop. Explos. Pyrotech. 24 (1999) 269.
[104] F. H. Ree, J. Chem. Phys., 84 (1986) 5854.
[105] H. D. Jones, and F. J. Zerilli, J. Appl. Phys., 69 (1991) 3893.
[106] M. van Thiel, and F. H. Ree, Int. J. of Thermophysics, 10 (1989) 227.
[107] L. E. Fried, and W. M. Howard, Phys. Rev. B, 61 (2000) 8734.
[108] M. S. Shaw, and J. D. Johnson, J. Appl. Phys., 62 (1987) 2080.
[109] J. A. Viecelli, and F. H. Ree, J. Appl. Phys,. 86 (1999) 237.
[110] J. A. Viecelli, and F. H. Ree, J. Appl. Phys., 88 (2000) 683.
[111] L. E. Fried, and W.M. Howard, J. Chem. Phys., 109 (1998) 7338.
[112] F. H. Ree: J. Chem. Phys., 70 (1979) 974.
[113] W. J. Nellis, F.H. Ree, R. J. Trainor, A. C. Mitchell, and M. B. Boslough: J. Chem. Phys., 80 (1984) 2789.
[114] W. J. Nellis, and A. C. Mitchell, J. Chem. Phys., 73 (1980) 6137.
[115] S. P Marsh, LASL Shock Hugoniot Data, (University of California Press, Berkeley, 1980).
[116] L. A. Weber, NTIS Report n78, 29 (1977) 16119.
[117] G. C. Straty, and B. A. Younglove, J. Chem. Thermodyn., 5 (1973) 305.
[118] E. H. Abramson, L. J. Slutsky, and J. M. Brown, J. Chem. Phys., 110 (1999) 10493.
[119] V. N. Zubarev, and G. S. Telegin, Sov. Phys. Dokl, 7 (1962) 34.
[120] W. J. Nellis, and A. C. Mitchell, J. Chem. Phys., 73 (1980) 6137.
[121] W. J. Nellis et al., J. Chem. Phys., 94 (1991) 2244.
[122] P. Malbrunt and B. Vodar, Physica, 66 (1973) 351.
[123] S. L. Robertson and J. S. E. Babb, J. Chem. Phys., 50 (1960) 4560.
[124] P. J. Kortbeck, N. J. Trappeniers, and S. N. Biswas, Int. J. Thermophys., 9 (1991) 103.
[125] J. M. Zaug, W. M. Howard, L. E. Fried, A. F. Goncharov, W. B. Montgomery, and J. C. Crowhurst, in *Chemistry Under Extreme Conditions*, ed. M. R. Manaa, Elsevier Science Ltd, 399-425, (2005).
[126] R. F. Trunin, M. V. Zhernokletoc, N. F. Kuznetsov, O. A. Radchenko, N. V. Sychevskaya, and V. V. Shutov, Khim. Fiz., 11 (1992) 424.
[127] Unpublished work at LLNL, J. C. Crowhurst, J. M. Zaug, (2004).

[128] A. F. Goncharov, M. R. Manaa, J. M. Zaug, R. H. Gee, and W. B. Montgomery, *PRL*, **94**(6), 065505 (2005).
[129] W. Montgomery, J. M. Zaug, W. M. Howard, A. F. Goncharov, J. C. Crowhurst, and R. Jeanloz, *JPCB* **109**(41) 19443 (2005).
[130] J. W. Stout and L. H. Fisher, J. Chem. Phys., 9 (1940) 163.
[131] R. C. Wihoit, J. Chao, and K. R. Hall, J. Phys. Chem. Ref. Data, 14 (1985) 123.
[132] W. Wagner, K. M. de Reuck, R. Schmidt, J. Ewers , R. B. Stewart, R. T. Jacobsen, in: Oxygen International Thermodynamic Tables of the Fluid State, vol. 9, (Blackwell Scientific Publications, Oxford, 1987).
[133] D. S. Tzikilis and A. I. Koulikova, Zh. Phiz. Khimii, 39 (1965) 1752.
[134] A. B. Belonoshko, and S. K. Saxena, Geoch. Cosmochim. Acta, 55 (1991) 3191.
[135] G. L. Schott, M. S. Shaw, and J. D. Johnson, J. Chem. Phys., 82 (1985) 4264.
[136] B. J. Baer and M. F. Nicol, J. Phys. Chem., 94 (1990) 1073.
[137] R. L. Mills, D. H. Liebenberg, and J. C. Bronson, J. Chem. Phys., 63 (1975) 1198.
[138] T. M. Reed, and K. E. Gubbins, Applied Statistical Mechanics (McGraw-Hill, New York, 1973) p 131.
[139] H. Shimizu, Physica, 139 (1986) 479.
[140] D. R. Allan and S. J. Clark, Phys. Rev. Lett., 82 (1999) 3464.
[141] P. G. Maiella and T. B. Brill, J. Phys. Chem., 102 (1998) 5886.
[142] J. A. Muller and E. Peytral, Memoires Presentes a la Societe Chemique, 34 (1920).